12-1997

Vertical Axis Rotation in the Silurian Hills: A Cenozoic Overprint on the Mesozoic U.S. Cordilleran Magmatic Arc

John E. Comstock
University of New Orleans, jcomstock105@gmail.com

VERTICAL AXIS ROTATION IN THE SILURIAN HILLS; A CENOZOIC OVERPRINT ON THE MESOZOIC U.S. CORDILLERAN MAGMATIC ARC

A Thesis

Presented to

the Faculty of the Graduate School

of the University of New Orleans

In Partial Fulfillment

of the Requirements for the Degree of

Master of Science in Geology

by

John E. Comstock

B.S., Sonoma State University, 1995

December 1997

The point is that whenever we try to propose a solution to a problem, we ought to try as hard as we can to overthrow our solution, rather than defend it. Few of us, unfortunately, practise this precept; but other people, fortunately, will supply the criticism for us if we fail to supply it ourselves.

Karl R. Popper
The Logic of Scientific Discovery

Acknowledgment

Professional:

The entire faculty and staff of the Department of Geology and Geophysics at the University of New Orleans was generous with both time and knowledge on many aspects of this project, but the countless hours of patience and support from my thesis committee, Dr. Terry Pavlis, Dr. Kathleen Johnson, Dr. Dale Easley, and Dr. Laura Serpa require particular thanks. The Oregon State University Radiation Center at Corvallis performed the neutron activation analysis, and Sonoma State University in Rohnert Park, California, allowed me to use their x-ray diffraction equipment to help with metamorphic mineral identification. Dr. Tom Anderson and Dr. Tony Prave's time in the field provided observations, important regional stratigraphic correlations, and encouragement that can not be overestimated.

Funding for this project was provided, in part, by a Graduate Research Grant from the Geological Society of America to the author, and a National Science Foundation grant EAR-9304715 to Dr. Laura Serpa and Dr. Terry Pavlis.

Personal:

Assistance in the field was kindly and cheerfully provided by Kim McLean, Cary Whitehill, Theresa Hartman, Bernard Guest and Tom Anderson. I am particularly indebted to Bernard for weeks of tireless effort and discussion both in and about the Silurian Hills, and for an extra day of reconnaissance mapping when I could not personally return to the field. At home, both Theresa Hartman and Nathan Hartman provided space, encouragement, and an occasional threat to allow me to finish this project.

In my discussions with fellow scientists I have discovered that many, if not most, of us chose to pursue science due to the influence of a single person. Sometimes it was an instructor, other times a relative or friend who sparked an interest in observing the world and provided the encouraging news that it could be a rewarding thing to do. For me, that person is Myrtle Richards. To you I owe a debt that can never be repaid.

Table of Contents

List of Tables

List of Figures

Abstract

New, detailed field work in the Silurian Hills, southeast of Death Valley, reveals a pattern of a complex Cenozoic brittle fault overprint of rocks containing evidence of at least three episodes of Mesozoic thermal-ductile deformation. The Cenozoic faulting consists of five distinct sets of structures ordered by cross cutting relationships. The oldest, BF1, are fragments of reverse faults trending NW and dipping 45-60 SW. BF2 consists of NW trending, en echelon, sinistral strike-slip faults. BF3 is a conjugate set of N-NE trending high-angle normal faults with 100's m offset. BF4 is a complex array of conjugate strike-slip and normal faults. NNW trending dextral and NNE trending sinistral faults offset and are offset by N and NW trending conjugate sets of high-angle normal faults. The youngest set, BF5, are low-angle normal faults with no consistent basal surface or transport direction. These are interpreted to be right lateral, strike-slip extension (dextral transtension, BF4 & BF5) preceded by right lateral, vertical axis rotation, and strike-slip shortening (dextral transrotation and transpression, BF2 & BF3), all related to the interaction of the Garlock fault and northwest trending dextral shear. 30° of clockwise vertical axis rotation is inferred to have affected the Silurian Hills since the Middle Miocene as the result of BF2 & BF3 deformation.

The Mesozoic deformations are; 1, a greenschist facies, low-strain but tightly folded N vergent, crystalline basement through Pahrump Group section; 2, a greenschist facies, high-strain, 100's m thick, mylonite zone with stretching lineations trending NE-SW; and 3, an upper amphibolite facies (high T, low P), high-strain, E-W trending, S plunging Pahrump Group section, syntectonically intruded by multiple igneous phases U-Pb dated from 177 Ma to 97 Ma. The two Pahrump Group sections are interpreted to form as the result of NW directed backthrusting in the hinterland of the Sevier orogeny and were juxtaposed by NNW normal, extensional transport along the mylonite zone after crustal thickening. K-Ar biotite cooling ages suggest the mylonite zone developed during Late Cretaceous to Eocene time.

Finally, the protolith of the tectonostratigraphic Riggs Formation to be two formations of the Pahrump Group, the Crystal Spring and Beck Spring Formations.

INTRODUCTION

The Neogene interaction between the sinistral Garlock fault zone and a zone of distributed dextral faulting associated with the Eastern California Shear Zone has created a complex Cenozoic overprint on the geologic features of the Mesozoic magmatic arc and foreland fold and thrust belts in southeastern California (e.g., Dokka and Travis, 1990). Accumulating evidence suggests that vertical axis rotation of crustal blocks is as important as horizontal translation by extensional and strike-slip faulting in the late Cenozoic tectonics of the southern Death Valley and northeastern Mojave Desert regions (e.g. Holm et al., 1993; Serpa and Pavlis, 1996; Schermer et al., 1996). Initially formulated based on data from the Mojave Desert (Garfunkel, 1974), the vertical axis rotation model has now been extended to the Death Valley region to explain paleomagnetic data (Holm et al., 1993), understand the interaction of the Garlock and Southern Death Valley fault zones, and account for ~65 km of slip on the Garlock fault within 15 km of its apparent termination (Serpa and Pavlis, 1996).

The Silurian Hills, and neighboring Halloran Hills and Shadow Mountains, lie 20 km southeast of the intersection of the Garlock and Southern Death Valley fault zones (Fig. 1). This area, bounded on the west and north by the Avawatz Mountains and Kingston Range respectively, and on the east and south by the Clark Mountains and Cima Dome, is composed of rocks with ambiguous structural and stratigraphic relationships to the surrounding, more thoroughly studied regions. This ambiguity is exemplified by the lack of consensus regarding the upper plate transport direction of the Riggs "Thrust" fault, a Mesozoic shear zone overprinted by brittle faulting exposed in the Silurian Hills (Kupfer, 1960). Interpretations of upper plate motion vary from south-southwest (Kupfer, 1960) to north-northeast (Walker and Wardlaw, 1989) to west (Bishop, 1994). These transport directions are not consistent with known Mesozoic thrust faults to the east in the Clark Mountains (Burchfiel and Davis, 1988), the north in the Nopah and Resting Spring Range (Burchfiel et al., 1983), the west in the Avawatz Mountains (Spencer, 1990), or the south in the New York Mountains (Burchfiel and Davis, 1977) and Old Dad Mountain (Dunne, 1977). However, recently mapped, complex, Cenozoic brittle faulting in the Silurian Hills

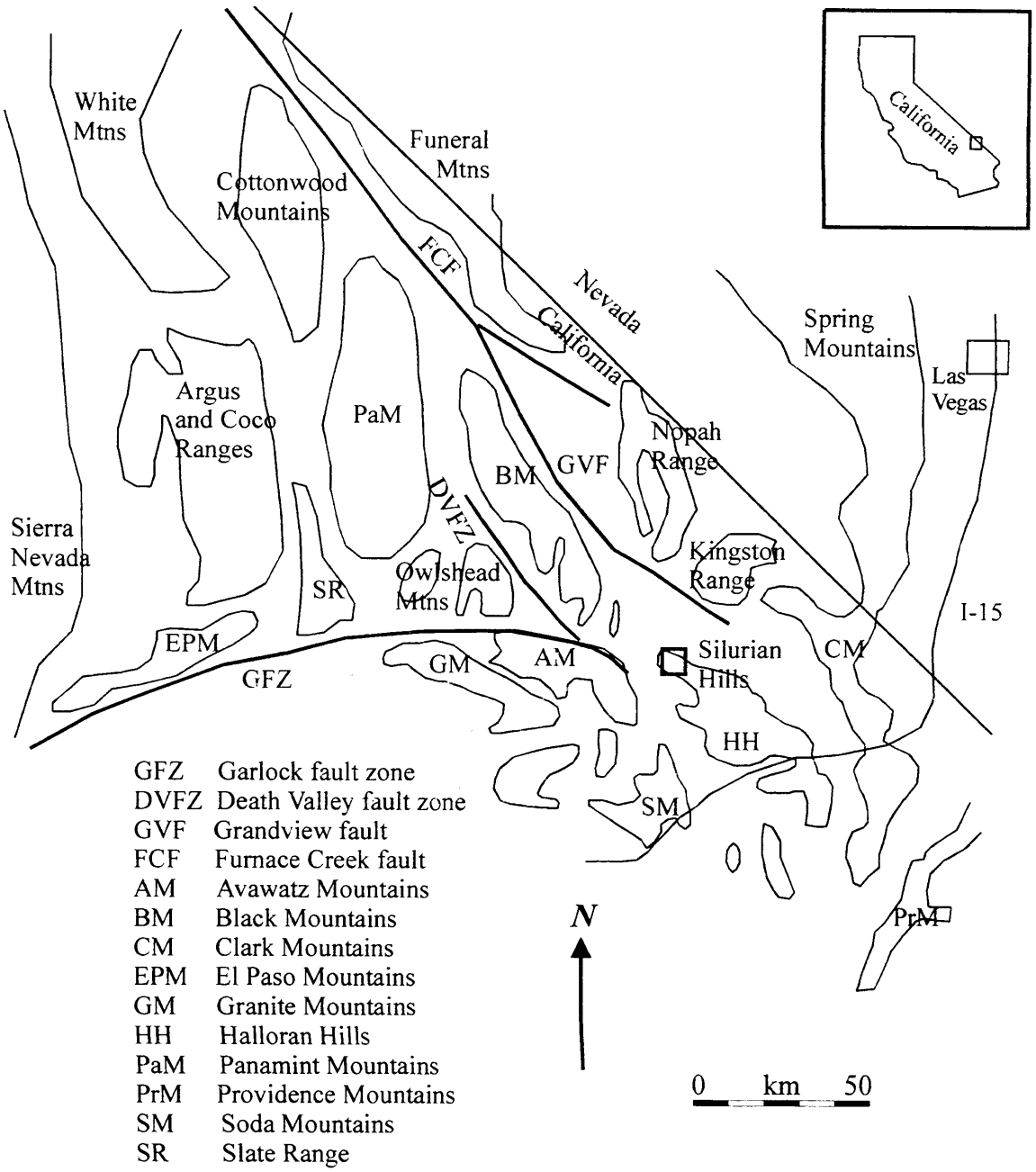

Figure 1. General location map. The study area is the outlined rectangle in the Silurian Hills.

suggests vertical axis rotation has affected areas to the east of the Avawatz Mountains (Comstock et al., 1996). Removal of the Cenozoic faulting and clockwise vertical axis rotation realigns the Mesozoic structures with recognized regional trends and is consistent with the Serpa and Pavlis (1996) model that extends vertical axis rotation into the Death Valley region.

New, detailed geologic mapping in the eastern Silurian Hills (Fig. 2), reported in this study, has revealed a polyphase Mesozoic ductile deformation recognized by basement-involved thrusting accompanied by syntectonic pluton emplacement and upper amphibolite-facies metamorphism. A subsequent greenschist-grade quartz mylonite zone places this high grade package over a tightly folded, lower greenschist-grade package of crystalline basement, Pahrump Group and younger miogeoclinal rocks. All of these rocks are crosscut by brittle high and low angle normal faults, dextral and sinistral transcurrent faults, and reverse faults. This study documents these structures and interprets the ductile events to be the result of Mesozoic back thrusting in the hinterland of the Sevier fold and thrust belt, followed by Late Mesozoic to Early Tertiary extension due to gravitational collapse of the thickened crust. The brittle faulting is interpreted to be the result of clockwise vertical axis rotation, southeast translation, and low angle detachment faulting in a broad dextral shear zone extending east from the present location of the Southern Death Valley fault zone. Secondary results of this study are the correlation of the tectonostratigraphic Riggs carbonates with rocks of the Pahrump Group and the resolution of the Riggs "Thrust" fault into two distinct components: a Mesozoic ductile, back thrust and fold shear zone, and a Miocene low-angle normal fault.

Geologic Setting

The Silurian Hills lie at the intersection of several geologic trends and structures affecting the Mesozoic and Cenozoic Cordilleran of the United States (Fig. 3). The Sevier fold and thrust belt is characterized by thin-skinned, brittle, southeast vergent, imbricate thrust stacks (Armstrong, 1968; Fleck, 1970). The Jurassic-Cretaceous magmatic arc is characterized by thick-skinned, ductile, crystalline-basement-involved, northeast vergent

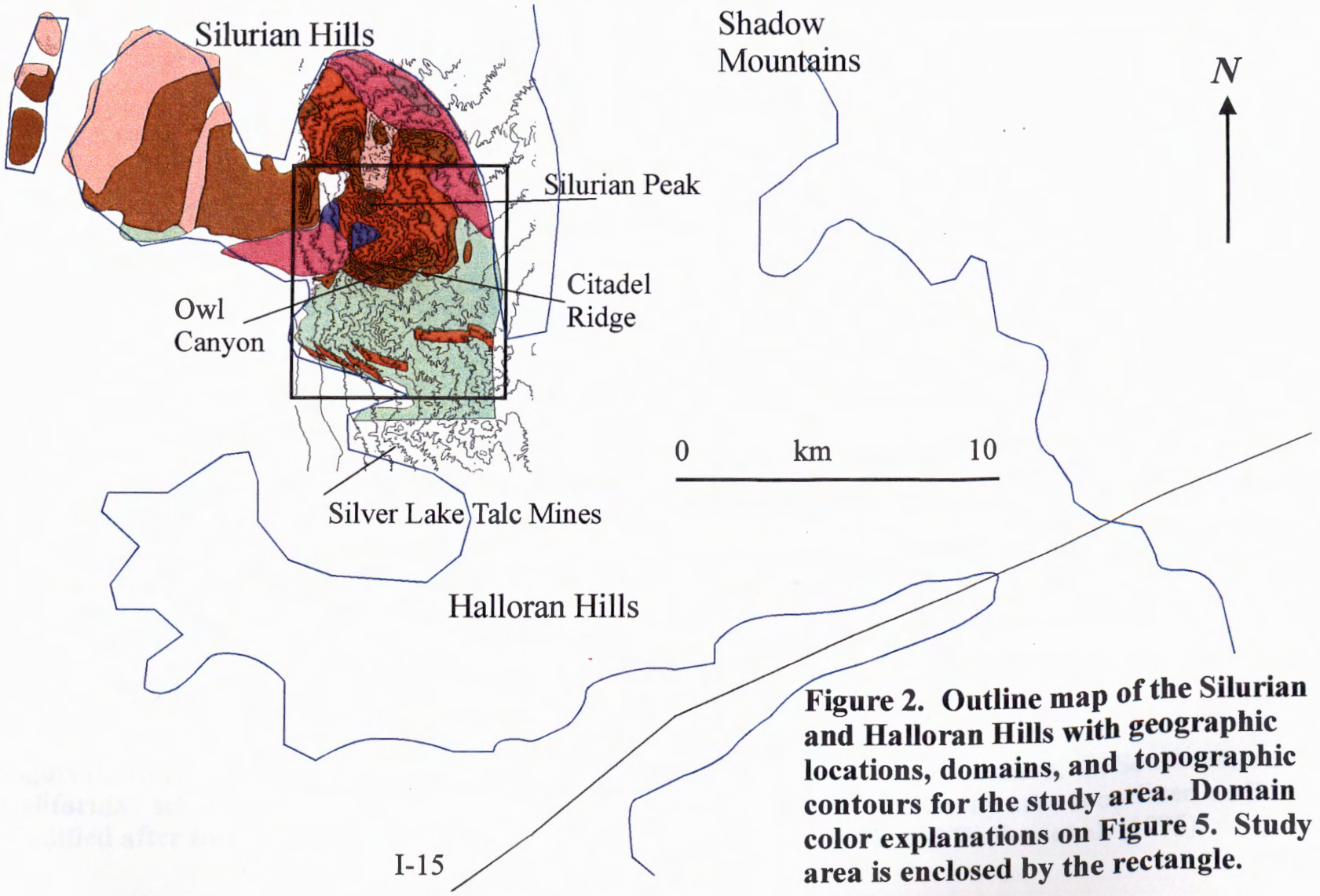

Figure 2. Outline map of the Silurian and Halloran Hills with geographic locations, domains, and topographic contours for the study area. Domain color explanations on Figure 5. Study area is enclosed by the rectangle.

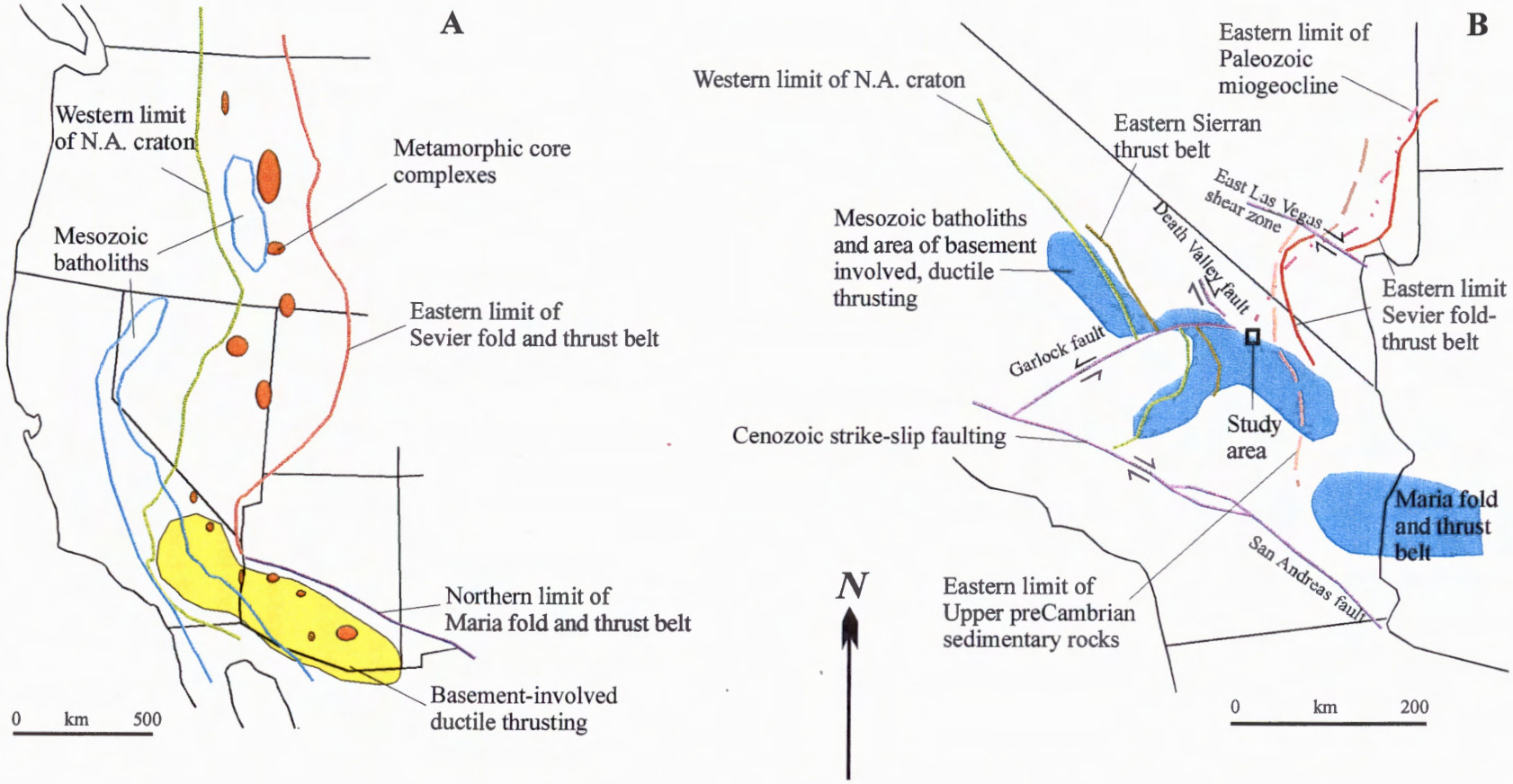

Figure 3. Regional geologic trends and structures. A. Conterminous U.S. Cordillera. B. Southeastern California - southern Nevada - eastern Arizona - southwestern Utah. The study area is outlined on B. Modified after Burchfiel and Davis (1988), Hodges and Walker (1992), and Walker et al. (1995).

thrusting and pluton emplacement (Dunne and Walker, 1993; Snow and Wernicke, 1989; Ward, 1995). East of the study area, the southernmost expressions of the Sevier fold and thrust belt are exposed in the Mesquite and Clark Mountains. In the eastern Clark Mountains younger , brittle allochthons (~96 Ma) involve Cambrian and younger sedimentary strata, while the more western thrusts (Pachalka/Winters Pass) involve ductiley deformed crystalline basement and Jurassic (~144 Ma) plutonic rocks (Fleck et al., 1994; Walker et al., 1995). West of the study area the East Sierran thrust system is exposed in the Slate Range (Wrucke et al., 1995), Avawatz (Dean, 1995; Spencer, 1990) and Tiefort Mountains (Stephens, 1994), and Cronese Hills (Walker et al., 1990). These thrust faults locally involve Precambrian basement and the Late Proterozoic to Early Cambrian terrigenous miogeoclinal wedge. The timing of these structures is constrained by pre-, syn-, and post-tectonic Middle to Late Jurassic plutonic rocks. South of the study area, in the Soda (Walker and Wardlaw, 1989) and Cowhole Mountains (Wadsworth et al., 1995), and Old Dad Mountain (Dunne, 1977), extensional Jurassic structures, surficial volcanic and sedimentary deposits are interpreted to represent an arc-graben setting (Busby-Spera, 1988). These extensional structures predate the East Sierran thrust system (Walker et al., 1990). Most of these Mesozoic structures are intruded by late Early to Late Cretaceous granitic plutons (DeWitt et al., 1984).

These Mesozoic structures are obscured by a complex Cenozoic overprint. The usual style of Cenozoic Basin and Range extension in the Death Valley region is an array of subparallel, listric normal faults coalescing at depth into a master, low-angle normal fault (Wright and Troxel, 1973). This produces a series of subparallel, fault-bounded, range blocks that have been rotated about a horizontal axis and translated along the master detachment (Wernicke et al., 1988). In the northern Mojave Desert and southern Death Valley region this pattern is disrupted by the interaction of the left lateral Garlock fault zone and a broad zone of distributed right lateral shear that includes the Southern Death Valley fault zone (Butler et al., 1988; Dokka and Travis, 1990; Wright, 1976). Recent paleomagnetic data from this region suggest that an additional component, vertical axis rotation, affects these crustal blocks (Burbank and Whistler, 1987; Ross et al., 1989).

Vertical axis rotation of intact crustal blocks is induced within many areas where there is distributed transcurrent shear (Dickinson, 1996; Luyendyk, 1991).

The Mesozoic and Cenozoic deformation of this region was imprinted on a miogeoclinal section that changes across the southern Death Valley region. The Pahrump Group unconformably overlies Proterozoic crystalline basement: arkosic strata of the lower Crystal Spring Formation underlie mixed carbonate and siliciclastic units of the upper Crystal Spring Formation and Beck Spring Dolomite (Link et al., 1993) and distinctive diamictite and olistostrome strata of the Kingston Peak Formation (Miller, 1987). All Pahrump Group formations exhibit abrupt lateral thickness and facies variations and contain numerous unconformities that regionally remove section (Prave, 1994; Mbuyi and Prave, 1993). A northwest thickening, terrigenous, detrital miogeoclinal section composed of quartzose sandstone and mixed siliciclastic and carbonate strata developed above the Pahrump Group (Poole et al., 1992). A carbonate miogeoclinal section extends from the Middle Cambrian Bonanza King Formation, (which forms the basal decollment of most Sevier style thrusts), through various middle Paleozoic rocks (Martin and Walker, 1992; Miller et al., 1992).

Mesozoic magmatic arcs were built upon and through these sedimentary units. Jurassic through Cretaceous plutons range in composition from diorite through two-mica, garnet-bearing granite, and where locally preserved, their time-correlative volcanic rocks are interbedded with Mesozoic siliciclastic and marine sedimentary sequences (Schermer and Busby, 1994). Overlying all of the above rocks are Tertiary sedimentary and volcanic deposits that record deposition in developing sedimentary basins (Fowler et al., 1995).

Detailed lithologic descriptions of Silurian Hills stratigraphy can be found in the following work: the crystalline basement is discussed by DeWitt (1980), the Pahrump Group through middle Paleozoic section is described by Kupfer (1960), the plutonic rocks are described by Abbott (1971), Sutter (1968), and DeWitt (1980), and the Tertiary sedimentary sections are described by Bishop (1994) and Fowler et al. (1995). A tectonostratigraphic unit, the Riggs Formation (Kupfer, 1960), is unique to the Silurian Hills region. It consists of highly deformed dolomite and calcite marble, quartzite, and calc-silicate rocks. Definitive correlation to regional stratigraphy has not been possible;

any fossils that may have originally been present have been destroyed by metamorphism and transposition of original bedding (Battey, 1991). Figure 4 summarizes the stratigraphy in the study area.

Methods

Reconstructing the geologic history of the Silurian Hills region involved tracing and correlating structures, fabrics and stratigraphy throughout the field area as well as determining grades of metamorphism and the amount and shear sense of penetrative strain. In the primary field area this was accomplished by detailed field mapping at the scale of 1:6,000 using enlargements of 1:24,000 USGS topographic maps and aerial photography. This detailed work was accompanied by reconnaissance observations throughout the Silurian and Halloran Hills and at selected locations in the Shadow, Clark, Avawatz, and Panamint Mountains, the Saratoga, Saddle Peak, Salt Spring and Alexander Hills, and the Kingston Range. Primary field mapping included collection of orientation data for foliation, mineral lineation, faults, slickensides, and fold axes. Stretched pebbles of the Kingston Peak Formation were measured to estimate finite strain in four locations.

Over 75 samples were selected, and over 150 thin sections examined, for petrography, metamorphic mineral identification, igneous rock identification and kinematic sense indicators. Most samples were oriented in the field with respect to foliation and mineral lineation. Thin-section examination was supplemented by X-ray diffraction analysis of metamorphic minerals.

Whole rock neutron activation analysis of plutonic rocks was conducted to analyze possible correlations with rocks in adjacent terranes. Samples for whole rock neutron activation analysis were powdered in an alumina ceramic shatterbox to minimize contamination. Sample splits, including one duplicate for reference, were analyzed at the Radiation Center of Oregon State University, Corvallis.

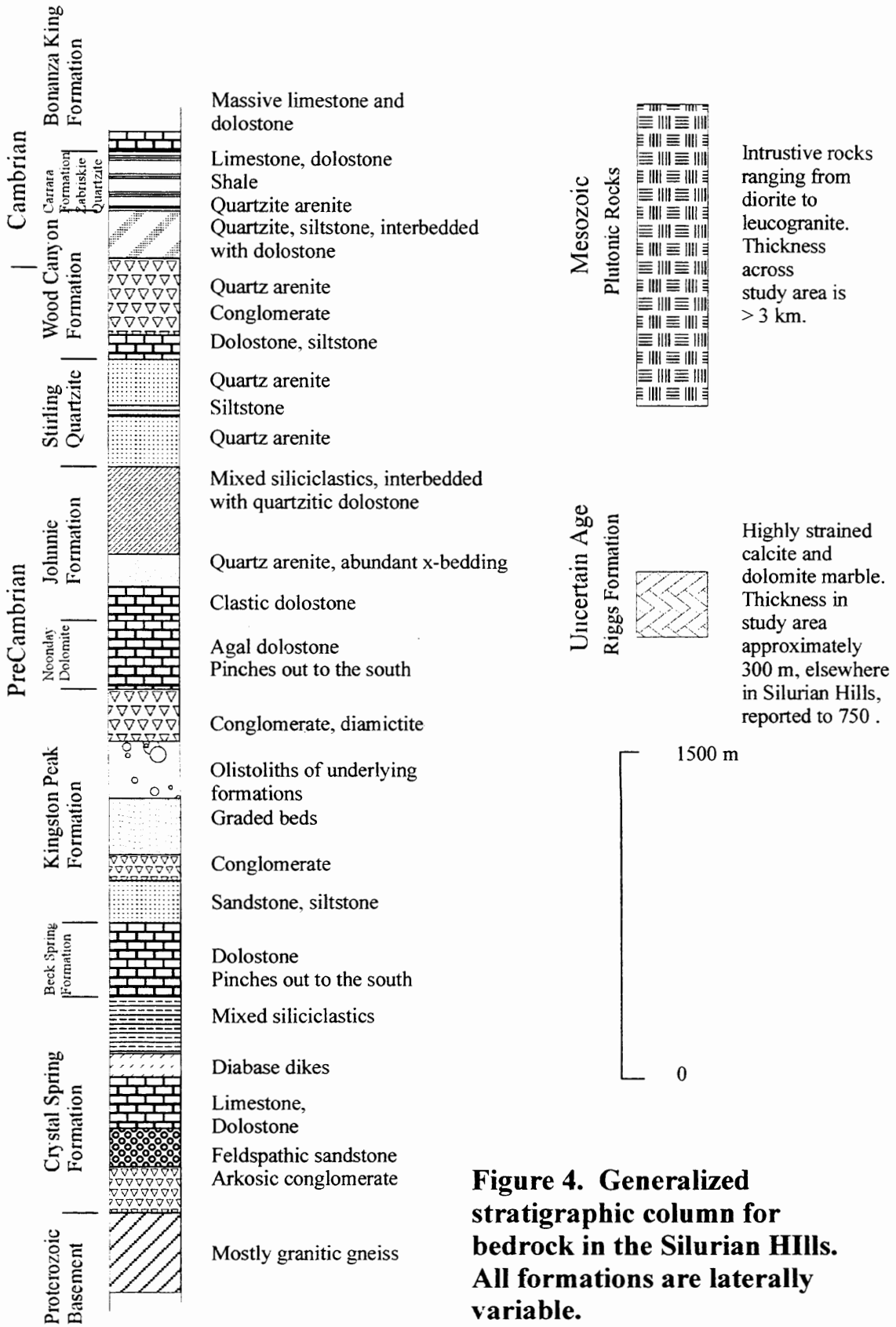

Figure 4. Generalized stratigraphic column for bedrock in the Silurian HIlls. All formations are laterally variable.

STRUCTURE AND METAMORPHISM

The Silurian Hills contain evidence of at least nine deformational events ranging from the formation of the Middle Proterozoic crystalline basement, through Mesozoic ductile thrusting and amphibolite grade metamorphism to complex Cenozoic strike slip and normal faulting. These deformation events are recognized by contrasts in fabric and mineral lineation orientation, styles of penetrative ductile deformation, metamorphic mineral assemblages, and contrasts of ductile and brittle deformation. Ages and relative timing are inferred from cross cutting relationships, metamorphic pressure - temperature - time paths, and previously published ages of intrusive rocks and metamorphic minerals.

Previous studies of the Silurian Hills have interpreted a simple Cenozoic deformation history of north-trending, high-angle, basin and range style normal faults producing a west to southwest directed extension. Mapping for this study reveals a more complex brittle Cenozoic history, and it is impossible to consider the Mesozoic history in the absence of this context. Thus, the Cenozoic structures are described first below, providing a framework for understanding the Mesozoic deformation. Metamorphism and ductile deformation clearly predate brittle deformation and are discussed between descriptions of Cenozoic and Mesozoic structure.

The Study Area

The study area covers approximately 35 km^2 in the southeastern Silurian Hills. The area consists of Quaternary alluvium, Miocene alluvial and lacustrine sediments, Mesozoic plutonic rocks, Pahrump Group siliciclastics and carbonates, and a tectonostratigraphic unit, the Riggs Formation carbonates and quartzites. This study groups these rocks by domains comprised of rocks of similar metamorphic grade and deformational style (Fig. 5). The Quaternary and Miocene sedimentary rocks flank both the east and west sides of the study area and are not given a domain designation. Greenschist facies Pahrump Group and Proterozoic basement, designated domain 1, comprise the north and northeastern section of the area. The central section of the study

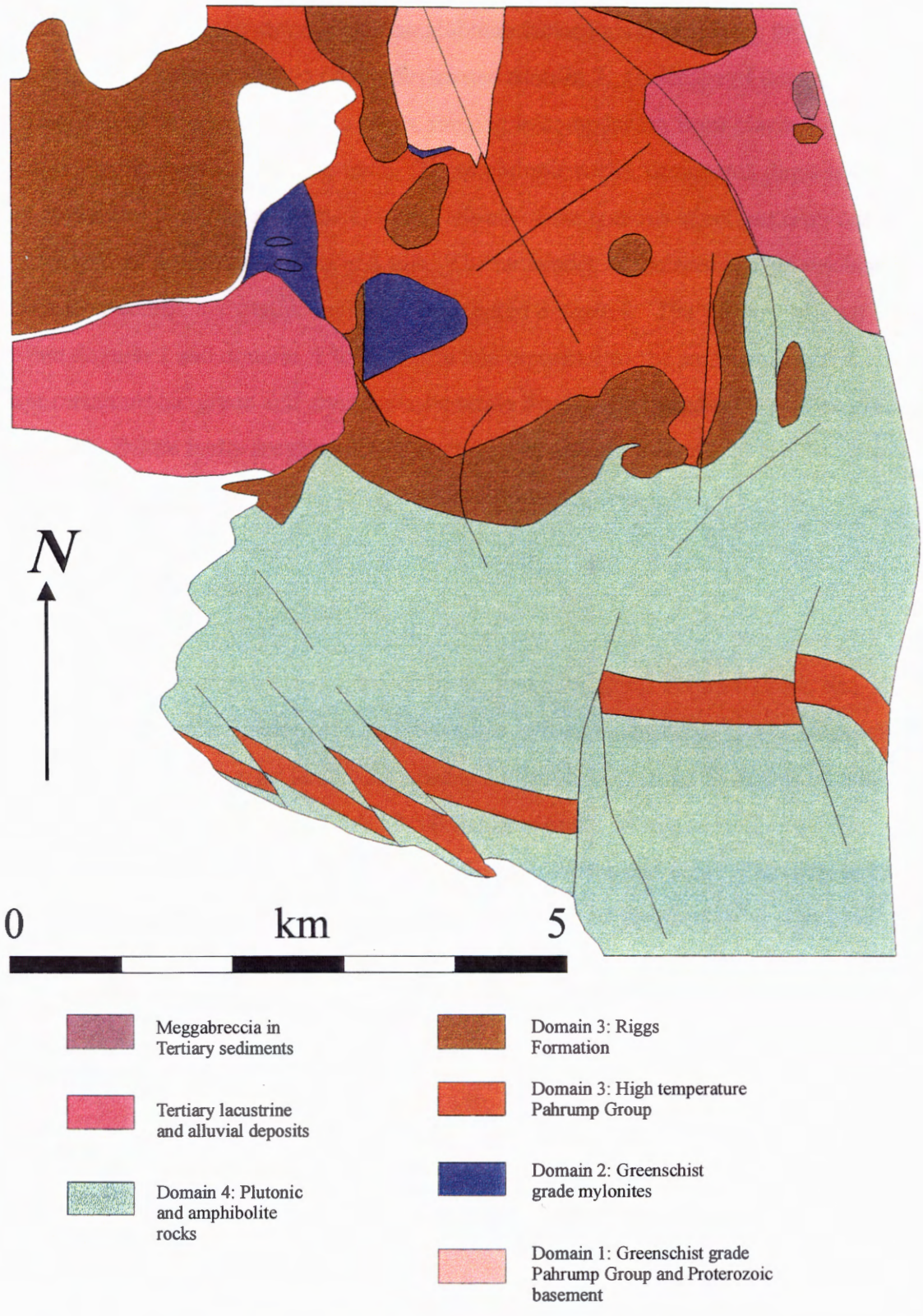

Figure 5. Generalized domain map of the study area in the Silurian Hills.

area is dominated by high strain, upper amphibolite facies Pahrump Group, Proterozoic basement, and Riggs Formation rocks, designated domain 3. Outcrops of domain 3 rocks are separated by Mesozoic plutonic rocks, ranging in composition from diorite to two-mica, garnet bearing, leuco-granite. These plutonic rocks, designated domain 4, show evidence of varying amounts of strain. Some of the igneous injections crop out in the main part of domain 3 as pods and sills. The remainder of the area is a greenschist facies, mica quartzofeldspathic mylonite, designated domain 2. The primary contact between domain 2 and domain 1 to the north and domain 3 to the south and east, is an abrupt metamorphic grade and crystal-plastic strain front. The transition is neither gradual nor faulted. Brittle faults are present in the study area and are inferred, by the disruption of the Miocene sedimentary beds, to be Middle Miocene and later.

Cenozoic Structure

Cenozoic structures are dominated by brittle faults, tilted Tertiary strata, and brittle folds. The faults include high and low angle normal faults, three sets of strike-slip faults, and high angle reverse faults. All normal and strike-slip faults disrupt the Tertiary sedimentary deposits, dated post 13.8 Ma (Friedmann et al., 1996), as well as all the Mesozoic and older rocks, and are therefore Middle Miocene and later. The reverse faults do not clearly cut Tertiary deposits and are therefore only constrained to be post Late Cretaceous, the youngest age of crosscut granitic intrusive rocks. The brittle faults (BF) are grouped and labeled BF1, oldest, through BF5, youngest. The relative ages of sets are determined by crosscutting relationships.

Low-angle normal faults:

The youngest brittle faults in the study area are low angle normal faults, BF5 (Figures 6 and 7A), that consistently place structurally higher over lower rocks. These faults place Riggs carbonates discordantly over Pahrump Group rocks and Tertiary sediments. The entire structural section of Riggs carbonates through domain 2 mylonites is partially repeated by a west dipping fault underlying the upper plate fragment that forms

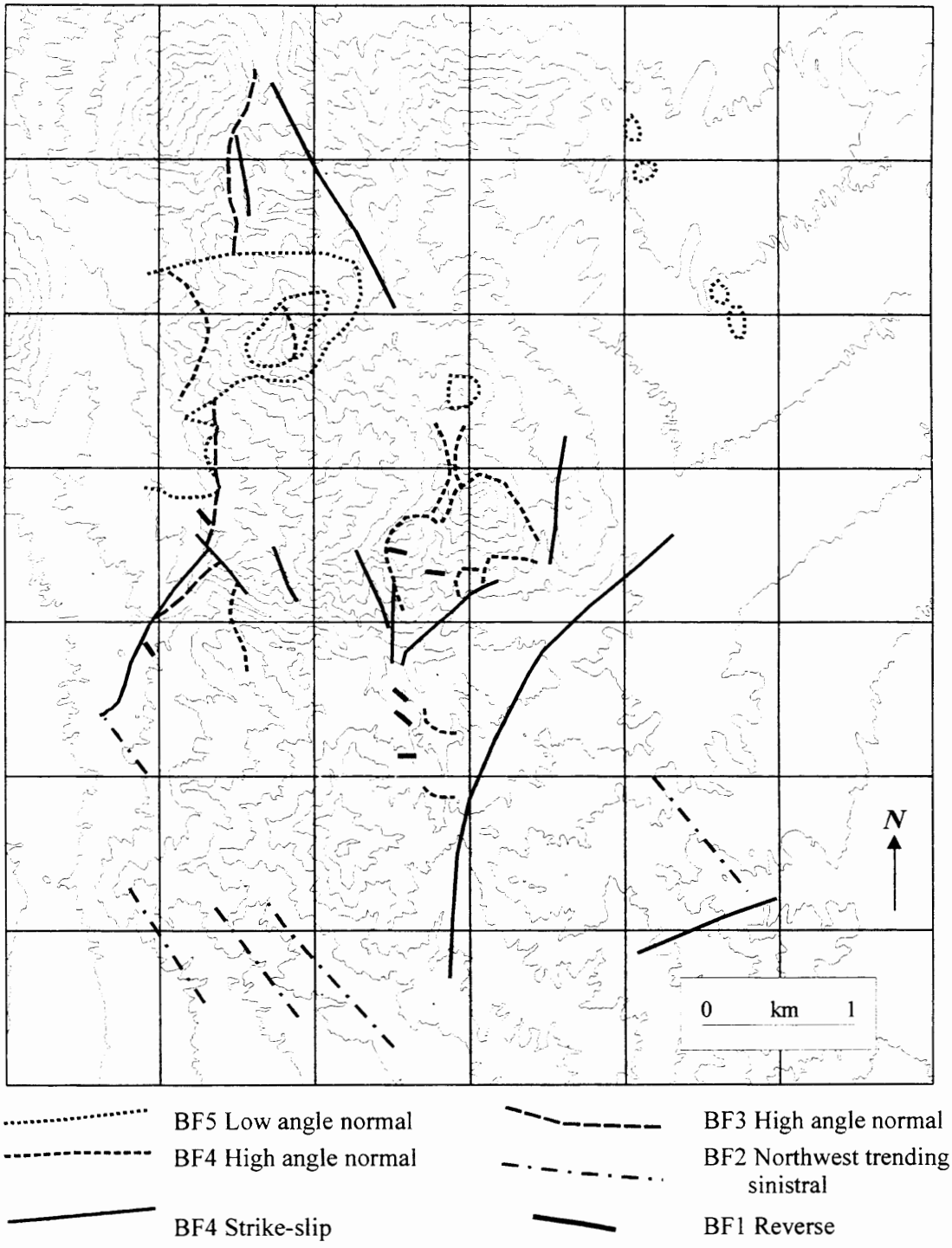

Figure 6. Generalized map showing surface traces of the brittle faults. Only the most continuous traces are shown. Most fault surfaces are not mappable as continuous traces due either to lack of stratigraphic control, or complex cross-cutting relationships with other faults.

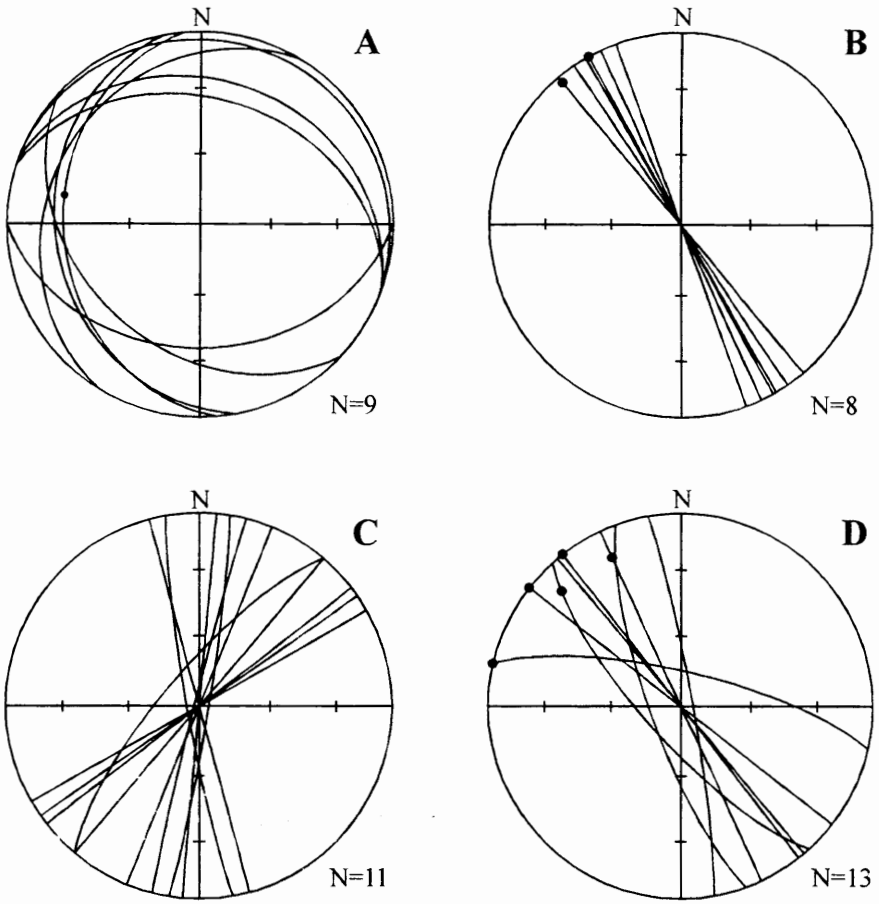

Figure 7. Stereonet summaries of brittle low-angle normal and strike-slip faults. Great circles are fault planes, black circles are slip vectors from slickensides. A. Low-angle normal faults, BF5. B. Northwest trending sinistral faults, BF2. C. Northeast trending sinistral faults, BF4. D. Northwest trending dextral faults, BF4.

Silurian Peak. This fault may have developed as a gravity slide surface formed in the weaker mylonite foliation. In the northeastern part of the study area, a low-angle normal fault is horizontal to gently northeast dipping and separates southwest dipping Tertiary strata from overlying Riggs carbonates. The lower plate rocks are disrupted by strike-slip faulting and the upper plate exists as isolated fragments or klippe. Thus, the low-angle faults may not represent one continuous fault surface, and some low-angle faulting may have preceded strike-slip faulting. These low-angle normal faults are similar to numerous examples mapped to the east and south in the Shadow Mountains and Halloran Hills (Fowler et al., 1995) that have been interpreted as gravity slide blocks.

Strike-slip faults:

A conjugate pair of strike-slip faults comprise BF4. Stereonet summaries (Figs. 7C and 7D) of BF4 faults show average trends of 318° for dextral faults and 023° for sinistral faults with a resultant acute angle intersection of 065°. The conjugate pair could be attributable to either plane strain with a north-south trending shortening axis or transcurrent shearing. In a transcurrent system, two shear zone orientations are possible (Fig. 8), northwest trending dextral shear or northeast trending sinistral shear. Figure 9 shows the regional distribution of sinistral and dextral fault systems and suggests that a dextral shear zone in the Silurian Hills would be concordant with regional trends. The variance of 065° and 075° about the dextral and sinistral averages suggests internal or external rotation accompanied shearing. BF4 faults prominently cut a set of en echelon, northwest striking, sinistral faults, BF2, that trend across the south central portion of the study area (Fig. 6).

These BF4 strike slip faults are clearly distinguishable from an older set of sinistral faults (BF2). A stereonet summary of BF2 sinistral faults is shown in Figure 7B. BF2 faults are clearly cut by the conjugate faults, BF4, and therefore must represent an earlier faulting event. However, as can be seen in Figure 9, these BF2 faults are not concordant with any recognized regional trend.

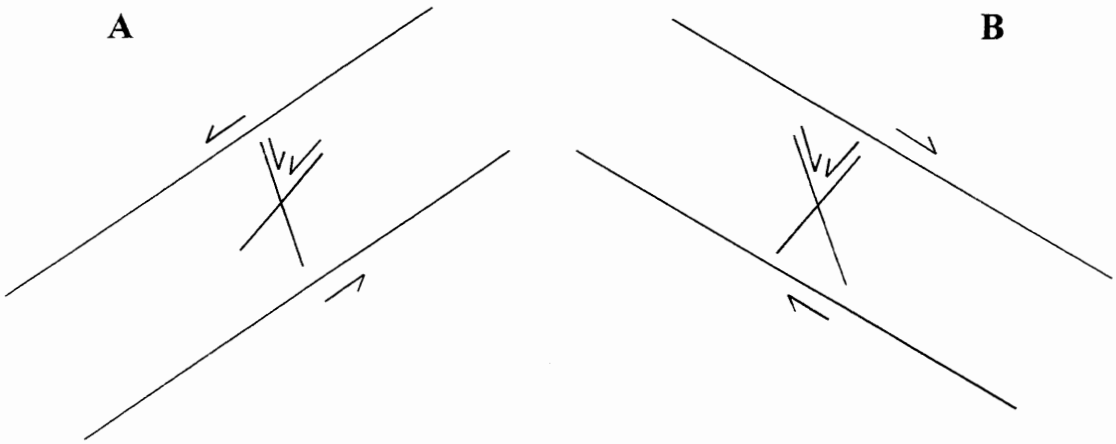

Figure 8. Identical patterns of conjugate strike-slip faults can develop in either a sinistral or dextral shearing system. Example A shows the development of a conjugate fault set within a sinistral shear system oriented northeast - southwest. Example shows the same conjugate fault set developed within a northwest - southeast trending dextral shear system. Conjugate strike-slip fault sets can also develop in a pure shear system as well.

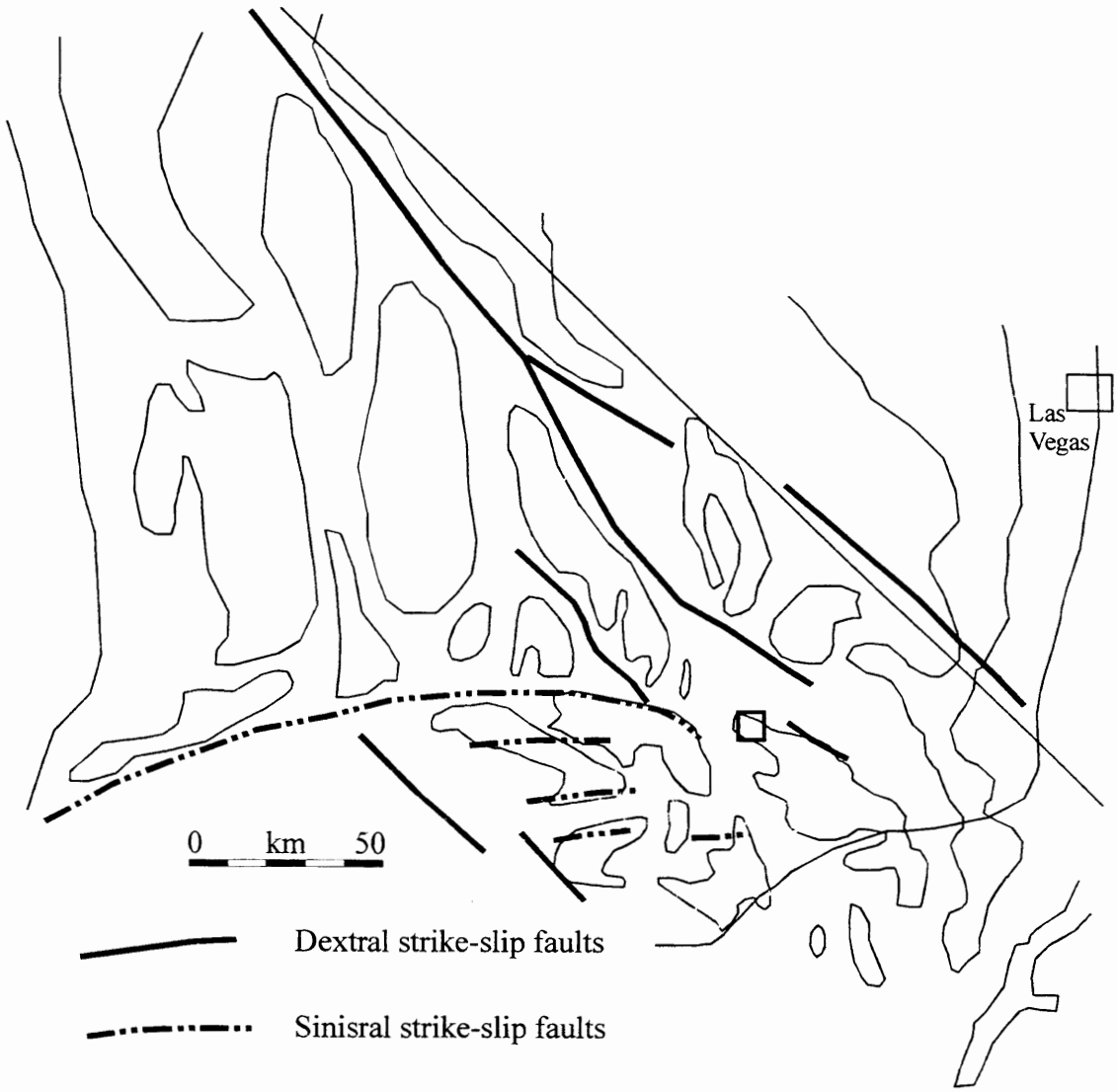

Figure 9. Regional trends of strike-slip faults. Sinistral faults trend east-west to slightly northeast while dextral faults trend northwest.

High-angle normal faults:

Normal faulting is ubiquitous throughout the study area. However, these faults are truncated by, or merge with, strike-slip faults or occur as localized conjugate sets that are not traceable for long distances. Figure 10 shows stereonet summaries of all normal fault data. Field relationships on the west side of the study area reveal that the set of northeast trending faults, BF3, produce at least 100 meters of west block down slip. BF4 faults truncate and offset the older BF3 faults. The relationship of BF3 faults to BF2 faults is more difficult to establish. The inferred intersection of the two faults is covered by alluvium. Examination of aerial photos of the central portion of the Silurian Hills, northwest along strike from the BF2 faults, show northwest trending lineaments, but reconnaissance field checks along the southern escarpment of the central Silurian Hills revealed right, not left-lateral offsets. The Tertiary beds, also along strike to the northwest from the BF2 faults, must have been displaced to their present position partly by the BF3 faults, (the Tertiary sediments do not contain clasts of any of the surrounding exposed bedrock). If BF3 predated BF2 the Tertiary beds should record evidence of the BF2 faulting. Instead, the Tertiary beds show lineament evidence of the conjugate BF4 faulting, but not of BF2 faulting. Thus, I conclude that BF3 normal faulting occurred between the conjugate BF4 episode and the earlier BF2 sinistral episode.

Two remaining sets of conjugate normal faults strike 355° and 315° (Figs. 10B and 10C). These minor faults show little offset or linear persistence and frequently merge with BF4 strike-slip faults. The acute angle intersection of 040° is consistent with conjugate fault sets arrayed in orthorhombic symmetry in response to a three-dimensional stress field (Reches, 1978; 1983). These faults are therefore inferred to develop during the BF4 episode.

Brittle folds:

Brittle folding of the foliation in the metamorphic rocks is displayed in two ways: the mylonitic rocks (domain 2) have developed southeast trending kink folds, and all highly strained lithologies, (the mylonites, metamorphosed Pahrump Group, Riggs carbonates and amphibolites), exhibit a broad, southeast trending arch in foliation (Fig.

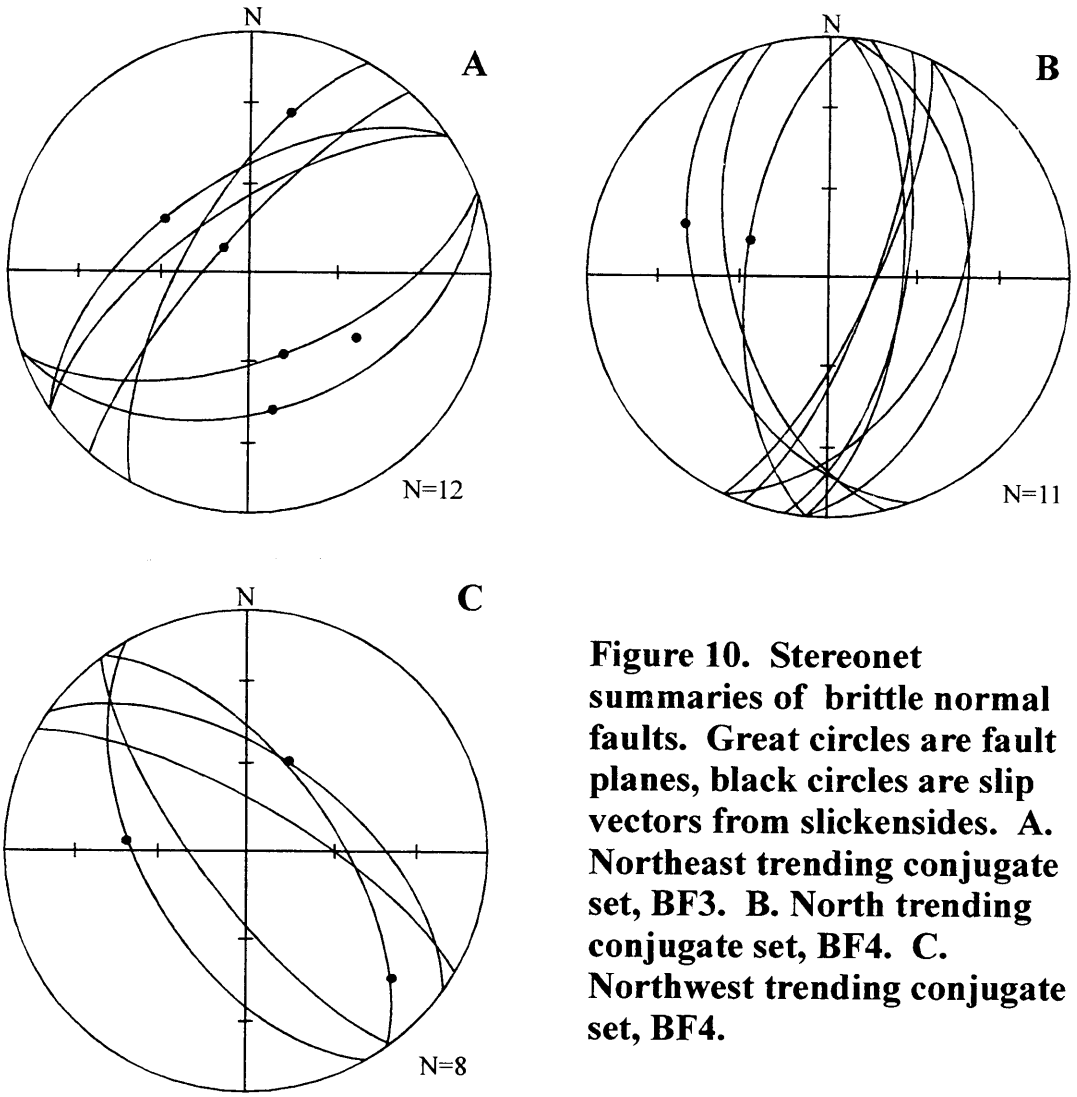

Figure 10. Stereonet summaries of brittle normal faults. Great circles are fault planes, black circles are slip vectors from slickensides. A. Northeast trending conjugate set, BF3. B. North trending conjugate set, BF4. C. Northwest trending conjugate set, BF4.

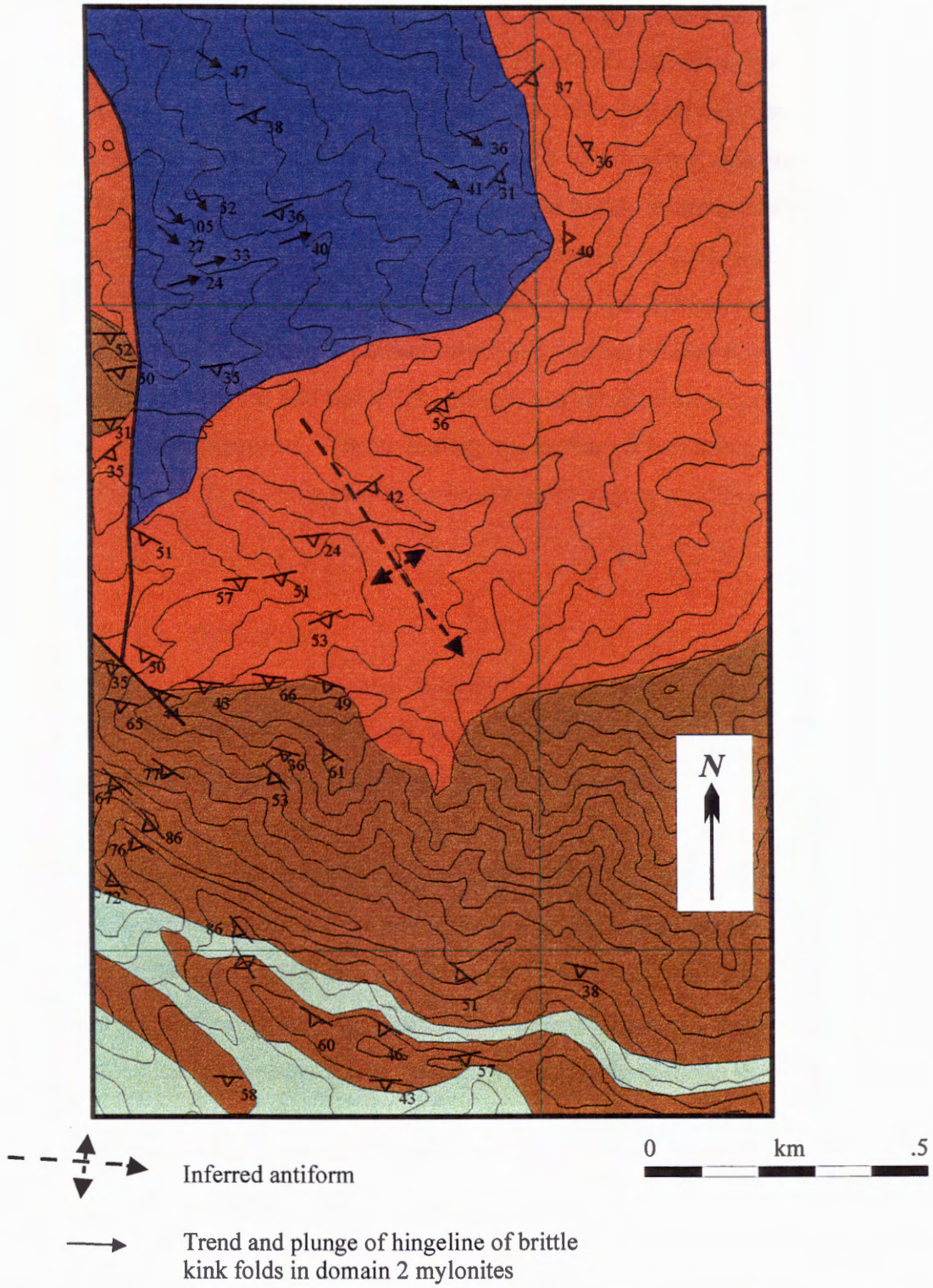

Figure 11. Arching of foliation in domain 3 (Riggs and Kingston Peak formations) and brittle kink folds in domain 2 mylonites. The arching forms a plunging antiform that is subparallel with the hingeline of the brittle kink folds in the mylonite. Domain colors are given in Figure 5.

11). Kupfer (1960) identified similar arching in the study area and in localities throughout the Silurian Hills. The stereonet data shown in Figure 12 summarize both examples of folding. The contoured hingeline trend of the kink folds and the calculated pi axis both show a southwest trend. Eighty percent of the kink folds show Z asymmetries viewed downplunge, implying dextral strain. I infer that the highly foliated, thinly laminated, and mineralogically segregated mylonites experienced flexural-slip kink-folding with relatively short wavelengths (outcrop scale) consistent with their thin laminations. In contrast, the other, more coherent rocks have thicker layers and folding produced only a broad arch. BF4 and BF3 faulting cut and disrupt the foliation of the southwest trending kink folds and arch. This is consistent with the folding and arching representing strain accumulation in the BF2 dextral shear zone prior to complete brittle failure resulting in BF3 and BF4 episodes.

Tilting of Tertiary beds:

Tertiary sediments are present in two separate localities, one each on the east and west sides of the study area. These are two fragments of the Tertiary Shadow Basin deposits described in detail by Bishop (1994) and Fowler et al. (1995). The eastern section contains lacustrine mudstone and carbonate strata and dips steeply southwest while the western section contains granitic cobble to boulder fanglomerate and conglomerate layers with rare interbedded quartz arenite and mudstone strata and dips moderately southeast. Significantly, no clasts were observed in this section that were derived from the adjacent and topographically higher bedrock (Pahrump Group, Riggs, and mylonites). This implies that the bedrock had to either underlie the basins at the time of deposition or rocks have been transferred laterally by faulting. These Tertiary sections could not have been deposited on top of the bedrock and then simply tilted into the current position by faulting and horizontal axis rotation of the underlying bedrock. Restoring the Tertiary beds to horizontal with concurrent tilting of the adjacent bedrock exacerbates the problem by increasing the slope of the bedrock to vertical or overlying, rather than an underlying position (Fig. 13). Restoring movement on normal fault BF3 elevates the western Tertiary exposures, but the bedrock west of BF3 is also elevated and

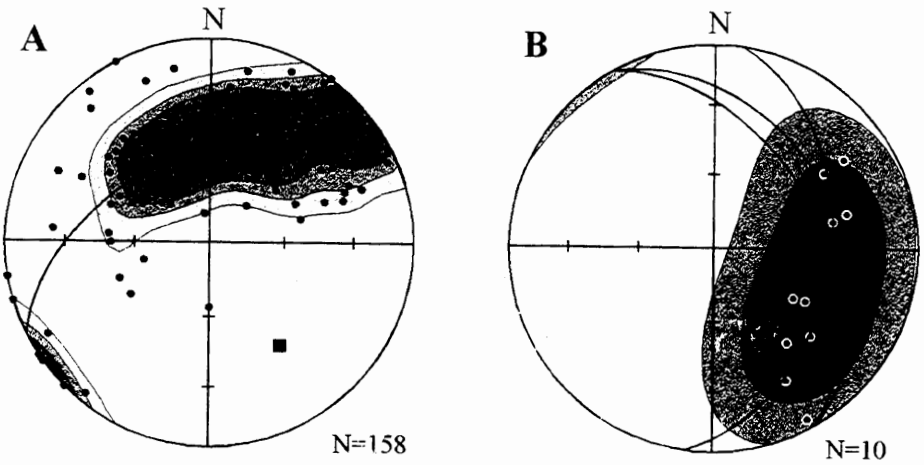

Figure 12. A. Pole to foliation of mylonites, Pahrump Group rocks, Riggs carbonates, and plutonic rocks. The black circles are poles to foliation, the great circle is the calculated best fit great circle to the data and the gray square is the pole to that great circle (pi axis). B. Brittle kink folds in mylonites. The black circles are the trend and plunge of fold hingelines and the great circles are the strike and dip of fold axial planes.

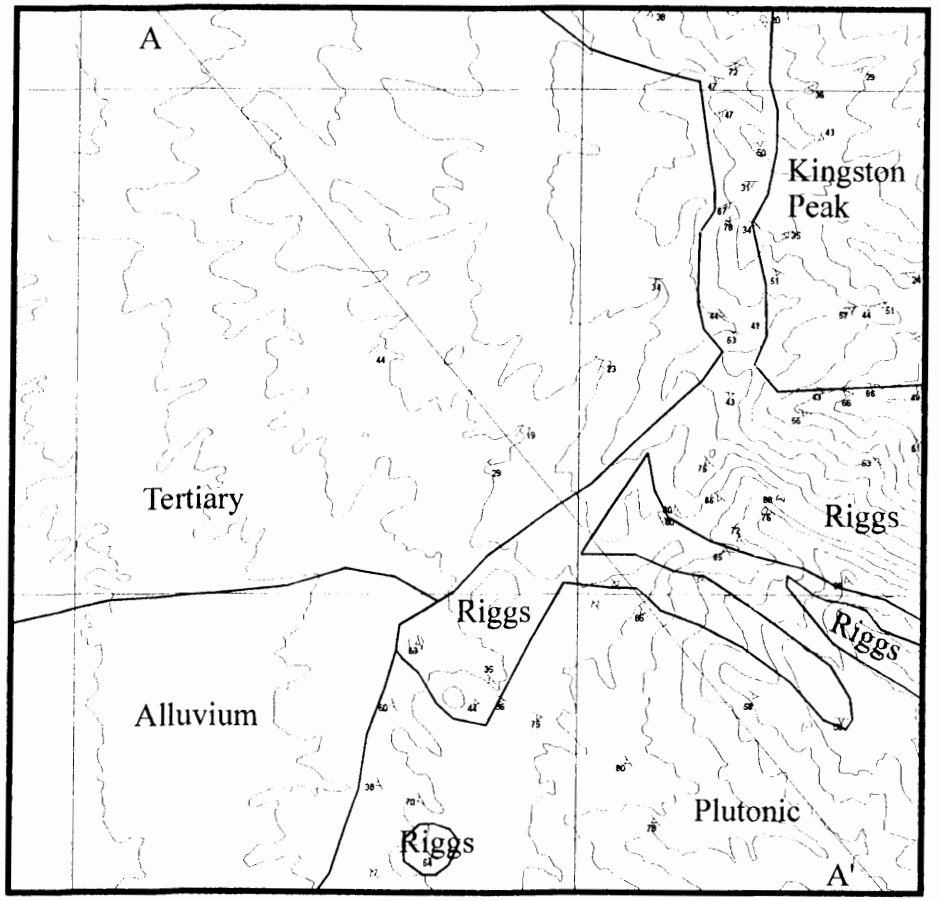

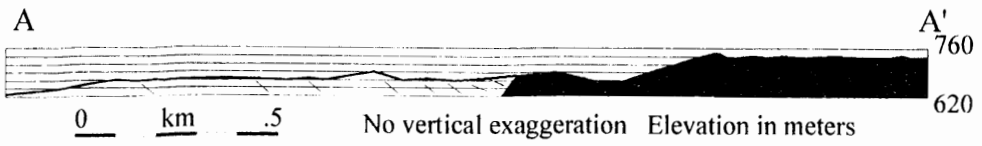

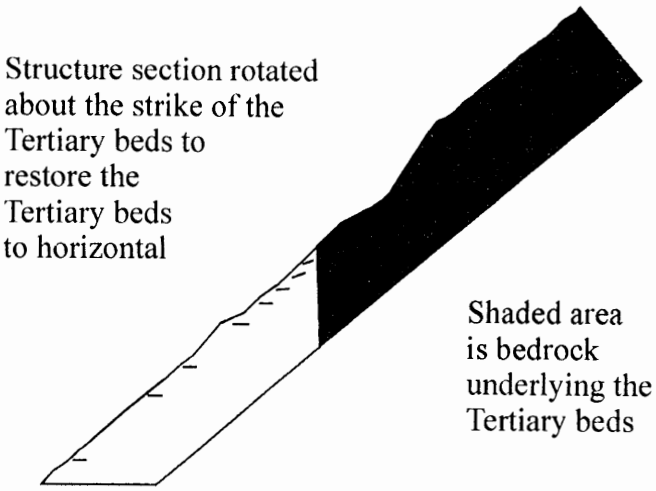

Figure 13. Generalized geologic map of the Tertiary beds at the west end of Owl Canyon. Structure section A-A' is perpendicular to strike of the Tertiary beds and extends into the adjacent bedrock of the Riggs, Kingston Peak and plutonic complex. The rotated section restores the Tertiary beds to horizontal and shows that the contact between the shaded bedrock and Tertiary beds would be vertical, an untenable position due to the absence of Riggs clasts in the Tertiary beds.

therefore is not restored to a position underlying the Tertiary sediments. Based on these relationships, the Tertiary sediments appear to have been deposited elsewhere and emplaced by either an as yet unidentified detachment surface that does not penetrate the adjacent bedrock, strike-slip faulting, or a combination of both.

Brittle reverse faults:

The oldest brittle structures are a scattered set of fault surfaces with slickensides indicating reverse slip (BF1). Figure 14 summarizes the data of these surfaces. These faults are primarily recognized in the Riggs carbonates where injected and ductilely deformed granitic sills or pods are cut off along the fault planes. They cut the Late Cretaceous granite and are offset by BF3 and BF4 faults, thereby loosely constraining the age of faulting to the latest Cretaceous or early Tertiary.

Metamorphism

All pre-Tertiary rocks in the Silurian Hills are variably affected by metamorphism and penetrative deformation. Four distinct metamorphic domains are recognizable based on contrasting metamorphic mineral assemblages, contrasting styles of dynamic recrystalization, or combinations of both. Metamorphism reached greenschist grade in domains 1 and 2 (Fig. 5) and upper amphibolite grade in domains 3 and 4. Metapelites in domain 1 exhibit slaty cleavage while all lithologies in domains 2, 3, and 4 experienced penetrative ductile deformation from crystal plasticity, recrystallization, or both. LS tectonites are dominate in domains 2 and 3, and both LS and S tectonites occur in domain 4. Domains 1 through 3 are defined on the basis of metamorphic and deformation affinities, regardless of lithology. Domain 4, however, includes amphibolite and igneous rocks from both the plutonic complex in the southern portion of the study area and injected pods and sills in domain 3.

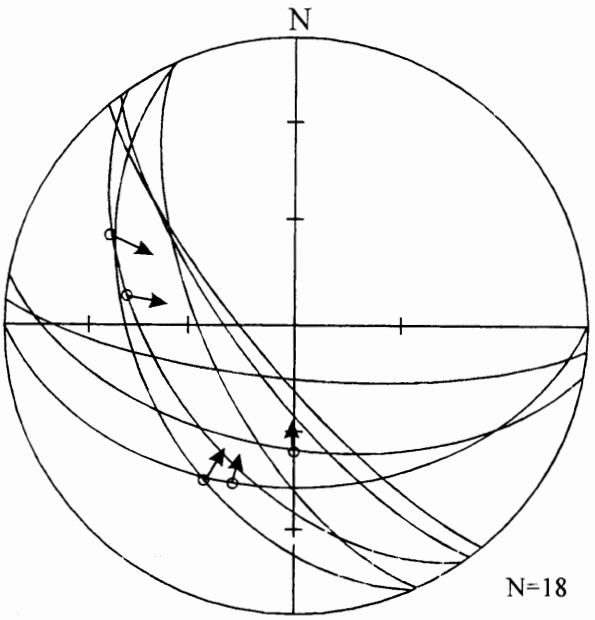

Figure 14. Reverse faults, BF1. Great circles are strike and dip of fault planes. Open circle and arrow are slip vectors determined from slickensides and field relationships.

Domain 1:

Domain 1 consists of an intact stratigraphic section including Proterozoic basement and overlying Pahrump Group strata. To both the east and west sides of the study area, and still within the Silurian Hills (Fig. 15), these sections also include the apparently intact stratigraphic succession overlying the Pahrump Group to the Middle Cambrian Bonanza King Formation. The mineral assemblage of epidote+chlorite+ tremolite/actinolite+quartz, indicating greenschist grade metamorphism (Spear, 1995), was found in marls of the Kingston Peak Formation and other mudstone strata. Pelitic strata show evidence of slaty cleavage oblique to original bedding, implying tight folding of the strata, although no large scale folds were recognized. Neither a continuous cleavage nor mineral lineation has developed. Original sedimentary structures are clearly identifiable and intact, and penetrative strain is insignificant.

Domain 2:

The main body of domain 2 consists of a greater than 250 m thick micaceous quartzofeldspathic mylonite exhibiting strong LS fabrics defined by the alignment of muscovite, biotite, and chlorite, and containing abundant attenuated polycrystalline quartz and feldspar ribbons (Fig. 16). The mylonite is so highly deformed and recrystallized that identification of the protolith is difficult. Field relationships and outcrop scale textures suggest that Pahrump Group diamictites, quartzites, and quartz cobble conglomerates, as well as Proterozoic gneissic basement, would be reasonable protoliths. The abundance of chlorite+biotite+quartz and the absence of garnet suggests deformation under greenschist facies conditions. This conclusion is also consistent with microstructures within the rocks showing brittle deformation of feldspars and crystal plasticity in quartz (see below).

Several thinner mylonite zones, up to 1 m thick, are found north of Silurian Hill (along the southern part of domain 1) and in domains 3 and 4 in the east-central portion of the study area. The mylonites in domain 4 occur within thin felsic dikes intruding amphibolites. While considerably thinner than, and separated from, the main body of domain 2, these outcrops share the same metamorphic grade, foliation, and mineral

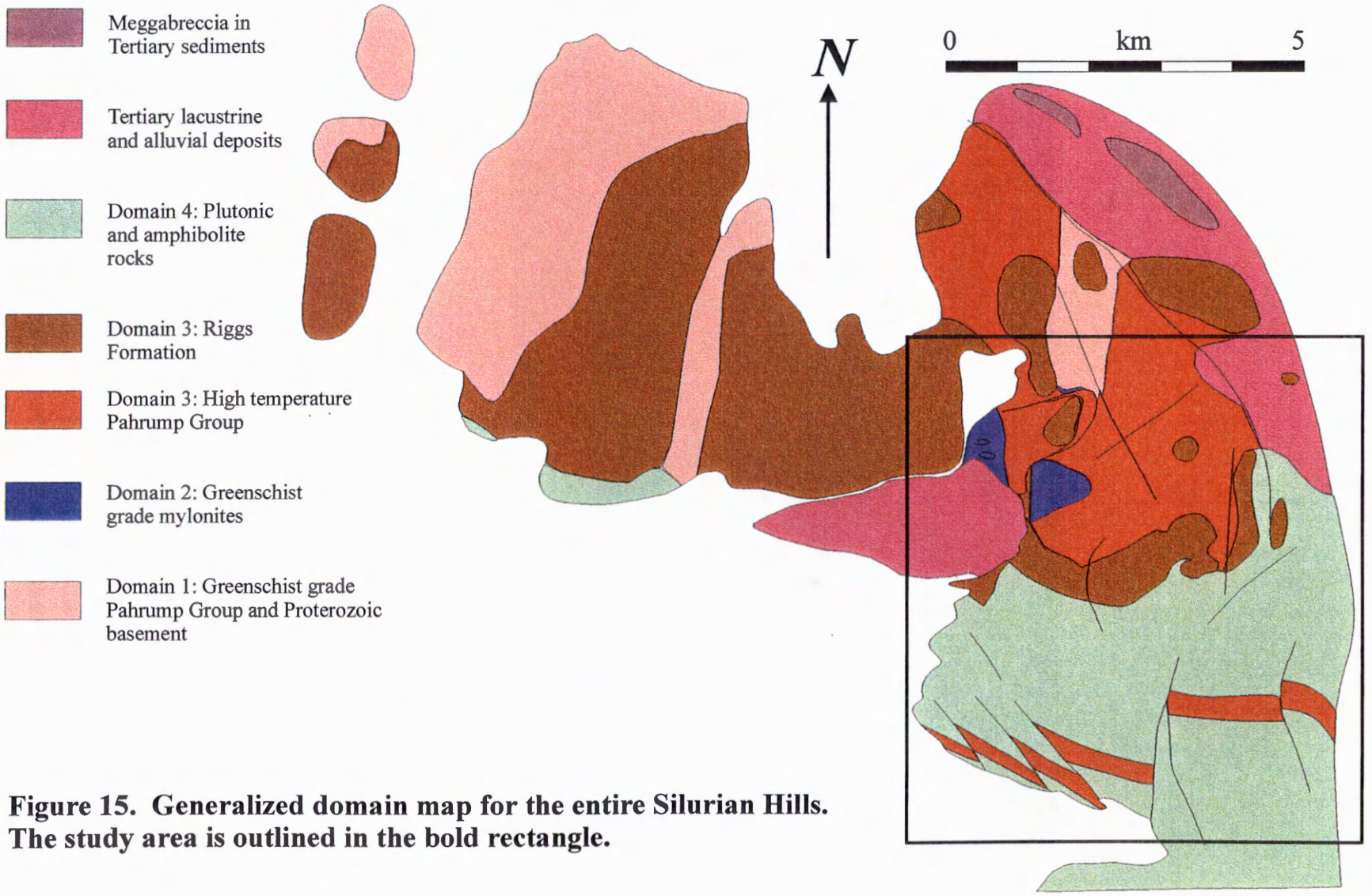

Figure 15. Generalized domain map for the entire Silurian Hills. The study area is outlined in the bold rectangle.

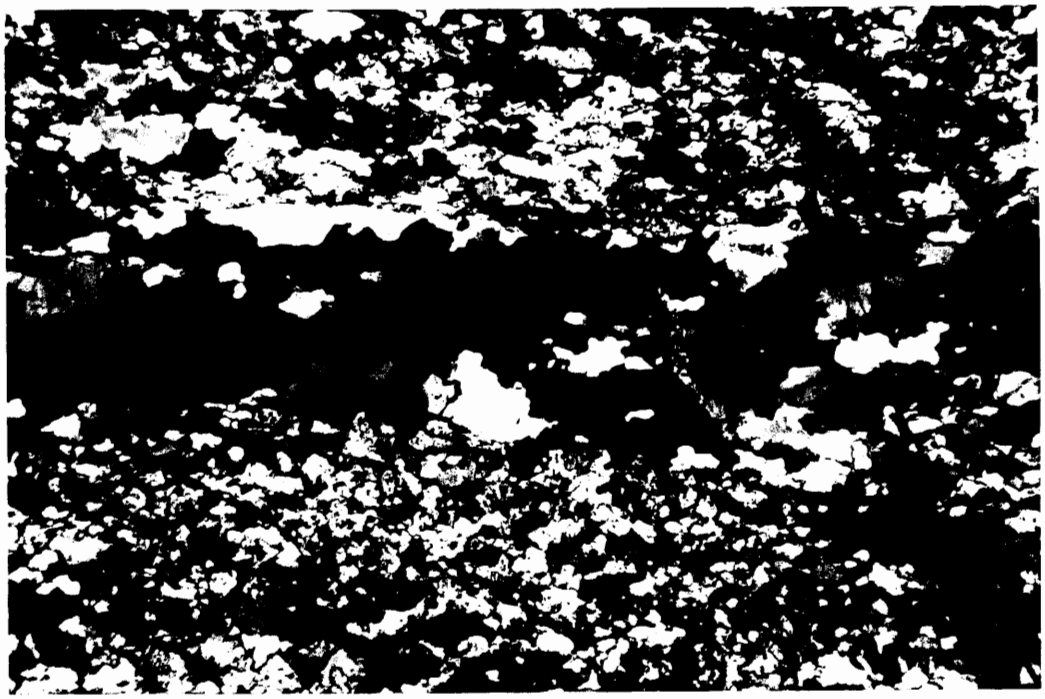

Figure 16. Quartz ribbons in sample 58, a domain 2 mylonite. The photomicrograph was taken under crossed Nicols with a field of view 3 mm wide.

lineation attitudes. Due to their metamorphic and structural similarity, these outcrops are included in domain 2 and are all interpreted to be the result of one deformational episode.

Domain 3:

Domain 3 consists of diamictite, carbonate, and quartzite strata of the Kingston Peak Formation (of the Pahrump Group) together with the dolostone and limestone marbles, quartzite, and calc-silicate strata of the tectonostratigraphic Riggs Formation. These rocks include the prominent exposures across the central portion of the study area but also smaller outcrops of carbonate, quartzite, and basement that are isolated within the plutonic complex in the southern portion of the study area (Fig. 5). While composed of widely varying protoliths, all the units in domain 3 consistently exhibit upper amphibolite or equivalent grade metamorphic mineral assemblages (Table 1) and strong LS fabrics.

TABLE 1. DOMAIN 3 METAMORPHIC MINERAL ASSEMBLAGES

Sample	Mineral Assemblage	Bulk Rock Type
79F	grossular, diopside, calcite, anorthite, quartz	calc-silicate
93A	diopside, calcite, quartz, tremolite, hornblende	calc-silicate
110	microcline, quartz, biotite, sillimanite, cordierite	pelite
130	orthoclase, biotite, sillimanite, andalusite, quartz, cordierite	pelite
155B	quartz, diopside, tremolite	quartzite

The degree of thermal metamorphism is consistent throughout the domain. Sillimanite is found in schists within one meter of the contact with domain 2 and within pelitic boudins in the Riggs Formation ten meters from the contact with domain 4. Sample 130 shows sillimanite, andalusite and cordierite (Fig. 17), which together with the absence of kyanite, places the reaction on or near the sillimanite-andalusite univariant line. There is ambiguous evidence that the "second sillimanite" reaction (direct formation of sillimanite by the reaction muscovite+albite+quartz=sillimanite+K-feldspar+H_2O) has been recorded. Muscovite and albite are absent but andalusite is metastable. Sample 110 (Fig. 18), from a different layer than 130, shows an abundance of sillimanite and cordierite, with neither

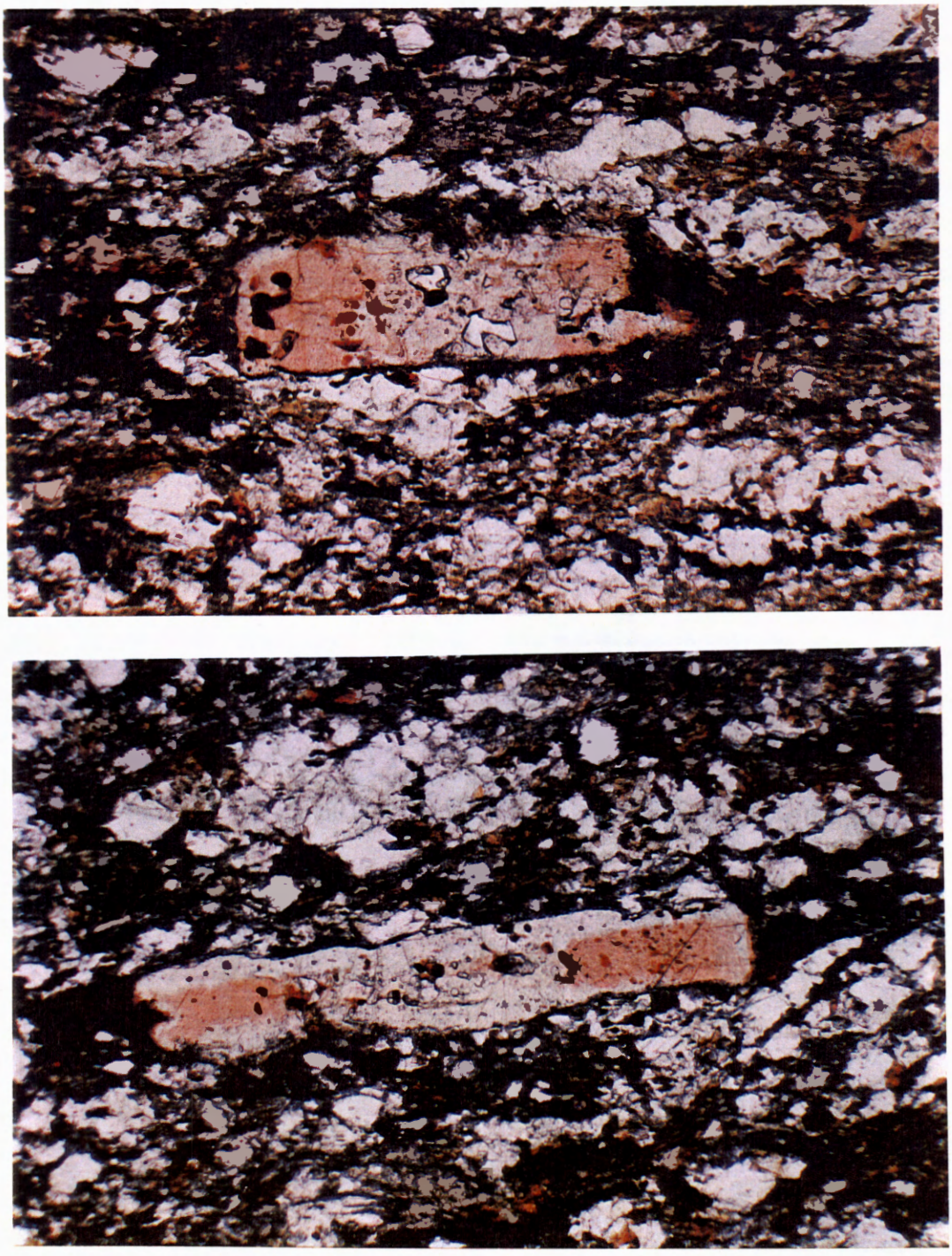

Figure 17. Two examples of the biotite-cordierite-sillimanite-andalusite schist, sample 130. The sillimanite is in the form of fibrolite and intergrown with the biotite indicating dynamic growth. However at the upper and lower edges of the andalusite crystals, radiating patterns of fibrolite crystals indicate static growth. Both photo-micrographs are under plane light with a field of view 3 mm width.

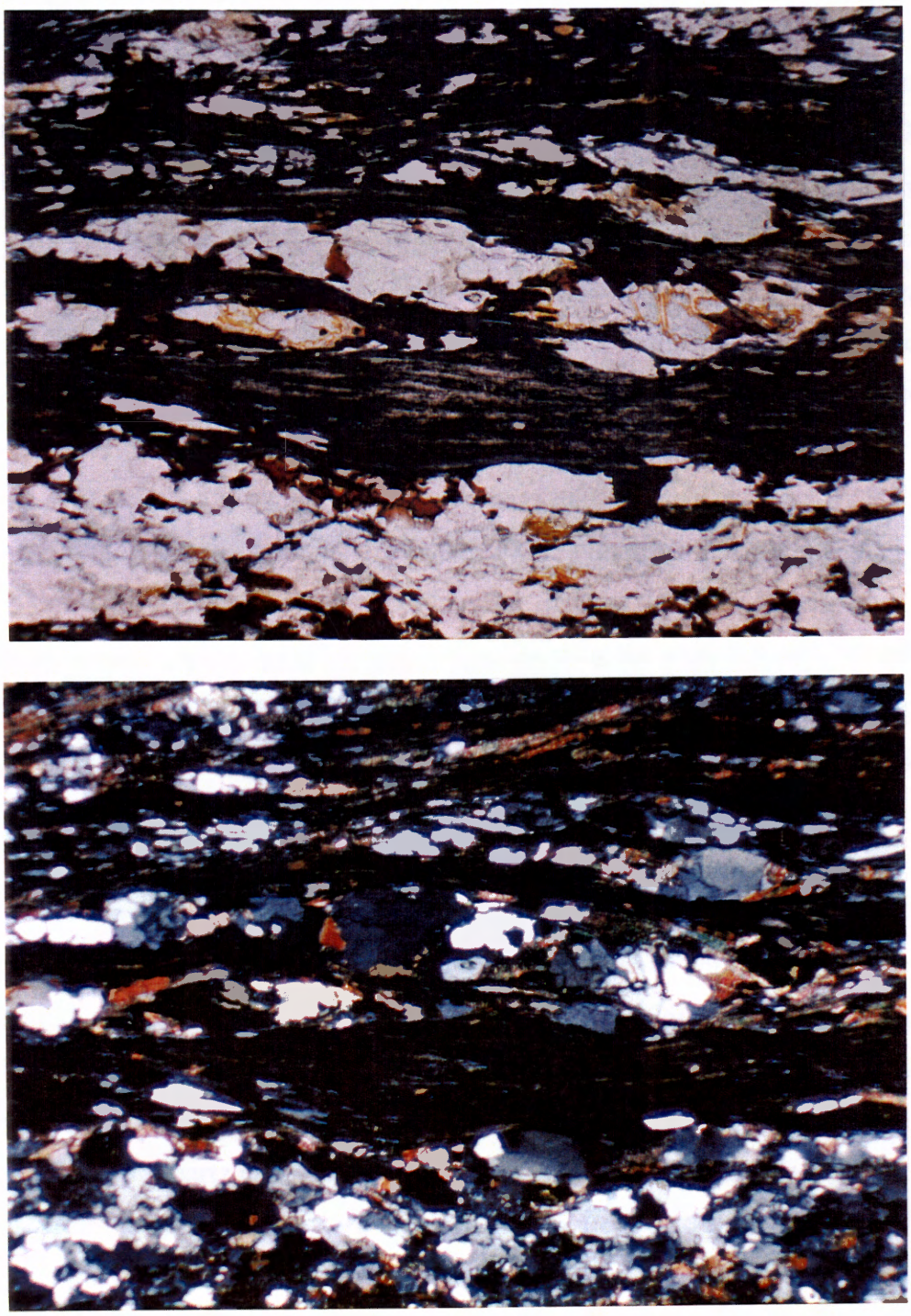

Figure 18. Sample 110, a pelitic schist, showing cordierite, quartz, biotite, and sillimanite. Also shown are S-C' shear sense indicators showing sinistral shear. Upper photo is in plane light, the lower photo under crossed Nicols. The field of view is 3 mm wide.

andalusite nor muscovite, an assemblage more strongly suggestive of the "second sillimanite" reaction. The presence of metastable andalusite in sample 130, however, implies P-T conditions close to the andalusite stability field. This combination constrains the pressure and temperature to 2 - 3 kbar and 600C to 640C (Fig. 19; Kerrick, 1990). The other mineral assemblages are less diagnostic of P-T conditions, but are consistent with the Al_2SiO_5 reactions (Fig. 19). While the degree of strain indicated by the penetrative cleavage varies throughout the domain, usually dependent on lithology, the strong LS fabric is consistent, regardless of rock type. The majority of the metamorphic minerals are strongly aligned parallel with the LS fabric, implying metamorphism coeval with strain. However, the static development of a small amount of sillimanite, randomly oblique to the fabric, implies some post-strain recrystallization. The upper amphibolite grade metamorphism and penetrative cleavage development are consistent with high temperature metamorphism at a depth not greater than the thickness of the normal stratigraphic succession in the region. Thus, considering the absence of similar metamorphic conditions elsewhere within the region, it seems clear the high T metamorphism was controlled by pluton emplacement, a conclusion consistent with structural evidence for syn-tectonic plutonism discussed below.

Domain 4:

Domain 4 consists of amphibolite and igneous rocks of both the plutonic complex to the south of the study area and intrusive pods and sills in domain 3. While comprised of widely varying specific textures and mineral percentages, these rocks can be grouped into five types (Streckeisen, 1976): (1) metadiorites and quartz-diorites (amphibolites), (2) granodiorites, (3) quartz monzonites, (4) granites, and (5) leucocratic, two-mica, garnet-bearing granites.

Amphibolite rocks in domain 4 contain mineral assemblages of biotite+plagioclase+hornblende+titanite$\pm$quartz and exhibit strong LS fabrics. At outcrop scale some exposures of amphibolite exhibit layering suggestive of a metasedimentary protolith and appear to be sedimentary country rock inclusions in a plutonic complex. However, in thin section most samples show zoned feldspar crystals (Fig. 20), implying an

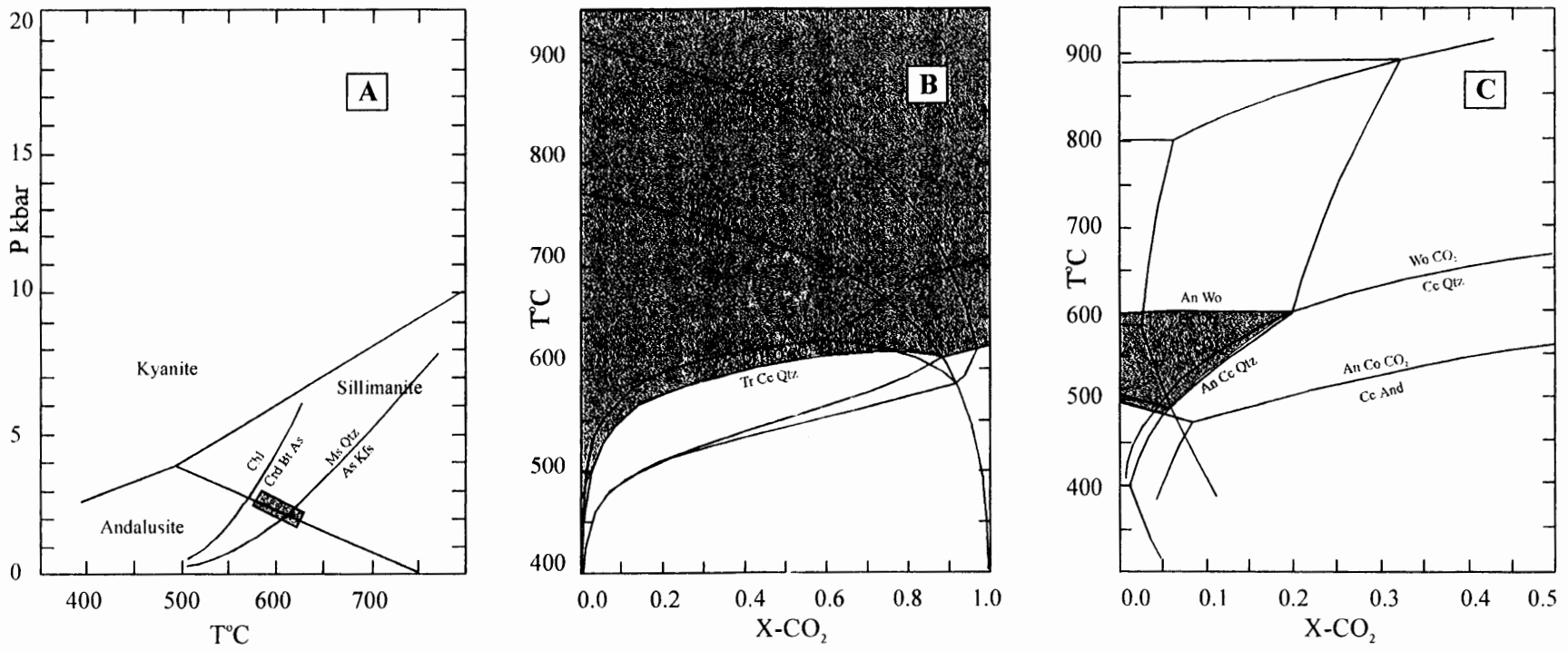

An Anorthite
And Andalusite
As Alumino silicate
Bt Biotite
Cc Calcite
Chl Chlorite
Crd Cordierite
Di Diopside
En Enstatite
Fo Fosterite
Gr Garnet
Kfs Potassium feldspar
Ms Muscovite
Qtz Quartz
Tr Tremolite
Wo Wollastonite

Figure 19. Pressure-Temperature and Temperature-XCO_2 for alumino-silicates (A) and calc-silicates (B and C). Chart A is for use with the pelitic schists, B and C are for use with calcite cemented quartzites and calc-silicates. The inferred P-T or T-XCO_2 conditions are shaded gray. Chart B is at p=5 kbar and chart C is at p=2 kbar. Charts A and B are modified after Spear (1995) and chart C is modified after Kerrick (1974).

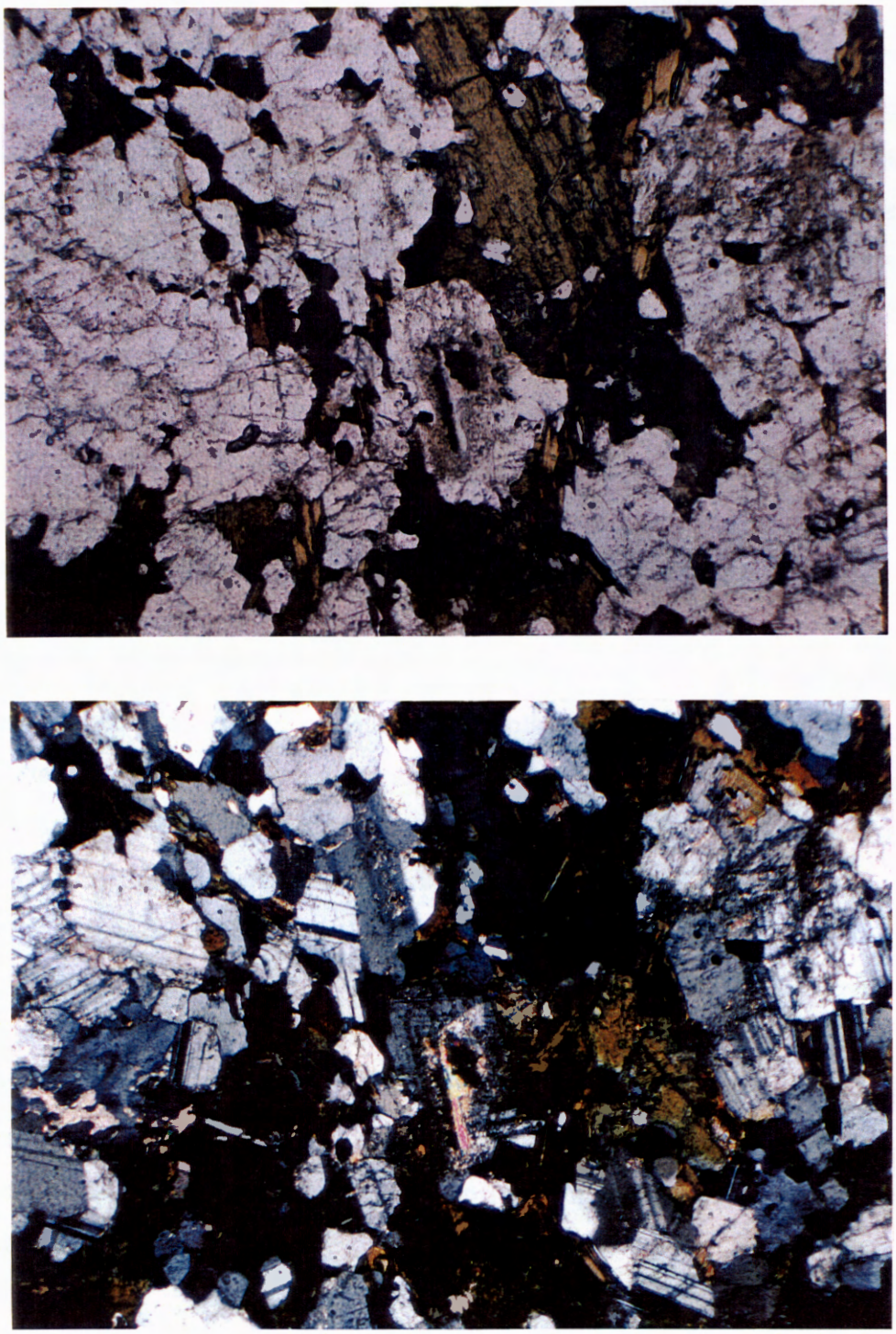

Figure 20. Photomicrographs of meta-diorite showing the original igneous zoning of a feldspar crystal and the recrystallization of quartz and feldspar grains. The upper photo was taken under plane light and the lower photo under crossed Nicols. The field of view is 3 mm wide.

igneous origin with a diorite to quartz-diorite igneous protolith. Regardless of protolith, the amphibolite rocks exhibit mineral assemblages and recrystallization indicative of amphibolite grade metamorphic P-T conditions consistent with those of domain 3. Hornblende crystals generally occur in aligned clusters that define both lineation and foliation and suggest dynamic recrystallization by grain size reduction of larger, pre-metamorphic crystals, and aligned titianite crystals also imply a solid state, metamorphic origin (e.g. criteria of Patterson, et al., 1989). Chlorite and white mica appear as static overprints of the peak metamorphic assemblage and are interpreted to be retrograde reactions.

The remainder of domain 4, the plutonic complex, is composed of granodiorite, quartz-monzonite, leucocratic two-mica garnet-bearing granite, and granite. Crosscutting field relationships and thin section examinations reveal a direct relationship among decreasing mafic content, decreasing crystal plastic deformation, and decreasing relative age of the igneous intrusions. The granodiorite shows the most pronounced foliation at outcrop scale and exhibits evidence of intrafolial folding during the injection of the equant, medium-grained quartz-monzonite (Figs. 21 and 24). While the quartz-monzonite appears undeformed in hand sample, thin section study shows pronounced dynamic recrystallization of quartz and fracturing of feldspars (Fig. 22). The granite is typically unaffected by solid state deformation, although occasional outcrops exhibit aligned orthoclase phenocrysts and mafic enclaves suggestive of magmatic flow (Fig. 23). Figure 24 shows an outcrop of the granodiorite, quartz-monzonite, and granite with the crosscutting relationships clearly evident. Two-mica granite outcrops display variable deformation ranging from the development of a mild foliation to undeformed. The only metamorphic mineral present is minor chlorite after biotite and is interpreted to be retrograde weathering.

Plutonic Complex Geochemistry

Neutron activation analysis for trace elements, rare earth elements (REE), and several major elements was performed on 12 samples from domain 4 to examine any

Figure 21. Interfolding of meta-diorite and granodiorite.

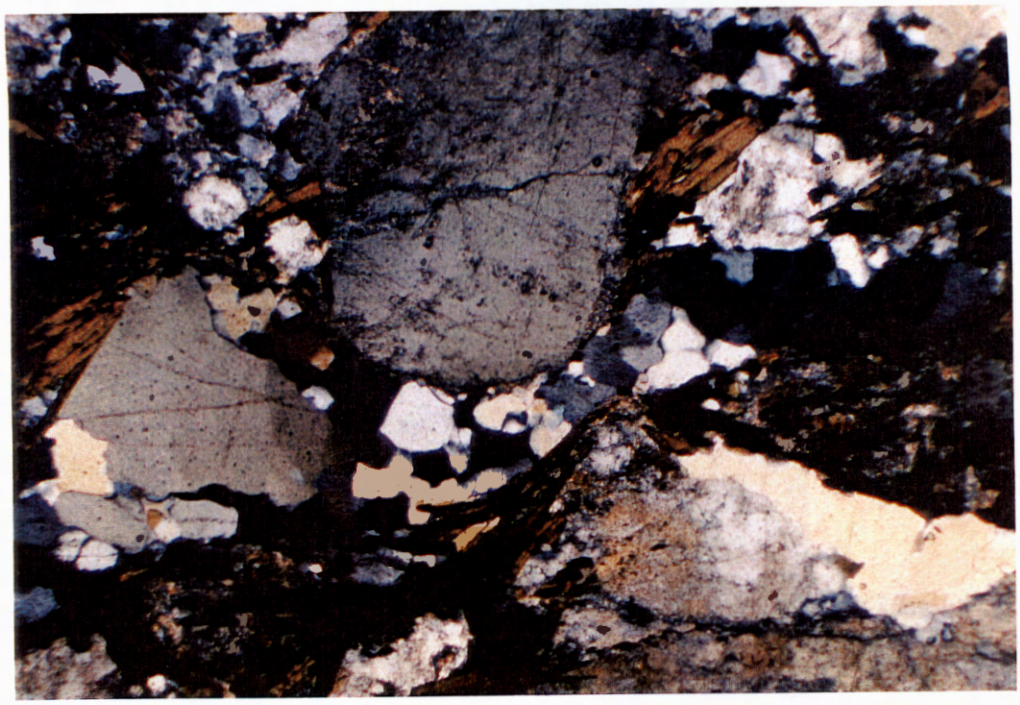

Figure 22. Photomicrograph of sample 129, a quartz monzonite, showing undulatory extinction and dynamic-recrystallization of quartz crystals. The photo is taken under crossed Nicols with a field of view of 3 mm.

Figure 23. Outcrop of aligned mafic inclusions in a granitic host. Host rock shows some alignment of magmatic crystals as well as crystal-plastic deformation.

Figure 24. Outcrop showing crosscutting relationships of plutonic rocks. To the upper right is interfolded metadiorite and quartz-diorite which is intruded by granodiorite (behind the rock hammer). Both of the above are intruded by granite.

readily apparent geochemical correlations. Samples of two groups of rocks were collected with two different objectives. First, the Silurian Hills contain exposures of the Riggs Formation, a tectonostratigraphic formation usually assigned a Paleozoic age (Kupfer, 1960; Abbott, 1971; Walker and Wardlaw, 1989; Battey, 1991; Bishop, 1994). However, in the study area the Riggs Formation is intruded by mafic sheets (amphibolite). This association is reminiscent of the Crystal Spring Formation where it is intruded by 1.1 Ga (Heaman and Grotzinger, 1992) mafic sills. Thus, samples of the diabase dikes were collected at Saratoga Springs, at the southern end of the Saratoga Hills, for comparison with amphibolite samples from within the Riggs Formation. Second, while field relationships and thin section analysis provide a relative timing and history of the plutonic complex in domain 4, the precise relationship between the igneous pods and sills found within domain 3 and the main plutonic complex of domain 4 is unclear. Thus, samples of the igneous pods and sills in domain 3 were compared with samples of the main plutonic complex to evaluate these relationships.

Figure 25 shows trace and REE abundance patterns for the samples listed in Table 2. Additionally, Figure 26 shows an XY plot of total Na_2O vs. FeO. This was done for an

TABLE 2. LITHOLOGY AND LOCATION OF TRACE AND REE SAMPLES

Sample	Hand Sample Identification	Location
99	amphibolite	within Riggs carbonates
129	quartz monzonite	pod within Riggs carbonates
131A	granodiorite	dike within Riggs carbonates
153B	quartz monzonite	pod within Kingston Peak domain 3
159	two-mica leucogranite	sheet intrusion in domain 4
162	quartz monzonite	intrusion in domain 4
166	granite	intrusion in domain 4
175A1	porphoritic granite	intrusion in domain 4
175A2	quartz monzonite	intrusion in domain 4
175A3	granodiorite	intrusion in domain 4
1131	amphibolite	within Riggs carbonates
180	amphibolite	within Riggs carbonates
SS2	diabase dike	Saratoga Spring
SS3	diabase dike	Saratoga Spring

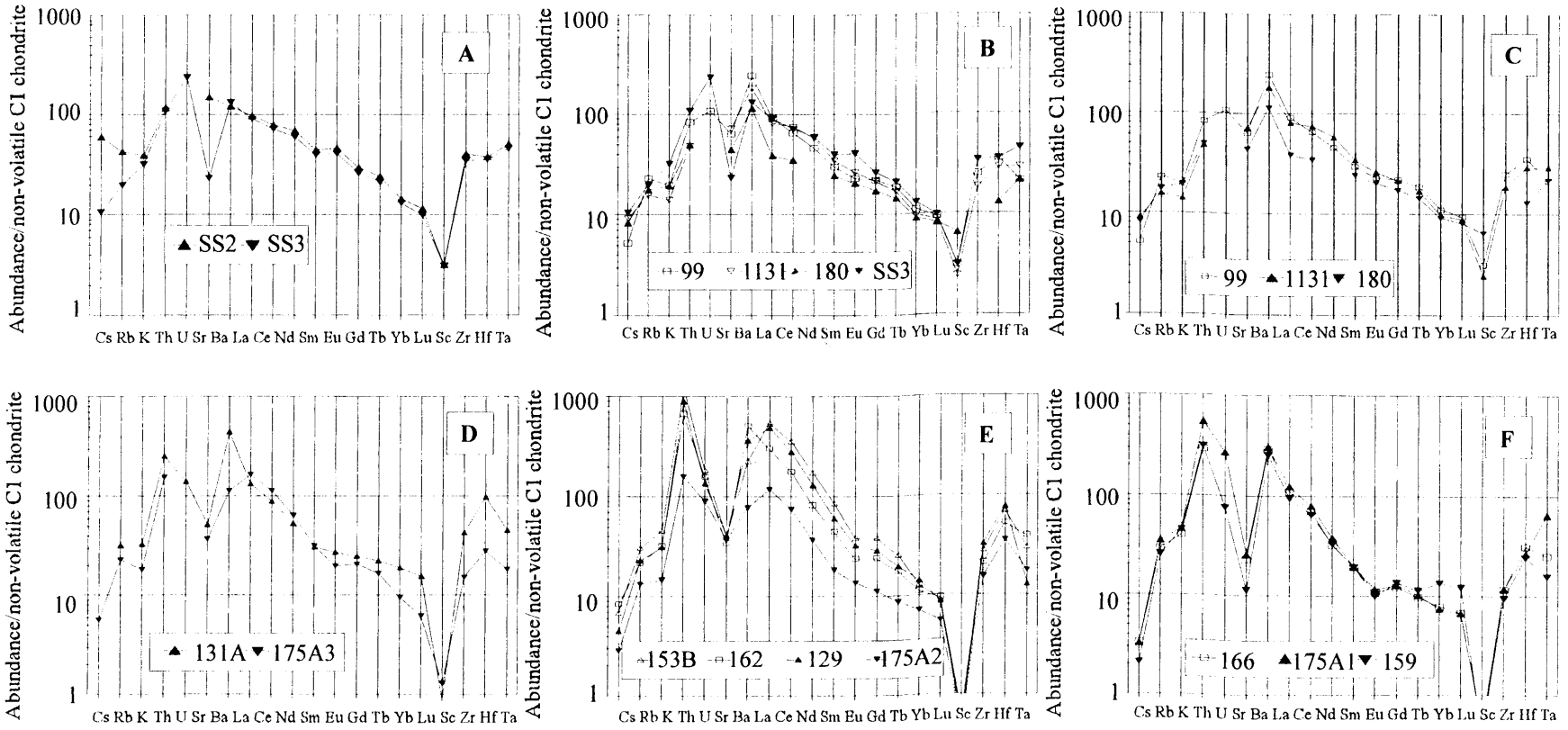

Figure 25. C1 Chondrite normalized, trace and rare earth element patterns for: A. Two samples of Proterozic Crystal Spring Formation diabase dikes from Saratoga Spring. B. Comparison of amphibolite samples from domain 3 and 4 and Proterozic diabase dike. C. Comparison of amphibolites from domain 3 and 4 only. D. Comparison of Mafic, metadiorites and quartzdiorites of domain 4. E. Comparison of intermediate igneous rocks from domain 4. F. Comparison of granitic rocks of domain 4.

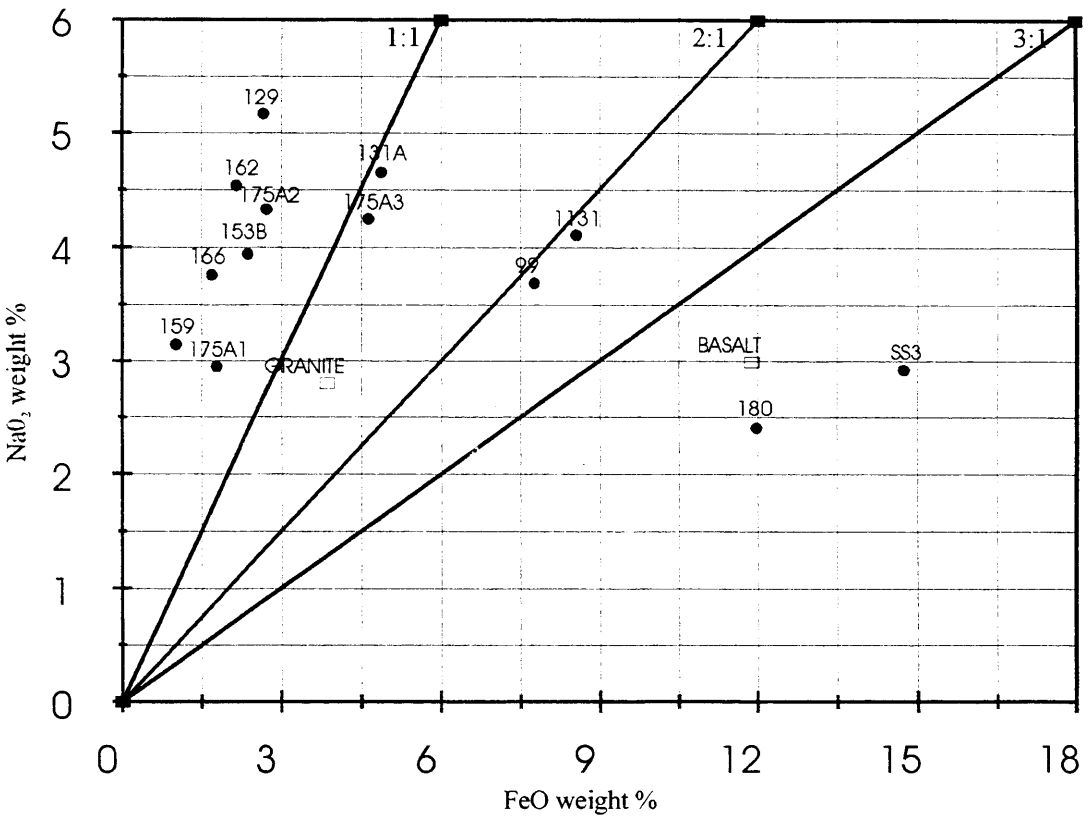

Figure 26. Ratios of Na to Fe as weight % oxides for identified samples. Granite is the GSP-1 standard prepared by the U.S.G.S. Basalt is the SRM 688 standard reference material prepared by the N.I.S.T. Diagonal lines represent 1, 2, 3:1 Fe/Na ratios.

approximate comparison of the mafic content of the samples. Also, Q and R mode factor analysis showed FeO and Na_2O to be the most significant factors differentiating geochemistry of the samples. Groupings were based on hand specimen and thin section classification, supplemented with Figure 26.

All of the amphibolites from the Riggs appear geochemically consistent with the Crystal Spring diabase dike (Fig. 25B). The Na_2O/FeO plot however, shows that only sample 180 contains sufficient iron, although Fe mobility during metamorphism could affect the Fe content of the other amphibolites. The slightly positive Eu anomaly of the Proterozoic diabase, sample SS3, with respect to the neutral Eu anomaly of sample 180 is the only discordant factor. Hammond's (1986) geochemical work on the Proterozoic diabase in the southern Death Valley region shows that both neutral and positive Eu anomalies are found throughout the region. All of the amphibolites in this study show a neutral Eu slope, in distinct contrast to the negative Eu anomalies of all the other samples. The geochemical data for the amphibolites, and sample 180 in particular, are consistent with an interpretation of Crystal Spring Formation diabase dike protolithology.

Not surprisingly, the geochemical analyses of the plutonic rocks are completely consistent with the hand sample and thin section classifications (Figs 25D-F). Taken together with field relationships, the geochemistry adds further support to an interpretation of multiple igneous injections over time, beginning with mafic magma and progressing through the felsic magmas. Based on chemistry and crystal plastic strain, the igneous pods and sills in domain 3 can be correlated with the mafic and intermediate but not the granitic magma (Fig. 25D-F). The decrease in the strain exhibited in each successive pulse is consistent with the geochemical and field relationships and is also consistent with the structural evidence for syn-tectonic plutonism discussed below.

Mesozoic Structure

The Silurian Hills contain several major, distinct, ductile structures, all of which are inferred, on the basis of published age data (DeWitt et al., 1984; Sutter, 1968; Walker and Wardlaw, 1989), to be of early-Late Cretaceous age or older. The structures are

recognized by the style of crystal plastic strain, the orientation of foliation and mineral stretching lineation, and the grade of associated metamorphism. These structural domains are coincident with the metamorphic domains discussed above.

Domain 1:

Domain 1 consists of an east-northeast striking, subvertical, homoclinal section of greenschist grade rocks ranging from Proterozoic basement through the Pahrump Group. In domain 1 rocks to the west of the study area, a south dipping slaty cleavage was found in some of the pelitic beds, indicating tight, north-vergent folding of the section (modern coordinates). This slaty cleavage was not recognized within the study area due to truncation of the section below the pelitic beds. However, in the north-central portion of the study area anticlinal folding about an axial trend of ~060° may be indicated by outcrop (see Plate 1 and Figure 27). This fold is offset by several dextral strike-slip faults which have brecciated the bedding.

While domain 1 and at least part of domain 3 are composed of the same stratigraphic formations, it must be emphasized here that the two domains exhibit completely different metamorphic grades and styles of deformation (see above). Direct contact between the two domains occurs only along brittle faults, and there are no gradations in metamorphic zones or deformational style at these contacts. Along the south-central section of domain 1 (north of Silurian Hill) is a contact with domain 2 mylonites. This contact is gradational in the sense that mylonitization clearly involves the domain 1 rocks, but while the metamorphic grade remains greenschist facies, the degree of strain increases, and the trend of foliation and lineation of the mylonites is discordant to the trend of bedding in domain 1 and concordant with the trend of foliation and lineation of domain 2.

Domain 2:

Domain 2 is dominated by a mylonite foliation, S_2, with northeast strike and dipping ~030° southeast with mineral stretching lineations, L_2, trending southwest-northeast (Fig. 28). These attitudes are uncorrected for rotation along brittle

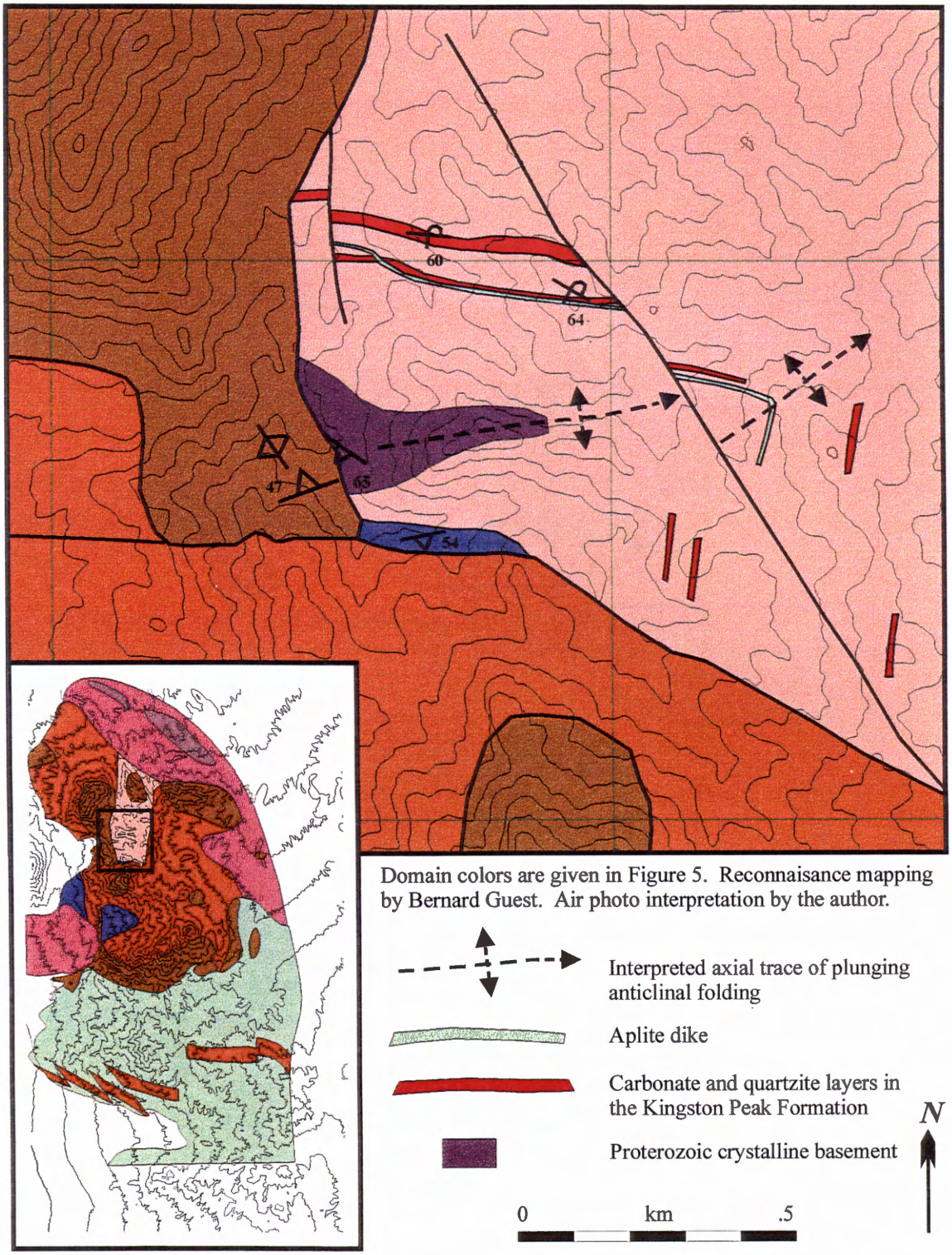

Figure 27. Detail of geologic map showing the outcrop patterns that are interpreted to represent north vergent folding structures in domain 1 rocks. Domain 1 rocks in the western part of the Silurian Hills exhibit a south dipping cleavage not mapped here. See text for details.

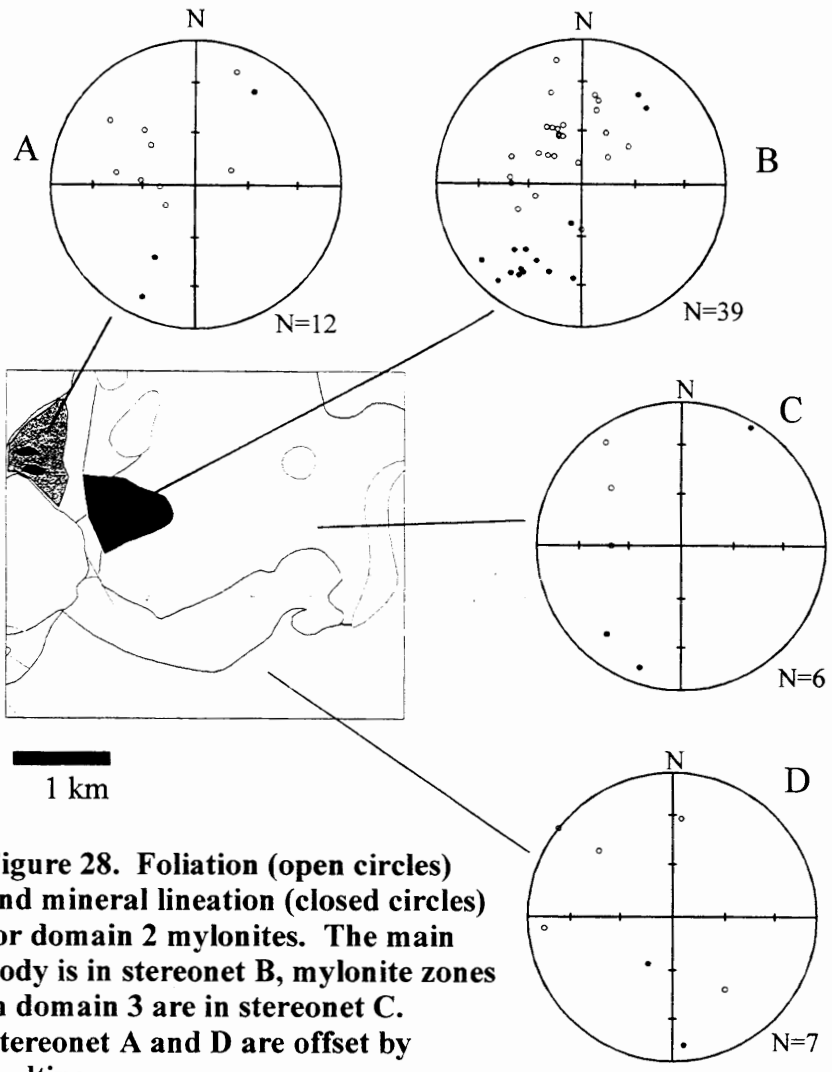

Figure 28. Foliation (open circles) and mineral lineation (closed circles) for domain 2 mylonites. The main body is in stereonet B, mylonite zones in domain 3 are in stereonet C. Stereonet A and D are offset by faulting.

faults, include variation due to the kink folding described above, and include attitudes from the mylonites in domains 1, 3, and 4. The mylonites in domain 4 are exposed in blocks of amphibolite bounded entirely by complex, brittle faults. The attitudes of both the amphibolites and mylonites within these blocks are discordant to S_1 - L_1 attitudes of the surrounding more intact rock. While there is insufficient fault kinematic data to determine the original orientation of these blocks, stereonet rotation of the host amphibolite S_1 - L_1 attitudes to concordance with the surrounding, more intact attitudes, carries the S_2 - L_2 attitudes into alignment with the main body of domain 2.

Thin-section analysis of oriented samples reveals numerous shear-sense indicators. These include mica fish, S-C' fabrics, delta and sigma rotation tails, and grain shape fabrics (Fig. 29). Table 3 lists the sample numbers and the interpreted direction of upper plate motion, which is uniformly top to the northeast.

TABLE 3. DOMAIN 2 MYLONITE SHEAR SENSE INDICATORS

Sample	Type of Indicator[1]	Direction of Movement
58	shear band cleavage	top to NE, up dip
287	sigma structures	top to NE, up dip
312	S-C' fabrics, sigma structures	top to NE, up dip
222	mica fish, sigma structures	top to NE, up dip
58-2	mica fish, sigma structures	top to NE, up dip

1. Passchier and Trouw (1996)

Domain 3:

Domain 3 contains the highest metamorphic grade in the study area and is characterized by a single prominent foliation, S_1, and mineral lineation, L_1. This D_1 fabric is the product of complete recrystallization of the rock with foliation and lineation defined by both dimensional and crystallographic preferred orientation of minerals. The foliation is layer parallel except in mesoscopic fold cores and locally along amphibolite contacts (see below). Figure 30 summarizes orientations for S_1 and L_1. Domain 3 rocks crop out within an area of approximately 20 km^2 and S_1 and L_1 have been cut by igneous intrusions and later brittle deformation. From west to east across the area, the strike of S_1 varies

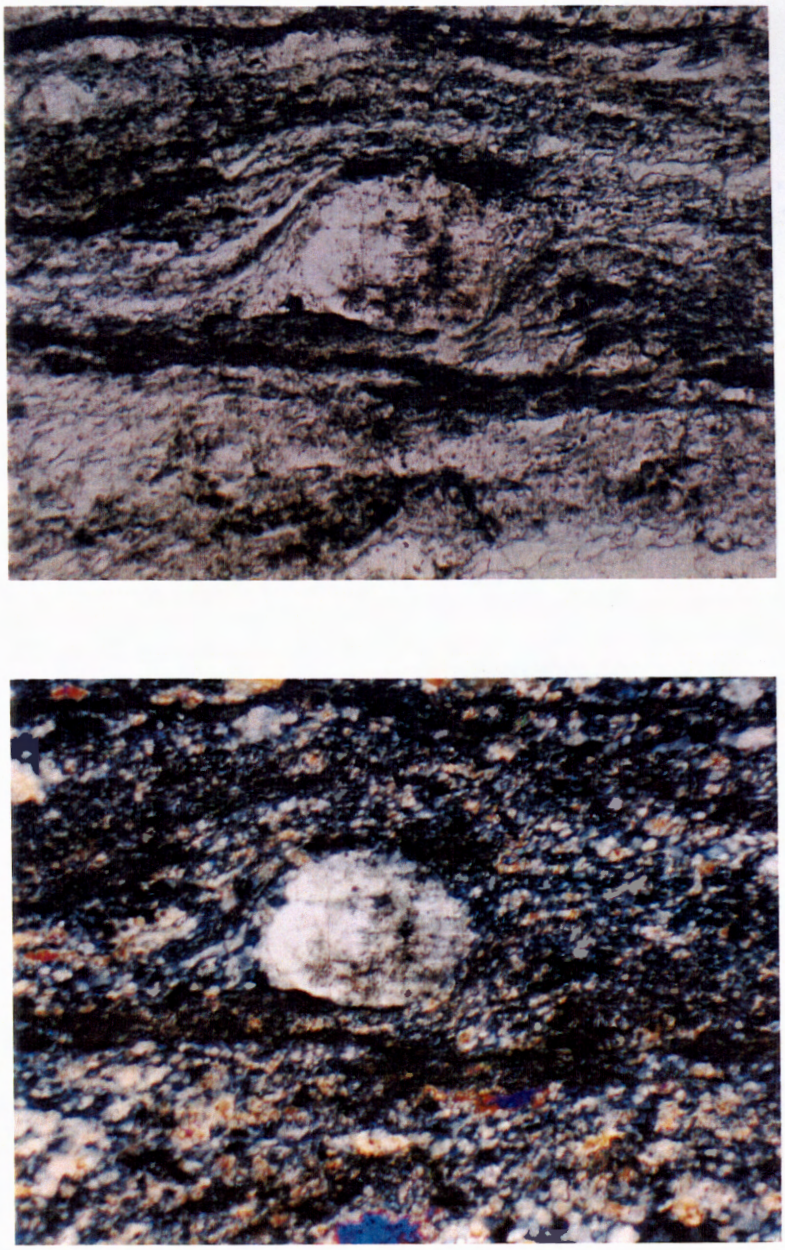

Figure 29. Sigma tails of a rotated feldspar grain showing a dextral shear sense. Sample 312, a domain 2 mylonite. The upper photomicrograph was taken under plane light, lower photograph under crossed Nicols. The grain is .5 mm across.

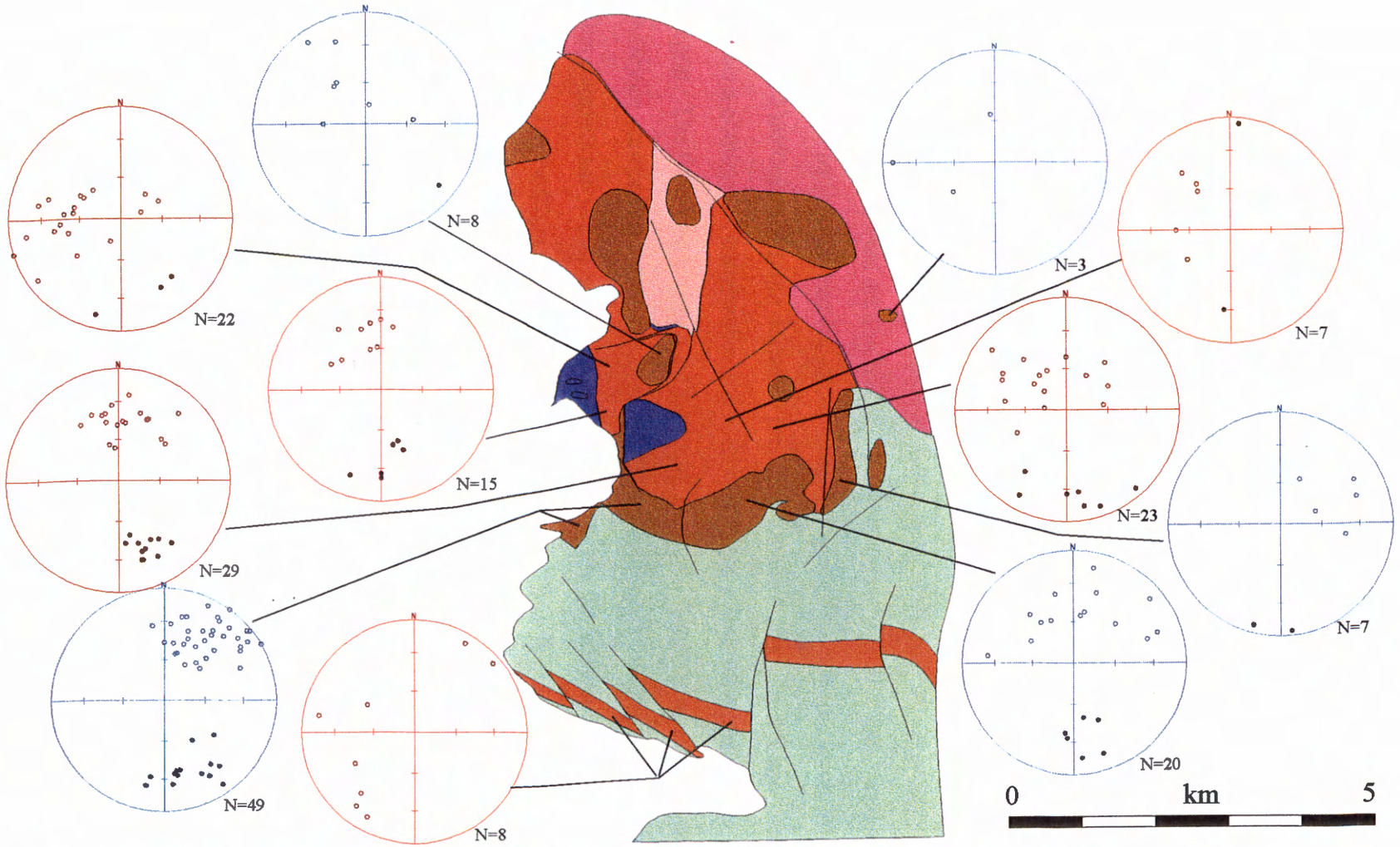

Figure 30. Stereonet summaries of mineral lineation (filled circles) and poles to foliation S_1 (open circles) for domain 3 rocks. The red nets are Kingston Peak Formation data and the blue nets are Riggs Formation data. All stereonets are equal area (Schmidt). Formation colors are the same as Figure 15.

from west-northwest to east-northeast. Foliation dips south and L_1 plunges to the south-southeast throughout the study area. These attitude variations across the study area are the product of the broad Cenozoic arching (see above).

It is important to note the concordance of S_1 - L_1 and the parallelism of foliation and lithologic layering in the two formations (Kingston Peak and Riggs) that comprise domain 3. Previous workers have interpreted the contact between the Kingston Peak and Riggs formations as a brittle (Abbott, 1971; Kupfer, 1960; Walker and Wardlaw, 1989) or combination of brittle and ductile (Bishop, 1994) thrust fault. While portions of this contact are clearly brittle faults, at those locations D_1 fabrics between the two formations are discordant, and the faults are part of the complex Cenozoic brittle faulting patterns (see above). The critical section is along the western portion of Citadel Ridge, a hogback ridge formed by the resistant Riggs carbonates (Fig. 31). A traverse south from the domain 2 mylonites through domain 3 and into domain 4 amphibolites and plutonic rocks reveals a continuous, metamorphosed section without a fault break within the structural section. The transition between the Kingston Peak and Riggs formations is welded, with D_1 fabrics concordant across the contact, and no evidence of fault gouge or brecciation. This suggests the youngest Mesozoic contact between the Kingston Peak and Riggs formations to be the result of high ductile strain, not brittle faulting. This does not preclude an older, brittle fault juxtaposition of the Kingston Peak Formation and a package of proto-Riggs rocks, but all trace of such an event has been obliterated by D_1 strain.

The Kingston Peak Formation contains several distinctive diamictite and quartz cobble conglomerate units which allow clear recognition of the formation and, in these ductilely deformed rocks, provide primary clastic material to measure and interpret the present state of finite strain. Table 4 summarizes the stretched pebble data obtained at four locations within the Kingston Peak Formation in domain 3, and Figure 32 is a Flinn diagram from the data. These data plot just within the constrictional field and, within error, along a line of constant slope coincident with plane strain. The differing magnitudes of shear strain imply heterogeneous strain. Assuming simple shear, the average γ of 1.9 integrated over the ~750 m structural thickness of domain 3 produces a minimum

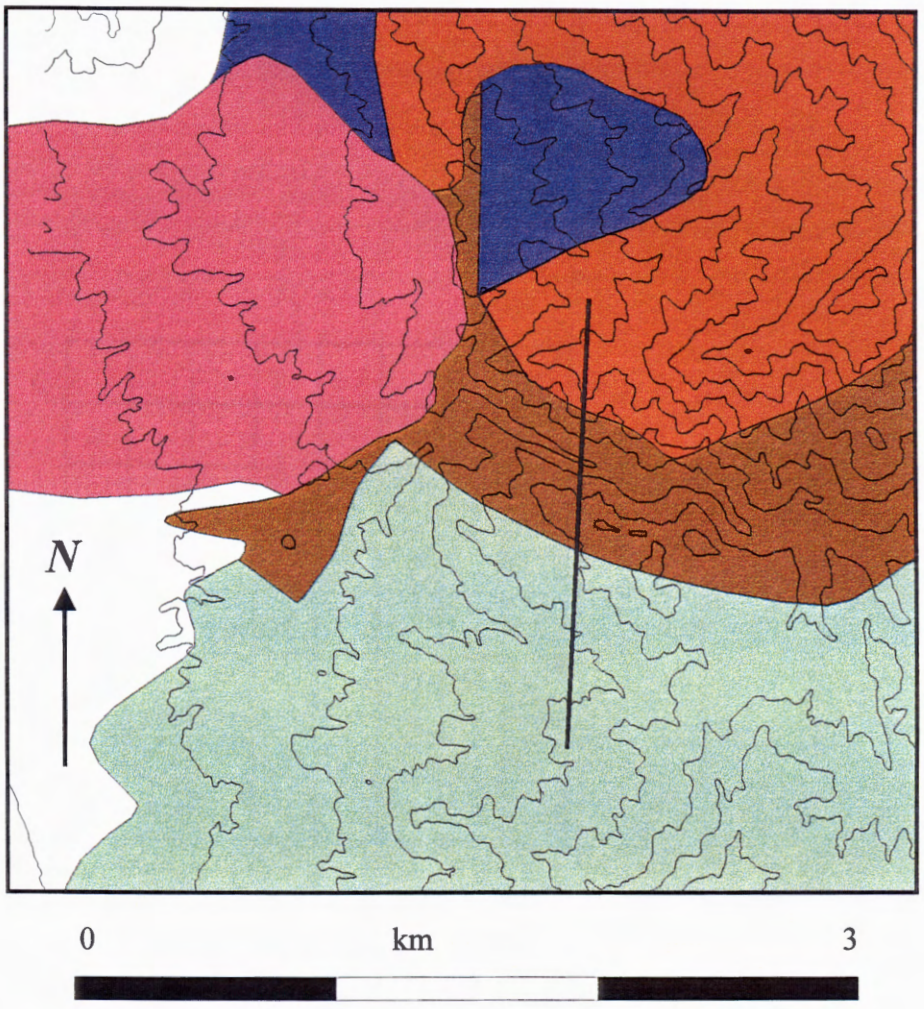

Figure 31. Location of intact N-S transect across the Kingston Peak and Riggs Formations of domain 3 and the plutonic complex, domain 4. Domain colors are given in Figure 5.

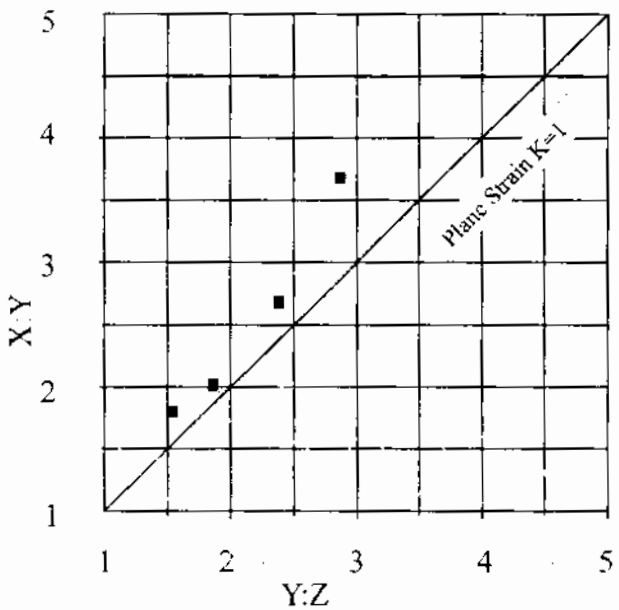

Figure 32. Flinn diagram of strain data from Kingston Peak Formation stretched pebbles.

displacement of 1.4 km across the shear zone (Ramsay and Huber, 1983). However, two factors suggest that the true displacement is much greater. First, higher amounts of strain

TABLE 4. DOMAIN 3 STRETCHED PEBBLE STRAIN DATA[1]

Sample	X:Z	Y:Z	X:Y	γ
155	3.76 (n=7)	1.86 (n=7)	2.02 (n=7)	1.4
238	6.40 (n=35)	2.38 (n=32)	2.69 (cal)[2]	2.2
298	10.54 (n=16)	2.87 (n=24)	3.68 (cal)[2]	2.9
TER[3]	2.78 (n=23)	1.54 (n=27)	1.80 (cal)[2]	1.1

1. Principle strain estimates made by measuring ellipticities on field exposures of joint faces perpendicular to L (Y-Z section) and parallel to L and perpendicular to foliation (X-Z section)
2. X:Y ratio calculated from harmonic means of measured X:Z and Y:Z sections
3. Data collected by Terry Pavlis

could be accumulated in the lower viscosity carbonate and pelitic rocks. Second, the full structural thickness of domain 3 is unknown due to the later mylonitic shearing of domain 2, and in domain 4 the injection of the plutonic complex obscures the original geometry of the zone.

Table 5 summarizes the thin section analysis of oriented samples for shear-sense

TABLE 5. DOMAIN 3 SHEAR SENSE INDICATORS

Sample	Rock Type	Type of Indicator[1]	Movement Direction
43	quartz-mica-schist	shear band cleavage	top to n, up dip
79D	quartzite	grain shape fabric	top to s, down dip
79E	quartzite	grain shape fabric	top to n, up dip
107	quartzite	mica fish	top to s, down dip
110	pelitic schist	shear band cleavage	top to n, up dip
154	quartzite clast	----	ambiguous
155A	granitic clast	----	ambiguous
155C	quartzite	grain shape fabric	top to n, up dip
170B	quartzite	lattice preferred orientation	top to n, up dip
299	quartz-mica-schist	----	ambiguous

1. Passchier and Trouw (1996)

indicators. Unlike the domain 2 mylonites, several samples reveal no clear kinematic

indicators. Those samples that do show shear-sense indicators are bipolar, with the majority indicating top to the north-northwest. This diversity of kinematic indicators is not consistent with the simple-shear plane-strain discussed above and suggests the rocks were either subjected to pure shear or "sub-simple general shear" in the sense of Simpson and De Paor (1993).

Domain 4:

Figure 33 summarizes the foliation and mineral lineation attitudes for the amphibolites and igneous rocks of domain 4. As discussed above, the plutonic complex consists of amphibolites (some possibly metasedimentary rocks, but most metadiorites) with a strong LS tectonite fabric and a suite of discrete igneous intrusive pulses showing a correlation of decreasing mafic content, decreasing post-emplacement ductile deformation, and decreasing relative age. These rocks crop out over ~20 km^2 of the study area and have locally been subject to considerable later, brittle disruption.

The most intact section of the study area is a southern extension of the traverse discussed in domain 3 (Fig. 31). Figure 34 compares the foliation and mineral lineation stereonet plots of the domain 3 and 4 rocks of this section. Taking the broad Cenozoic arching into account, the plots are concordant. Due to the similarity of metamorphic grade, and the coincidence of the foliation and lineation attitudes of domains 3 and 4, the solid state fabric of domain 4 is correlated with D_1. Although many of the quartz monzonites and granites do not appear foliated in hand sample (in both the plutonic complex and pods and sills in domain 3), these rocks show microscopic evidence of quartz recrystallization around feldspar grain boundaries, fracturing of feldspar grains, and occasional weak development of S-C' fabrics by the alignment of micas (Fig. 35). The leucocratic granites that are unaffected by solid state deformation occasionally exhibit alignment of both euhedral feldspar grains and mafic enclaves (Fig. 23) that are concordant with D_1 fabrics, although this could be a coincidence of magmatic flow alignment. Finally, the large and small screens of domain 3 rocks exposed as xenoliths in the plutonic complex (Fig. 36) exhibit both external alignment of the entire xenolith and

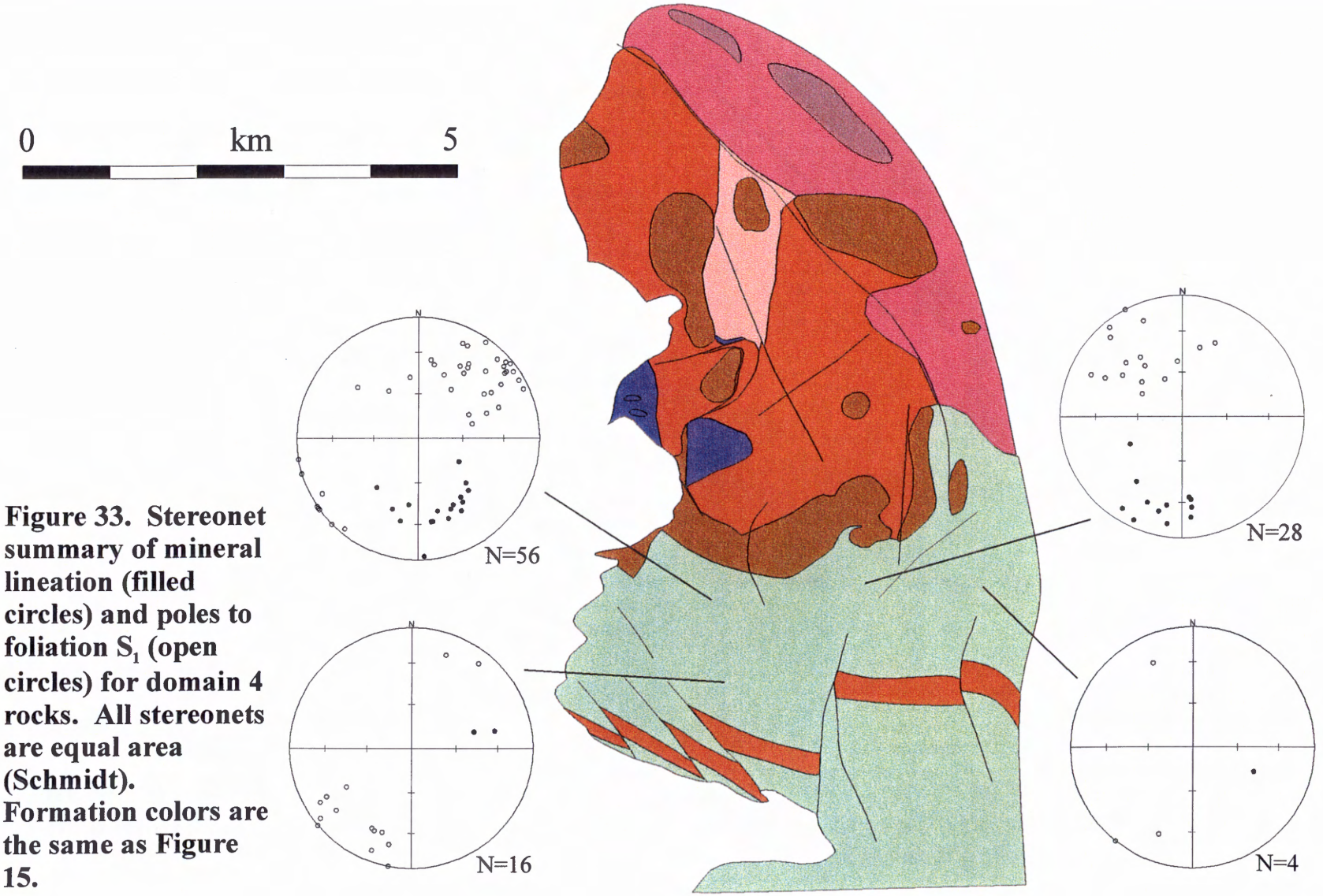

Figure 33. Stereonet summary of mineral lineation (filled circles) and poles to foliation S_1 (open circles) for domain 4 rocks. All stereonets are equal area (Schmidt). Formation colors are the same as Figure 15.

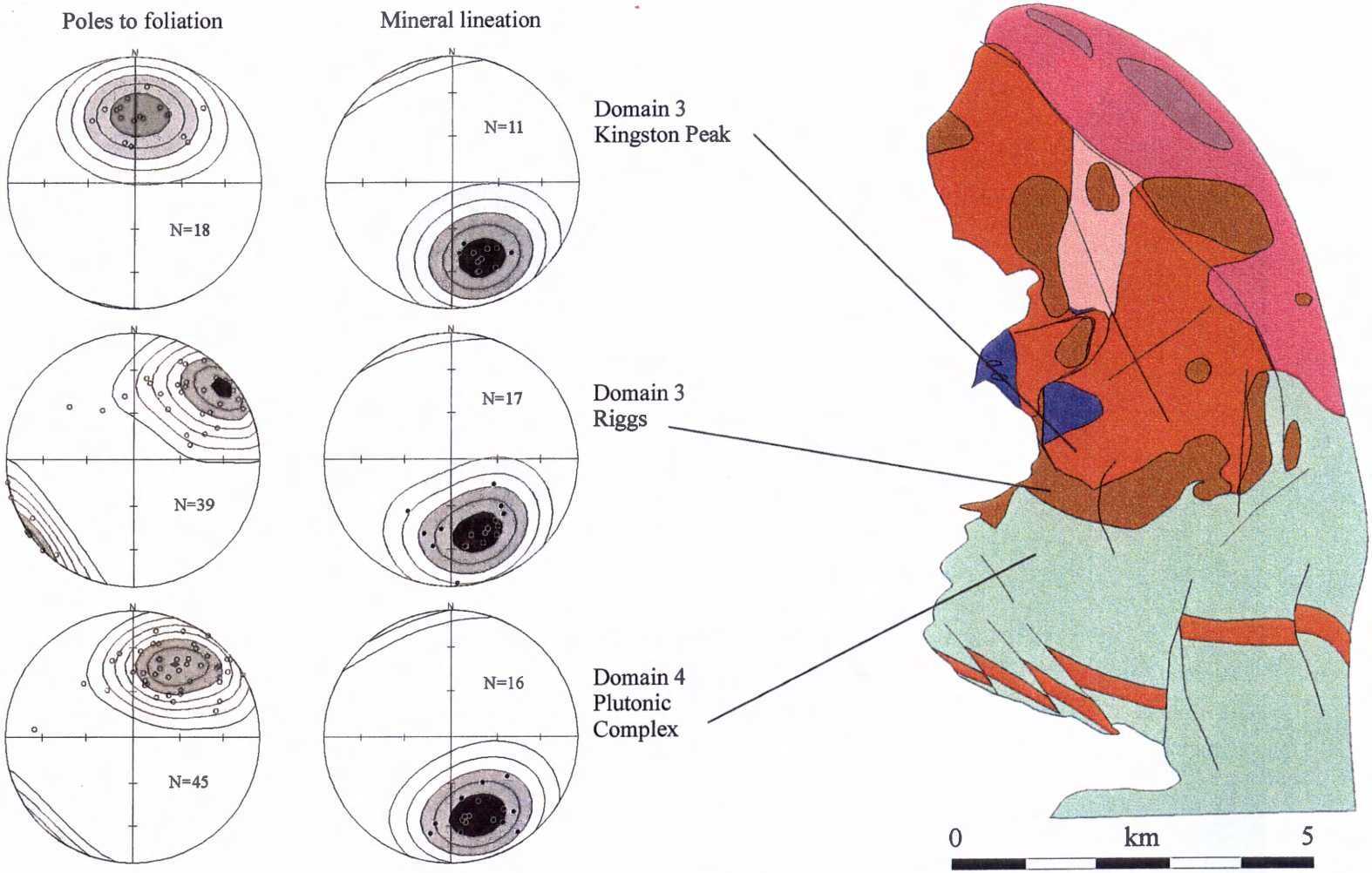

Figure 34. Stereonet summaries comparing poles to S_1 foliation (open circles on left) and mineral stretching lineation (closed circles on right) of domain 3 Kingston Peak and Riggs with the domain 4 plutonic complex. All stereonets are equal area (Schmidt). Formation colors are the same as Figure 15.

Figure 35. Photomicrograph of granitic sample 175B showing undulatory extinction in some large quartz crystals and dynamic recrystallization of quartz along feldspar-quartz grain boundaries. The field of view is 3 mm wide, under crossed Nicols.

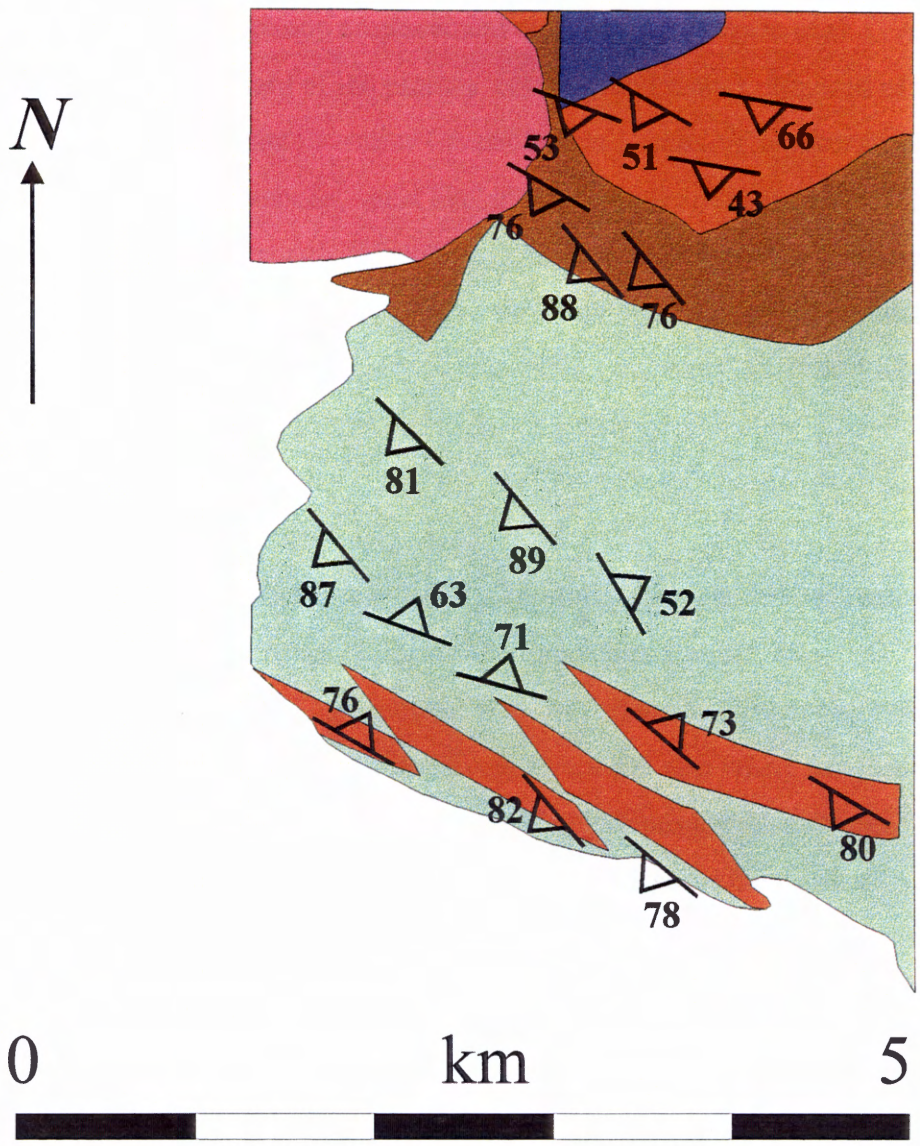

Figure 36. Foliation of the main body of domains 3, 4, and the screens of domain 3 in the southern part of the plutonic complex. The internal foliation of the screens is concordant with the foliation of both the main body of domain 3 and the plutonic complex (domain 4). Additionally, the external orientation of the screens is concordant with the trends of both the main body of domain 3 and the plutonic complex. The domain colors are given in Figure 5.

internal foliation subparallel with D_1 fabrics. Together, these observations represent all of the major criteria for syntectonic pluton emplacement outlined by Patterson et al. (1989).

Figure 37 shows an air photo of the plutonic complex and a reconstruction of the air photo removing movement along the major Cenozoic brittle faults. The reconstruction reveals a complex of continuous, tabular, sheet like, intrusive bodies, each at least .5 km thick and up to 5 km long. The strongly foliated mafic bodies are internally concordant with S_1 - L_1 and are separated and intruded by felsic plutons along contacts subparallel with S_1. The unfoliated sheets trend parallel to S_1 and exhibit magmatic alignment of euhedral crystals and mafic enclaves subparallel to S_1.

Evidence for older deformation, superposed folds:

Complex, type 2 (Ramsay and Huber, 1987), intrafolial fold interference patterns were observed in Riggs carbonate rocks of domain 3. Exposures are rare, two-dimensional, and limited to the flash-flood scoured walls of ephemeral stream channels (Fig. 38). The patterns are visible in some calc-silicate layers and also where penetrative mineral staining reveals an internal structure of the marble. It is possible that striped penetrative staining patterns visible on some marble layers may also be the result of complex intrafolial interference patterns. The deformation represented by these patterns was not investigated, because of insufficient 3-D control, but could be the result of either a pre-D_1 deformation history or one progressive D_1 event.

Possible large scale structure, a Mesozoic nappe?

A macroscopic north-northeast vergent, recumbent anticline, is suggested by comparison of outcrop patterns of metasedimentary and crystalline basement rocks across the southern part of the study area with similar rocks 2 km south in the Silver Lake Talc Mine area. In the Silver Lake Talc Mine area, mapping by Wright (1954), DeWitt (1980), and reconnaissance for this study reveals lithologies, metamorphic grades, and foliation and lineation attitudes similar to those found in domains 3 and 4. However, the lithologic sequence in outcrop is reversed in the Silver Lake Talc Mine area relative to domains 3 and 4. The structure is best seen in cross sectional view (Fig. 39). From north to south

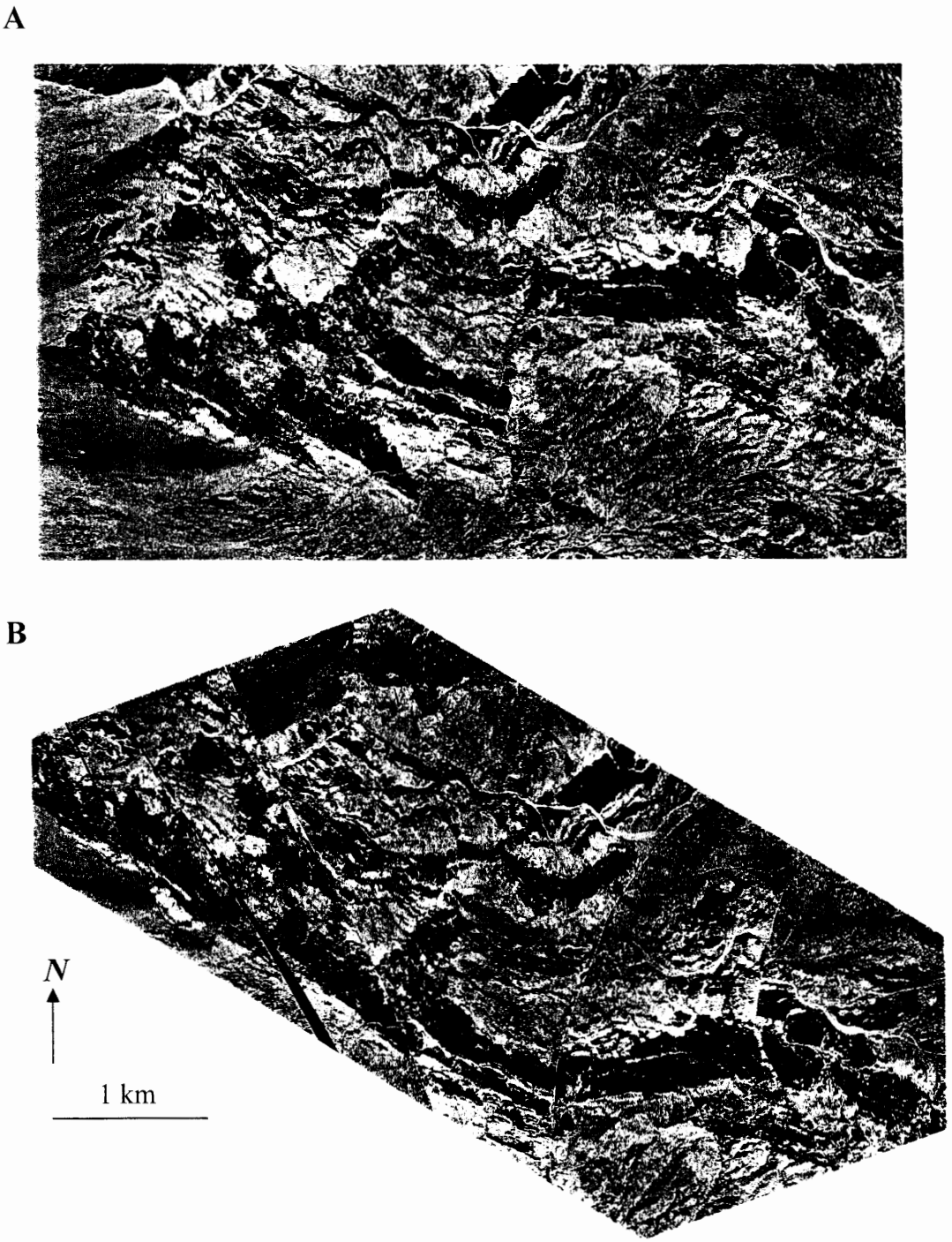

Figure 37. Air photos of domain 4 plutonic complex. A. Present day distribution of rocks appears to be a randoma distribution of stocks, sills, and dikes. B. With major Cenozoic strike-slip faults removed, the intrusions are more sheeted in appearance.

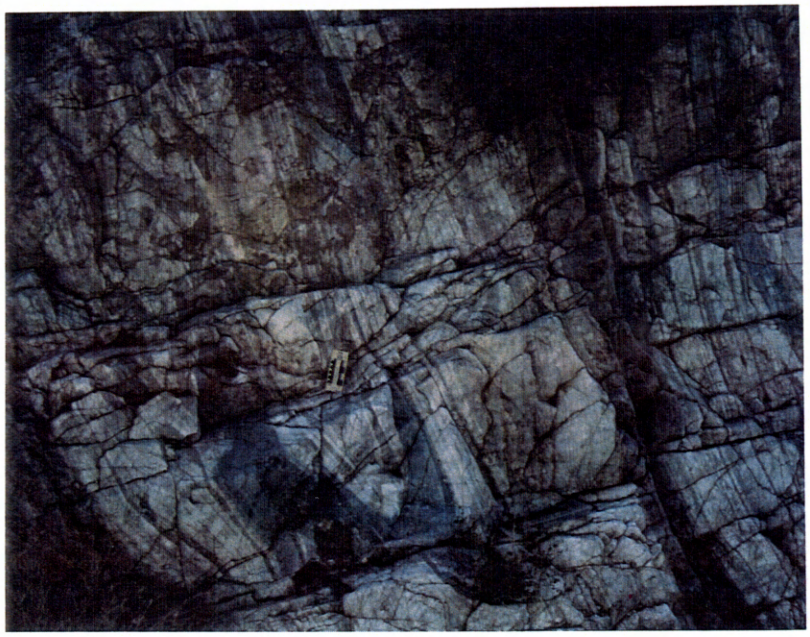

Figure 38. Type 2 interference fold pattern. Exposed on a scoured wall of Owl canyon, the interference pattern is in the primary S_1 foliation of the Riggs Formation carbonates.

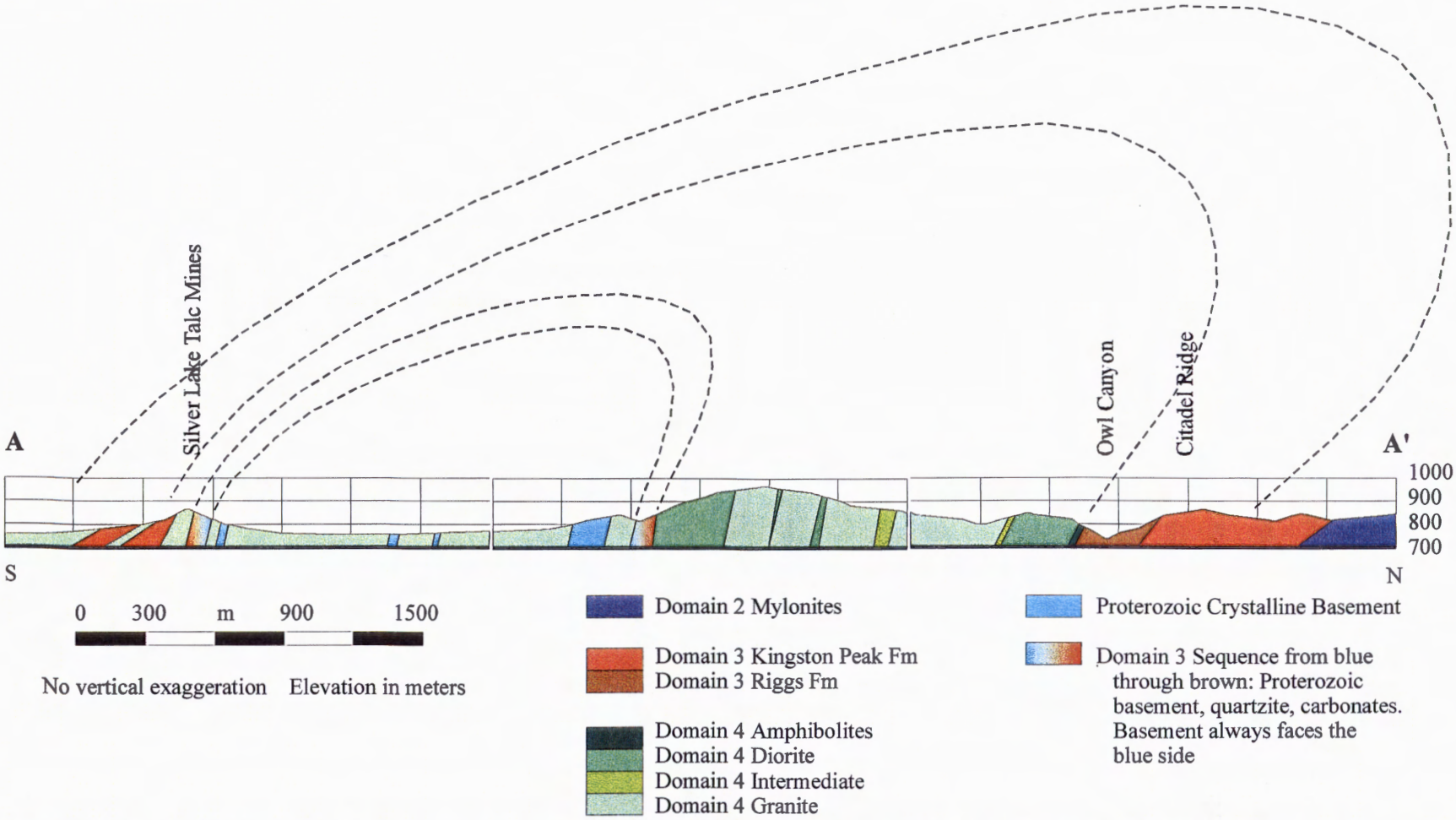

Figure 39. Diagramatic N-S structure section from domain 2 through the Silver Lake Talc Mine area. The interpreted north vergent antiform does not involve the domain 4 rocks. The domain 4 rocks are inferred to intrude syn- or post-tectonically with the deformation that produced the antiform in the domain 3 rocks. The domain 2 mylonites are post-domain 4 intrusion and therefore also not involved (see text).

across domains 3 and 4 the lithologic sequence is carbonates, quartzites, Proterozoic basement, and the plutonic complex. In the Silver Lake Talc Mine area the sequence is the plutonic complex, Proterozoic basement, quartzites and the carbonates. Cenozoic faulting and displacement of the Silver Lake Talc Mines and the possible correlation of the Riggs Formation with Pahrump Group rocks (see below) make this interpretation speculative. However, it would be consistent with the mirrored distribution of rock types and either pre-D_1 deformation or one progressive D_1 event (see above).

DISCUSSION

Vertical Axis Rotation

Complex Cenozoic brittle faulting overprints all other structures in the Silurian Hills and must therefore be interpreted before the older structures can be reconstructed and analyzed. Models of vertical axis rotation for the Mojave Desert and Death Valley regions have been developed to explain paleomagnetic data (e.g., Ross et al., 1989; Holm et al., 1993), the distribution and orientation of strike-slip faults (e.g., Dokka and Travis, 1990; Schermer et al., 1996; Serpa and Pavlis, 1996), slip rate discrepancies between the Pacific and North American plates (Dickinson and Wernicke, 1997), and the apparent clockwise rotation of the Independence Dike Swarm (Schermer et al., 1996). While differing in detail and implication, the models agree on basic descriptive mechanisms that produce vertical axis rotation. In the general case, adjacent crustal blocks are rotated, like dominos, between subparallel strike-slip fault zones (Fig. 40). The crustal blocks rotate within the active shear boundaries and passive stike-slip faults develop with an opposite sense of slip to that of the active faults between the adjacent blocks. Dextral active faults induce clockwise rotation and sinistral passive faults; sinistral active faults induce counterclockwise rotation and dextral passive faults. Features already present on the blocks, such as dikes, paleomagnetic declinations, or preexisting structures, are rotated

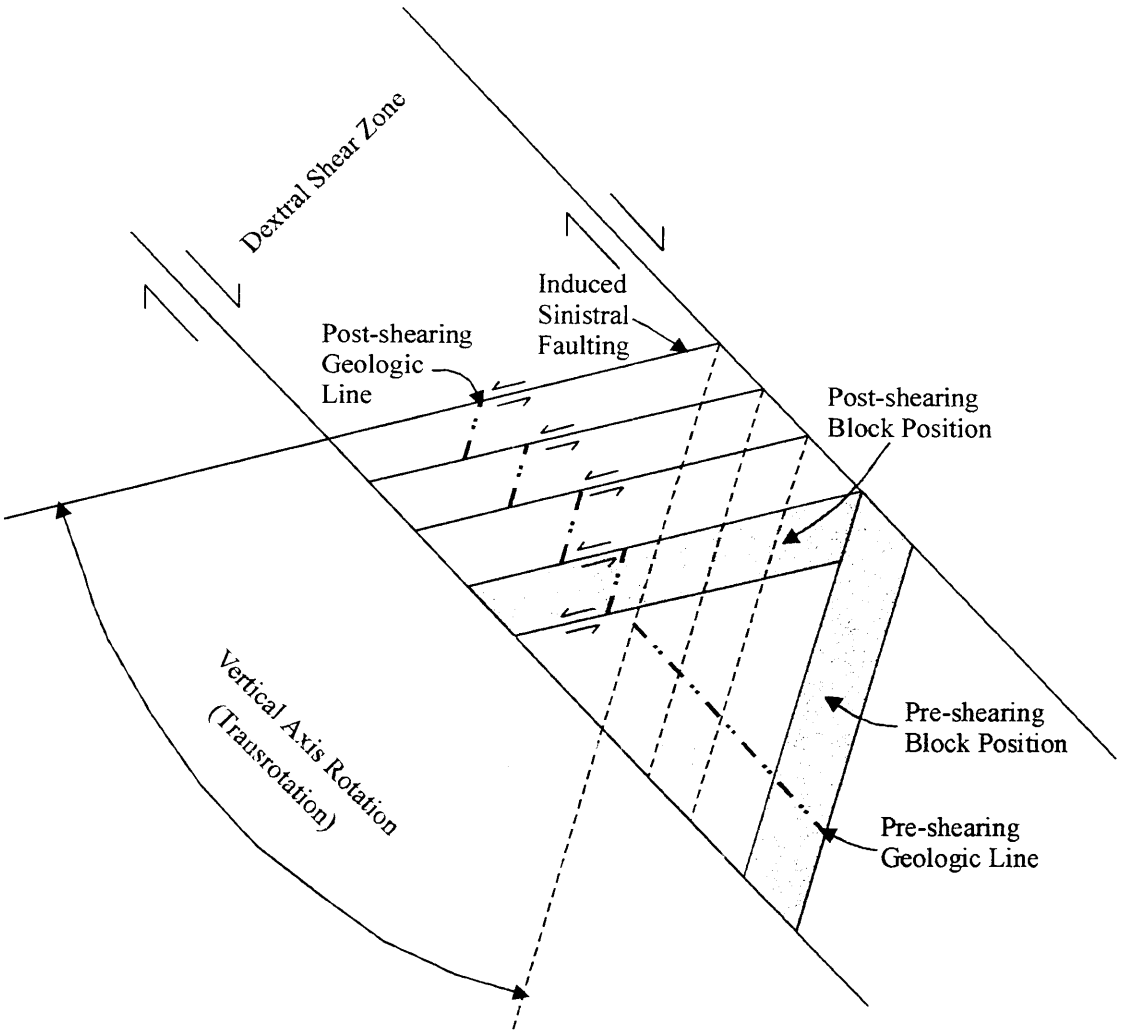

Figure 40. Vertical axis rotation (transrotation) within a dextral shear zone. Pre-shearing positions of crustal blocks and a generic geologic line are shown, along with post-shearing positions of both features. The geologic line is segmented by the induced sinistral faults as well as rotated along with the crustal blocks. Modified after Dickinson 1996.

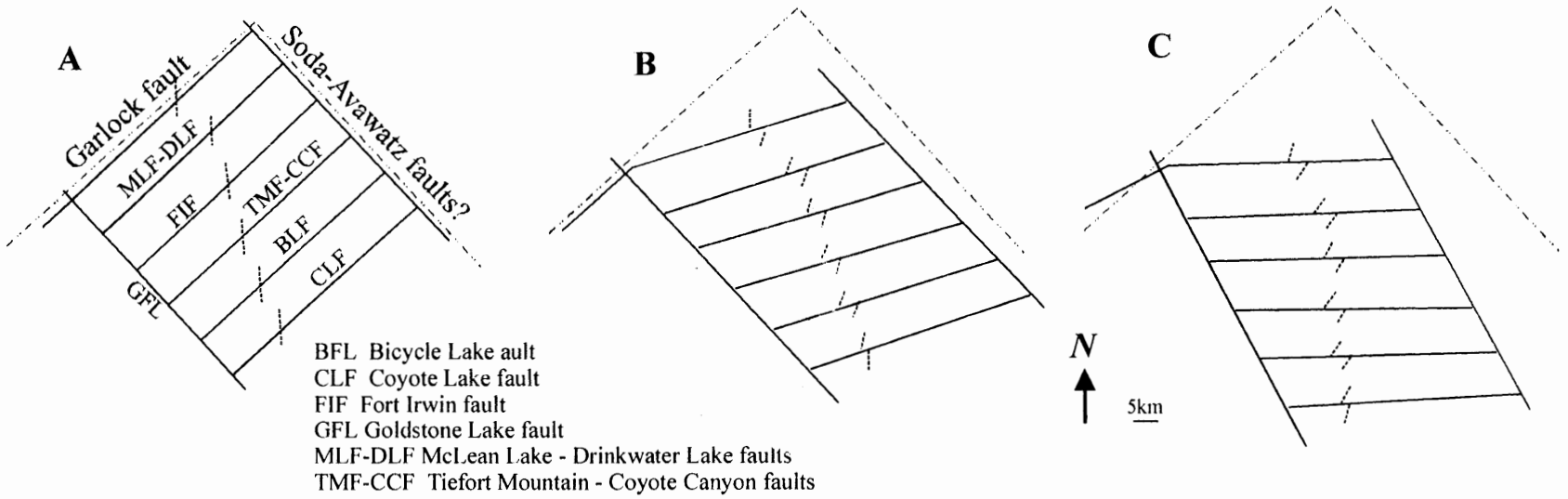

Figure 41. Bending of the Garlock fault as the result of transrotation. A. Before deformation. B. Internal transrotation between the Soda - Avawatz fault and Goldstone Lake fault produces bending of the Garlock, initiation of sinistral faulting within the fault bounded block, and vertical axis rotation of the individual blocks. C. External rotation of the entire block produces additional vertical axis rotation without increasing offset along sinistral faults. Rotation may not have occured in two distinct stages. Modified after Schermer et al. (1996).

along with the block. The passive, opposite sense faults between blocks are rotated, or deflected, in the same sense of direction as the adjacent blocks (Fig. 41).

The details are controversial, but it is generally accepted that northwest trending, dextral shear zones have induced both clockwise vertical axis rotation of blocks and sinistral faulting between blocks of the northeastern Mojave Desert and Death Valley regions. These rotations are also interpreted to contribute to the clockwise deflection of the eastern end of the Garlock fault (Schermer et al., 1996; Serpa and Pavlis, 1996; Fig. 41). In these regions, the descriptive mechanisms have been applied to intact blocks 5 to 10 km wide and several 10's of km long. The recognition and quantification of the effects of vertical axis rotational on smaller blocks, such as those exposed in the Silurian Hills, is not clear. The Silurian Hills contain conjugate strike-slip and normal fault sets, BF4, suggesting distributed dextral shear, but not necessarily implying vertical axis rotation. The older set of northwest trending sinistral faults, BF2, are overprinted by BF4 faulting and do not correlate with regional, northeast to east-west, sinistral fault trends.

The BF2 faults could represent evidence for two models of vertical axis rotation. First, they could be splays of a northeast to east-west trending sinistral fault that were subsequently rotated between transcurrent faults. This would imply at least 60° of rotation (either clockwise in a dextral system or counterclockwise in a sinistral system) of the BF2 faults and the intact Silurian Hills from an original east-west orientation to the present north-northwest orientation. Second, the faults are induced between blocks rotated within a dextral zone of distributed shear.

Model 1 is unlikely for two reasons. First, the Silurian Hills are permeated by strike-slip and normal faults, implying distributed shear throughout the block, not rotation of the entire block. Second, the rotation of an intact Silurian Hills requires significant east and west bounding dextral structures, which have yet to be found. To the west Rodosta (1997) and Hartman (1997) found no evidence of through-going dextral structures, and to the east, dextral faulting is distributed (e.g., McMackin, 1992; Fowler, et al., 1995).

Model 2, however, is consistent with several observations. First, only ~30° of vertical axis rotation is required to restore displacement along the BF2 faults. This amount was determined by rotating the fault bounded blocks both empirically and using

Dickinson's (1996) formula. This rotation is accommodated over a much smaller area, and therefore does not require large bounding structures. Second, the angular relationship of the sinistral faults to northwest trending dextral shearing implies the rotations occuried past a line perpendicular to the shear zone in restored coordinates (Fig. 42). This type of rotation is most indicative of a transpressional shear zone (Luyendyk, 1991; Dickinson, 1996). North of the study area, along the north part of the Silurian Hills, Tertiary sediments appear to be concordant with underlying bedrock and are uplifted by horizontal-axis rotation of the underlying bedrock through normal faulting effects. In most cases, however, the structural elevation of bedrock relative to Tertiary exposures could not be the result of normal faulting (see above), but another mechanism. A transpressive component of shear provides the mechanism and is regionally recognized along the Garlock and southern Death Valley fault zone intersection (Butler et al., 1988; Willis, 1993). Third, paleomagnetic studies in the Shadow Basin east of the study area indicate clockwise vertical axis rotations of less than 60° (Friedmann et al., 1996). Finally, 30° of rotation is consistent with several interpretations of the amount of vertical axis rotation in the northeastern Mojave Desert and Death Valley regions (Schermer et al., 1996; Serpa and Pavlis, 1996). The Silurian Hills appear structurally cut off from the northeastern Mojave and southern Death Valley regions, but concordance with trends in those regions suggests a stronger structural affinity than previously assumed.

The BF3 and BF4 overprint would occur as the BF2 faults continue rotation past perpendicular to the shear zone. At some point the induced sinistral shear cannot be maintained against the dextral shear of the primary shear zone. With continued dextral shearing, the conjugate strike-slip pattern of BF4 is produced. The BF4 pattern of dextral nonrotational shear extends east of the study area as documented by McMackin (1992), McMackin and Prave (1994), and Friedmann et al. (1996). The same pattern is reflected in the outcrop distribution of pre-Tertiary bedrock exposures across the Silurian and Halloran Hills as mapped by Bishop (1994). The progression from the BF2 (vertical axis rotation) to BF4 (dextral shearing without rotation) fault patterns has not been discussed in the literature or modeled either experimentally or mathematically. However, taken individually and sequentially, the Silurian Hills data are consistent with the Dickinson

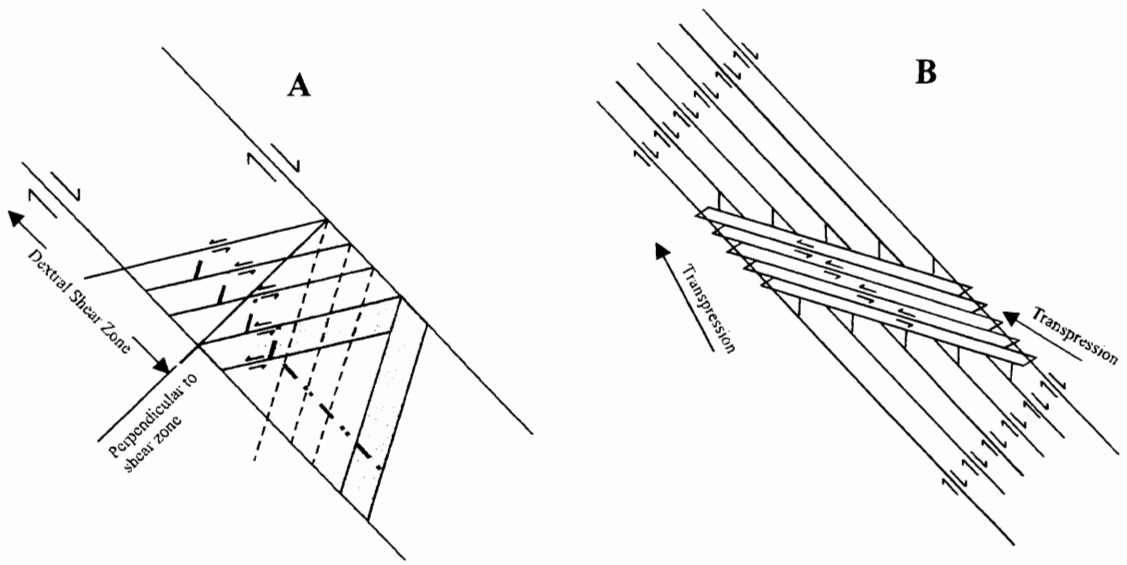

Figure 42. Transrotation in a dextral shear zone. A. Northwest trending dextral shear zone and the perpendicular to the shear zone. B. When the transrotated blocks rotate pass the perpendicular, continued rotation requires transpression in both the shear zone and between the rotating blocks. Modified after Dickinson (1996).

model (1996) for rotation and both the Withjack and Jamison (1986) and Fossen and Tikoff (1993) models for nonrotational transcurrent systems.

For completeness, a third hypothesis for the BF2 to BF4 progression is possible. The sequence could be due to changes in the orientation of the local stress field over time, without vertical axis rotation. Undoubtedly, the interaction of the Garlock and southern Death Valley fault systems have produced erratic, localized stress-field variations. If further study shows that vertical axis rotations could not have occurred, then there is no choice but to accept this hypothesis. None the less, I suggest that model 2 is most consistent with the observed dextral shearing across the region from Middle Miocene time forward, with paleomagnetic studies to the east indicating vertical axis rotation, and with theoretical and experimental transcurrent strain theory.

Mesozoic deformational history

Regional Mesozoic deformation at the latitude of the Silurian Hills is characterized by contraction associated with either the Sevier fold and thrust belt or the East Sierran thrust belt. Both fold and thrust belts trend north to northeast and are associated with east to southeast directed thrusting. The following discussions of the Mesozoic structural history of the Silurian Hills assume the removal of the ~30° clockwise rotation discussed above. This restoration of the Silurian Hills Mesozoic structural trends aligns them with the prevalent regional trends.

Structural relationships among domains:

The four structural and metamorphic domains of this study represent at least three spatially and/or temporally distinct events. Ductile structures in domain 4 are interpreted to be spatially and temporally continuous with those of domain 3. Although domains 1 and 3-4 both consist of Pahrump Group rocks, the differences in metamorphism and strain between the two domains imply a spatial, if not temporal, separation during the deformational events. Domain 2 is structurally continuous beneath domain 3 in the sense that the abrupt mylonite and metamorphic facies front between domains 2 and 3 involves

the lower strain rocks and is not a brittle fault contact. Similar contact relations are apparent at the domain 1 - 2 contact on the north side of Silurian Peak. However, the differences in strain magnitude, mineral lineation trends, and metamorphic facies between domain 2 and both domains 1 and 3 indicate a third, later event.

Syn-tectonic plutonism in domains 3 and 4:

In this study I interpret domains 3 and 4 to be the result of syn- and post-tectonic plutonism. The concordance of foliation and mineral stretching lineation attitudes between the two domains, the decreasing post-emplacement strain implied by fabric development in the successively younger plutonic phases, and the static, thermal metamorphic overprint all suggest syn-tectonic plutonism as described by Patterson et al. (1989). These observations are also consistent with models for syn-tectonic intrusive sheets as discussed by Pavlis (1995). The contrasting viscosity and post-cooling strength of the igneous intrusions, and rheological differences of the plutonic vs. country rock caused by heat transfer during pluton cooling and thermal softening of the country rock, produce low-pressure high-temperature "contact metamorphic" mineral assemblages within a regional tectonic deformation. Therefore, previous interpretations of thrust faulting (in variously vergent directions) followed by igneous intrusion across fault contacts (Kupfer, 1960; Bishop, 1994), are reinterpreted in this study to be successive, syn-tectonic sheets, intruded into a northeast trending and northwest vergent, reverse, ductile shear zone. After restoration of Tertiary motions, mineral stretching lineations trend 130° and plunge 030° with an interpreted sense of motion toward 310°.

This interpretation aligns the Silurian Hills reverse shearing with the general trend of the Sevier fold and thrust belt, but with an opposite sense of vergence. Recent models of convergent plate boundaries (Koons, 1990; 1994; Willett et al., 1993) require some degree of reverse-sense back-thrusting in the hinterland of the orogen depending upon specific physical conditions. Back-thrusts and folds have been observed to the north in the Cottonwood and Grapevine Mountains as well as other localities (Snow and Wernicke, 1989; Snow, 1992). The Mesozoic structure and associated metamorphism of domain 3 and 4 in the southeastern Silurian Hills are interpreted to be the result of back-thrusting

during the youngest (Late Cretaceous?) episodes of Sevier thrust emplacement. While several radiometric dates have been obtained on plutonic and metamorphic rocks in or near the study area, it is not clear which rocks in the present study can be correlated with previously dated rocks. The youngest dates on undeformed granites in the area are K-Ar cooling ages which range from 94 to 83 Ma (Fleck et al., 1994), constraining the end of shearing to early Late Cretaceous. Sutter (1968) obtained biotite K-Ar cooling ages of 95 to 85 Ma for plutonic rocks found within the Riggs carbonates, and DeWitt et al. (1984) obtained U-Pb zircon dates of 97 Ma and Ar-Ar amphibole cooling ages of 90 Ma for granitic rocks with a similar lithologic description in the Halloran Hills. Assuming these dates are from rocks similar to the domain 4 quartz monzonites found within the Riggs carbonates, then these dates would be near the end of shearing. U-Pb zircon dates of ~170 Ma reported by DeWitt et al. (1984) for granodiorites in the Halloran Hills may record earlier plutonic emplacement, but may not correlate with the granodiorites in the Silurian Hills. Further study of the geochronology of the individual intrusive pulses is required to constrain the dates of emplacement, cooling, and coincident shearing.

Mylonite development by gravity collapse of a tectonically thickened crust:

The domain 2 mylonites are a distinctive feature of the Silurian Hills. Mylonites are reported to crop out 40 km to the east in the Clark Mountains (Burchfiel and Davis, 1988) and Kingston Range (McMackin, 1992), and 45 km west in the Avawatz Mountains (Dean, 1995). Burchfiel and Davis associate the Clark Mountain mylonitic layers with Sevier age crustal shortening. McMackin associates the Kingston Range mylonitic development to both Mesozoic shortening and Miocene extension along the Kingston Range detachment fault. However, the reported thickness of the mylonite zones in those areas are in the range of 10's to 100 m and occur exclusively as retrograde zones in crystalline basement. In contrast, the minimum thickness of the mylonite zone in the Silurian Hills is 250 m and involves prograde metamorphosed Pahrump Group, crystalline basement, or both. The mylonite zone in the Avawatz Mountains is associated with the eastern Sierra thrust system and involves at least a 1 km thick section of Mesozoic volcanic rocks. Thus, the Silurian Hills mylonites do not appear to correlate with any of

these mylonite zones. While differences in structural thickness and protolith suggest these mylonites have a different origin, this inference is not as compelling as the timing constraints implied by the discussion of the syn-tectonic plutonism. The domain 2 mylonites clearly postdate the strain and metamorphism of domains 1 and 3-4 dated at ~pre-85 Ma (see above) and shear sense indicators show a clear top to the northeast displacement in present coordinates. Thus, the mylonite development postdates the reported youngest dates of Sevier thrust faulting in the Clark Mountains (Walker et al., 1995) and the eastern Sierran thrust faulting in the Avawatz Mountains (Dean, 1995). Moreover, the transport direction indicated by the mylonites is 180° from the SW directed Miocene detachment faulting in the Kingston Range.

Consideration of the Cenozoic clockwise rotation discussed above and restoration of the mylonite zone to a pre-Miocene orientation produces a top to the north-northwest (~170°) sense of movement. While the majority of data indicate a shallow mineral lineation plunge to the southeast (in restored coordinates), these are located in the kink-folded section of the mylonites. Up structural section and away from the kink folds, restored stretching lineations plunge north-northwest, down dip in foliation. The consistent northwest-southeast trend of mineral lineation and the down-dip plunge of the least disrupted mylonites suggests that the top to the north-northwest (~350°) directed shear would be normal displacement. Thus the mylonites apparently record west directed extension.

In the Death Valley region extensional mylonite zones are commonly associated with Miocene and later exhumation of metamorphic core complexes (e.g., Davis and Anderson, 1991). However, several studies suggest that extensional features also occurred during Late Cretaceous to Eocene time as the result of gravitational collapse of the crust thickened during the Sevier orogeny (Wells et al., 1990; Livaccari, 1991; Hodges and Walker, 1992). Recent work by Miller et al. (1994) in the New York Mountains, 95 km southeast, found a normal shear-sense mylonite zone, dated by metamorphic biotite at ~70 Ma, that cuts 92 Ma granites. This relationship was interpreted to be the result of Late Cretaceous extension. The Silurian Hills lie within the area where Mesozoic to early Tertiary extension has been inferred (Fig. 43).

Given this regional setting (Fig. 43) and the mismatch with other extensional features, the Silurian Hills mylonite zone is interpreted to be the result of Late Cretaceous to Eocene extension driven by gravitational collapse of the thickened Sevier orogen. The interpreted normal extension places domains 3-4 structurally above domain 1 by north-northwest translation along the mylonite shear zone. Unfortunately, domain 2 does not contains recognizable markers to calculate finite strain, and the total structural thickness is not known; therefore the displacement distance cannot be estimated.

Correlation of Riggs Formation with the Pahrump Group

Several lines of evidence suggest that the tectonostratigraphic Riggs Formation was derived from the Pahrump Group and not Paleozoic rocks. There is a continuous section from unequivocal Kingston Peak Formation diamictite (Pahrump Group) into the Riggs Formation carbonates, quartzites and amphibolites. While transposition and ductile strain can repeat sections or reduce the stratigraphic thickness of sections, it does not (in the absence of other evidence) remove section. The only way that section could be removed would be from a pre-metamorphic normal or strike-slip fault, a cryptic structure for which there is no evidence. As discussed above, the shear strain of ~1.9 calculated from stretched pebbles in the Kingston Peak Formation is significant but not of a magnitude required to condense the stratigraphic section by more than 50% near the region of contact between the Riggs and Kingston Peak Formations. Moreover, these strains are sufficiently low that a pre-metamorphic high-angle fault cutoff of Riggs - Kingston Peak would not be completely transposed into layering. Thus, the only allowable pre-metamorphic configuration of the system is a stratigraphic contact or a low-angle "flat-on-flat" normal fault. The latter seems highly unlikely. Therefore, the Riggs Formation protolith must be stratigraphically continuous with, and not more than a few hundred meters from, the Kingston Peak Formation.

This implies two possibilities for the protolith of the Riggs Formation: (1) the Noonday Dolomite, which is stratigraphically above the Kingston Peak Formation, and, (2) the Beck Spring Dolomite, which together with the underlying Crystal Spring

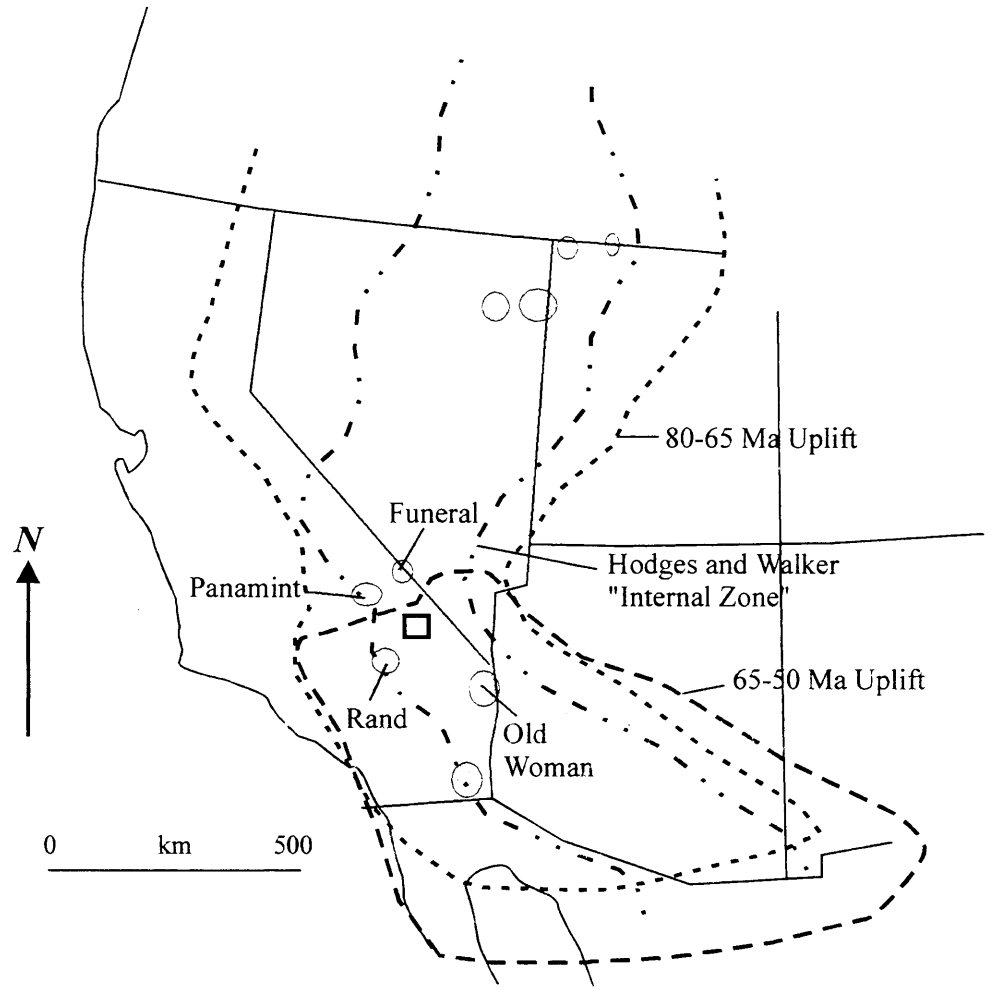

Figure 43. Mesozoic crustal thickening and extension. Uplifted regions identified by Livaccari (1991) as potential extensional collapse settings. Shaded areas are locations cited by Hodges and Walker (1992) as exhibiting evidence of Late Cretaceous to early Tertiary extension. The black outline rectangle is the study area.

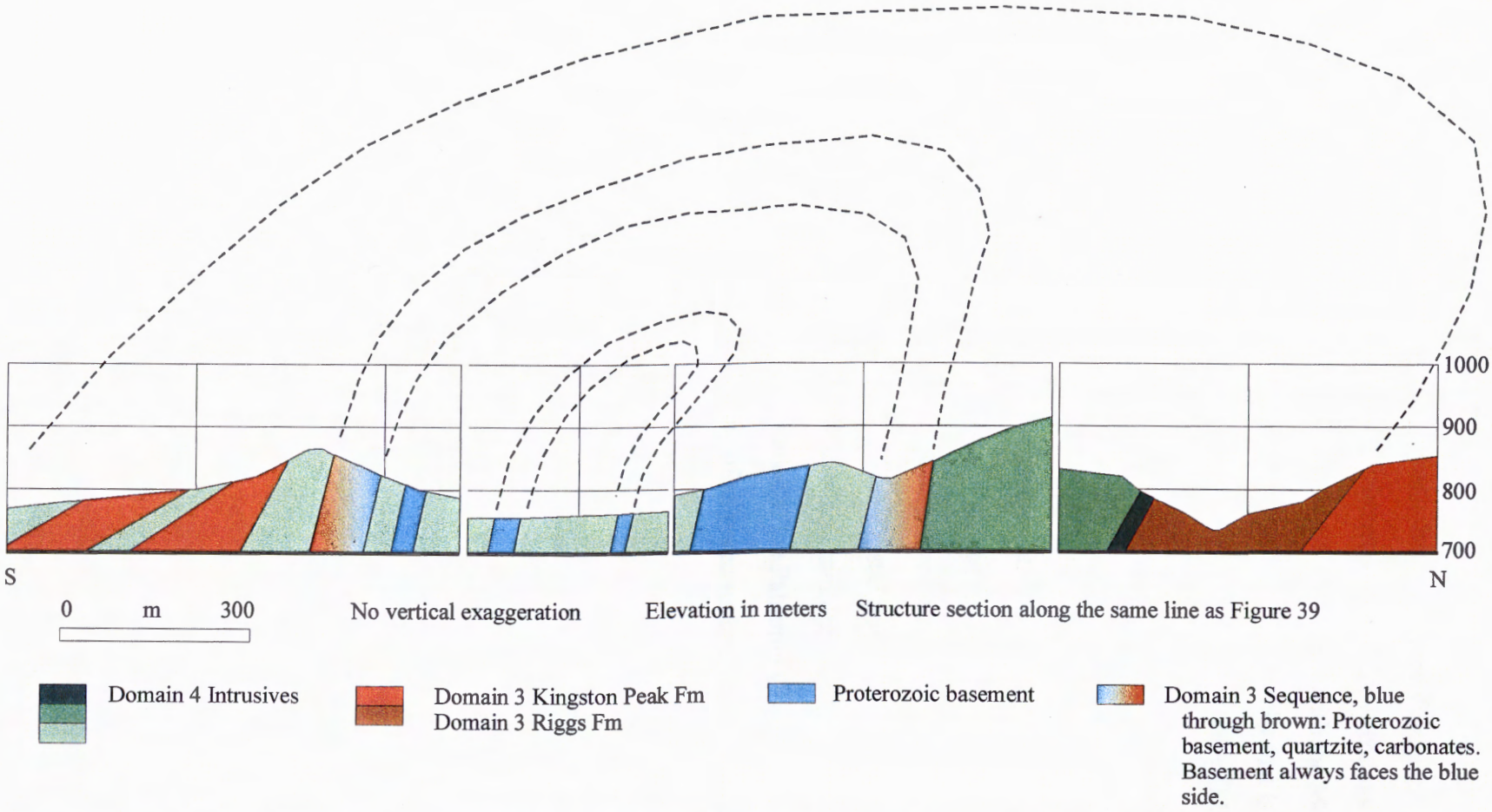

Figure 44. Stratigraphic correlation of the Riggs Formation with the Pahrump Group. With most of the Mesozoic intrusives removed from the section, the mirrored pattern of lithology about the Proterozoic basement is clearer. As with Figure 39, the domain 4 intrusives are not necessarily involved in the anticlinal strain.

Formation, are stratigraphically below the Kingston Peak Formation. Ductile deformation and regional facies variation make detailed, direct stratigraphic comparisons between domain 3 and unmetamorphosed Pahrump and Noonday sections ineffective. However, an examination of the north-south structural section with the Mesozoic plutonic injection removed (Fig. 44), provides a gross lithologic stratigraphy that is consistent with an overturned Pahrump Group section. While itself regionally variable (Mbuyi and Prave, 1993), the Crystal Spring Formation contains interbedded siliciclastic and carbonate (both limestone and dolostone) layers resting on Proterozoic crystalline basement consistent with the modified structure section. The southern (basin) facies of the Noonday Dolomite consists of predominately clastic dolomite mixed with 10 to 50 percent coarse sand grains (Williams et al., 1976), and is not consistent with a correlation to the Riggs Formation. The Beck Spring Dolomite pinches out to the south on a regional scale, which allows the Kingston Peak Formation to directly overly the Crystal Spring Formation (Roberts, 1976). Thus, if this correlation is correct, the domain 3 metamorphic of Pahrump Group (and Riggs Formation) represents a different facies of the Pahrump Group that that seem in domain 1 and would require the existence of an unrecognized thrust fault, strike-slip fault, or both.

Finally, the geochemical analysis of the Proterozoic diabase dikes found in the Crystal Spring Formation is consistent with the geochemical analysis of the amphibolites found within the Riggs Formation. In particular, the Eu anomaly of the amphibolites is flat, the only samples from the Silurian Hills that do not have a negative anomaly. Thus, the amphibolites are consistent with the regional geochemistry of the Proterozoic diabase dikes, and taken together with the lithologic and structural observations suggest a correlation of the Riggs Formation with the Crystal Spring and Beck Spring Formations of the Pahrump Group.

Reconstruction

The Silurian Hills are structurally, and to a large degree stratigraphically, cut off from the surrounding ranges. Through-going structures and the continuity of stratigraphy

are not apparent from bedrock exposures in nearby ranges. These relationships must be inferred by the contrasts and similarities of trends and styles of deformation, degrees of metamorphism, absolute and relative timing of events, and regional facies variations within stratigraphic formations between what is observed in the Silurian Hills and the surrounding ranges. Thus, although the internal evidence of vertical axis rotation and distributed dextral shear may be compelling, a precise quantification of translation of the Silurian Hills relative to surrounding ranges is impossible due to the lack of stratigraphic and structural control across the region. At the same time, many of the features found in the Silurian Hills (e.g., syn-tectonic sheeted intrusions, the Late Cretaceous to early Tertiary mylonite zone, the Riggs Formation, west vergent thrust shearing) do not have recognized correlations in the surrounding ranges. Nevertheless, based on the conclusions of this study and regional relationships, the following speculative late Cenozoic reconstruction is offered.

The most recent movement in the Silurian Hills is by distributed dextral shear with a slight transtension component as indicated by the conjugate strike-slip and normal faulting patterns. This was preceded by clockwise vertical axis rotation (transrotation) with a slight transpression component (Fig. 45) as indicated by the oldest generation of northwest trending sinistral strike-slip faults and the uplift of the underlying bedrock to structurally higher levels than the Tertiary cover. This sequence of events suggests an initial proximity to a transpressive faulting interaction similar to what is now found at the Garlock and southern Death Valley fault zone intersection, followed by movement into the more diffuse dextral shearing at the present location of the Silurian Hills.

Several qualitative, regional stratigraphic observations contribute to the reconstruction. In the Avawatz Mountains, the Pahrump Group is not observed south and west of the Mule Spring fault, the northernmost discrete strand of the Garlock fault zone (Spencer, 1990). This contrast in Pahrump Group outcrop patterns across the Mule Spring fault is striking, and suggests that the scattered outcrop fragments of Pahrump Group rocks found east and south of the fault termination beneath alluvium bear a structurally affinity to those rocks north of the Garlock fault zone. Indeed, the qualitative removal of the documented dextral shearing in the Silurian Hills and Shadow Mountains

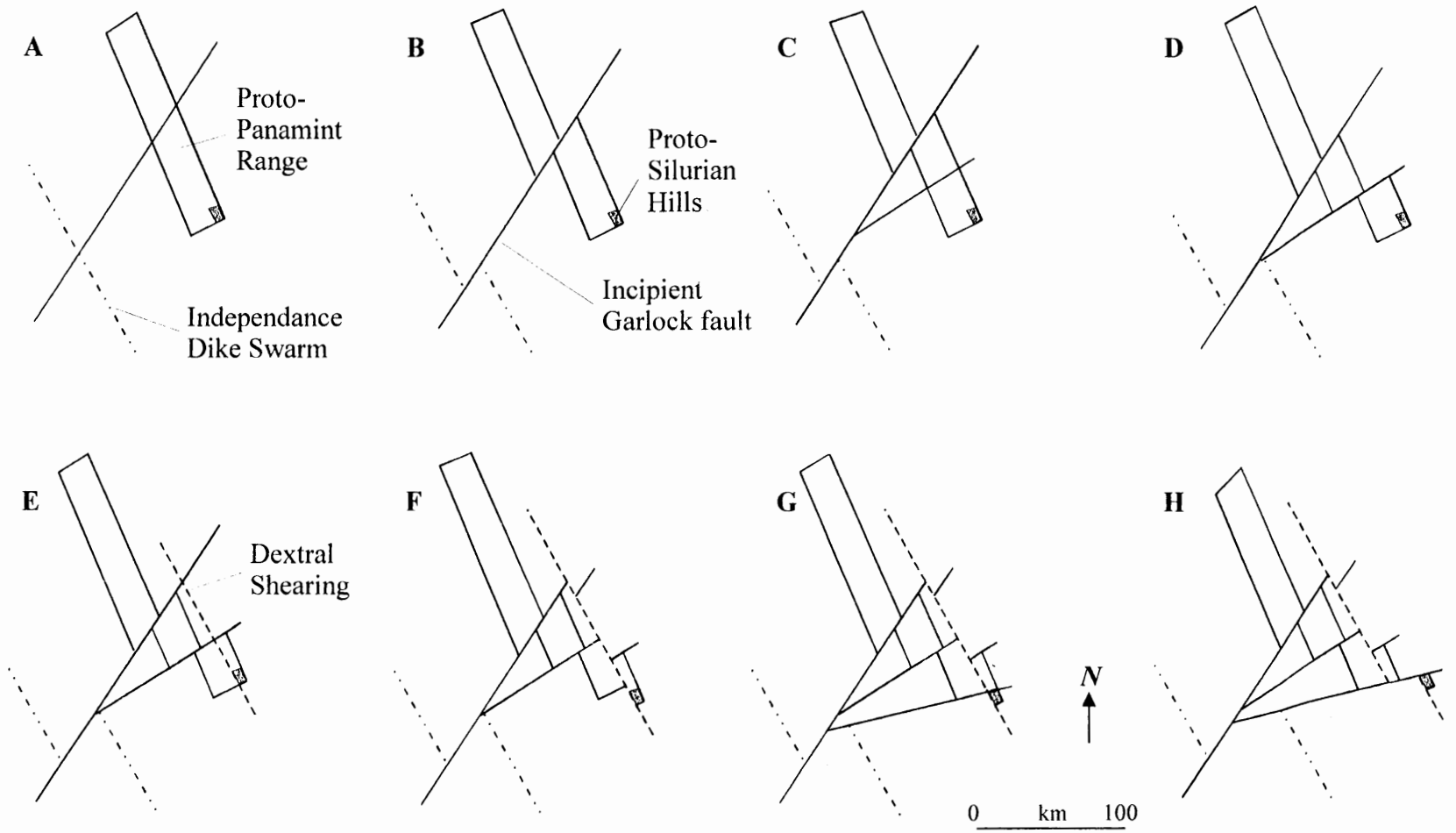

Figure 45. Diagramatic removal of Cenozoic brittle faulting with a reconstruction of the Silurian Hills to their pre-12 Ma relative position. Figures A - H are not sequential time slices, but a general representation of interactions of the Garlock fault zone with distributed dextral shearing. Sinistral faulting on the Garlock is assumed to occur first, but the order of subsequent events is not critical to this reconstruction. (cont'd)

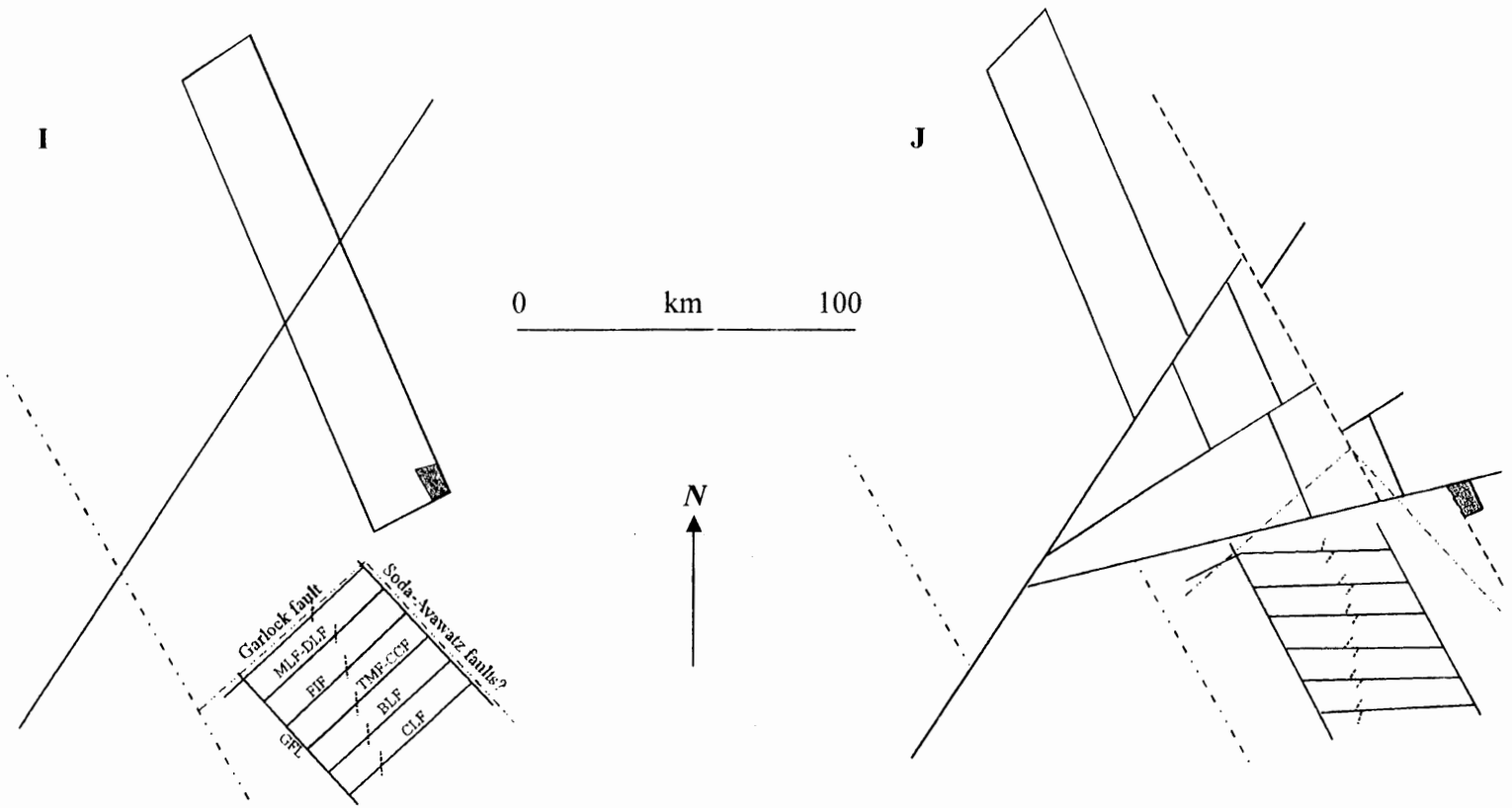

Figure 45 (cont'd). This model assumes a three tailed splay of the Garlock, with 20 km of relative offset along each splay for a total of 60 km offset of the Independance Dike Swarm. 10 km of dextral offset was introduced to separate the Silurian Hills block from the Avawatz Mtns. Figures I and J are the 12 Ma and present configurations overlain by the Schermer et al. (1996) model of transrotation in the NE Mojave (Fig. 41) for the same times with equal scale and consistent relative position. This model does not illustrate west directed extension and transrotation in Death Valley (Serpa and Pavlis, 1996) relative to the Mojave, but it would be required to unroof the Panamints from the Black Mtns., and account for the full relative offset along the Garlock.

restores the Pahrump Group to a more northern location (Fig. 45). A further implication of this hypothesis is that an eastern extension (if one exists) of the Garlock fault would have to occur south of the Silurian Hills, presumably offset by the dextral southern Death Valley fault. Unfortunately, this is not supported by the work of Hartman (1997) and Rodosta (1997) that found no evidence of through-going dextral structures in the Silver Lake or Soda Mountains areas. Nor is it supported by the work of Martin et al. (1993) and Martin and Walker (1995) that conclude Paleozoic and early Mesozoic depositional trends through the east central Mojave are disrupted by Early Miocene, west-directed extension, but not by later sinistral offsets of the ~65 km magnitude observed near the eastern termination of the Garlock fault.

The model of Serpa and Pavlis (1996) provides a solution to this apparent conundrum. They propose that offset of the Garlock is accommodated by trifurcation at fault termination, vertical axis rotation, and differential extension between the Death Valley and Mojave Desert regions across Garlock fault (Fig. 45). This model requires transpression at, and to the east of, the branching nodes of the Garlock, but does not require an eastern extension of the Garlock fault. It also reconstructs Proterozoic, Paleozoic, and Mesozoic lithologic and structural trends to reasonable pre-Tertiary positions.

CONCLUSIONS

The Silurian Hills contain evidence for northwest vergent, Mesozoic syn-tectonic plutonism and amphibolite grade metamorphism that temporally accompany the southeast vergent Sevier fold and thrust belt, and are interpreted to be the result of back-thrusting in the hinterland of the Sevier orogeny. A subsequent greenschist-grade quartz-mylonite zone places this high grade package over tightly folded lower greenschist grade basement, Pahrump Group and younger rocks due to gravitational collapse of the thickened crust during Late Mesozoic to Early Tertiary extension. All of these rocks are overprinted by complex Miocene and later brittle high and low angle normal, dextral and sinistral transcurrent faults. This faulting is interpreted to be the result of northwest trending

dextral shear across the eastern Mojave Desert that induced clockwise vertical axis rotation of crustal blocks within the shear zone. Secondary results of this study are the correlation of the tectonostratigraphic Riggs carbonates with the Crystal Spring Formation of the Pahrump Group and the resolution of the Riggs "Thrust" fault into two distinct components, a Mesozoic ductile, back-thrust shear zone and Miocene low and high angle normal faults.

REFERENCES

Abbott, E.W., 1971, Structural geology of the southern Silurian Hills, San Bernardino County, California [M.A. thesis]: Houston, Texas, Rice University, 48 p.

Armstrong, R.L., 1968, Sevier orogenic belt in Nevada and Utah: Geological Society of America Bulletin, v. 79, p. 429-458.

Battey, T.F., 1991, Neogene evolution of the Garlock - Death Valley fault junction, southeastern California, [M.S. thesis]: Los Angeles, University of Southern California, 170 p.

Bishop, K.M, 1994, Mesozoic and Cenozoic extensional tectonics of the Halloran and Silurian Hills area, eastern San Bernardino County, California [Ph.D. dissert.]: Los Angeles, University of Southern California, 252 p.

Burbank, D.W., and Whistler, D.P., 1987, Temporally constrained tectonic rotations derived from magnetostratigraphic data: Implications of the initiation of the Garlock fault, California: Geology, v. 15, p. 1172-1175.

Burchfiel, B.C., and Davis, G.A., 1977, Geology of the Sagamore Canyon - Slaughterhouse Spring area, New York Mountains, California: Geological Society of America Bulletin, v. 88, p. 1623-1640.

Burchfiel, B.C., and Davis, G.A., 1988, Mesozoic thrust faults and Cenozoic low-angle normal faults, eastern Spring Mountains, Nevada, and Clark Mountains thrust complex, California, *in* Weide, D.L., and Faber, M.L., eds., This extended land: Geological journeys in the southern Basin and Range: Las Vegas, University of Nevada - Las Vegas Department of Geoscience, p. 87-106.

Burchfiel, B.C., Hamill, G.S., and Wilhelms, D.E., 1983, Structural geology of the Montgomery Mountains and the northern half of the Nopah and Resting Spring Ranges, Nevada and California: Geological Society of America Bulletin, v. 94, p. 1359-1376.

Busby-Spera, C.J., 1988, Speculative tectonic model for the early Mesozoic arc of the southwest Cordilleran United States: Geology, v. 16, p. 1121-1125.

Butler, P.R., Troxel, B.W., and Verosub, K.L., 1988, Late Cenozoic history and styles of deformation along the southern Death Valley fault zone, California: Geological Society of America Bulletin, v. 100, p 402-410.

Comstock, J.E., Pavlis, T.L., Serpa, L., 1996, Sinistral and dextral strike-slip fault interaction: an example from the southern Death Valley region: Geological Society of America, Annual Meeting, Abstracts with Programs, Denver, v. 28, n. 7, p. A451.

Davis, G.A., and Anderson, J.L., 1991, Low - angle normal faulting and rapid uplift of mid-crustal rocks in the Whipple Mountains metamorphic core complex, southeastern California: Discussion and field guide: in Walawender, M.J., and Hanan, B.B., eds, Geological excursions in southern California and Mexico, Geological Society of America Guidebook: San Diego, California, p. 417-446.

Davis, G.A., Fowler, T.K., Bishop, K.M., Brudos, T.C., Friedmann, S.J., Burbank, D.W., Parke, M.A., and Burchfiel, B.C., Pluton pinning of an active Miocene detachment fault system, eastern Mojave Desert, California: Geology, v. 21, p. 627-630.

Dean, M.C., 1995, Geologic mapping and kinematic analysis of a shear zone near the Garlock - Southern Death Valley fault zone intersection, Fort Irwin, California [M.S. thesis]: New Orleans, Louisiana, University of New Orleans, 57 p.

DeWitt, E.H., 1980, Geology and geochronology of the Halloran Hills, southeastern California, and implications concerning Mesozoic tectonics of the southwestern Cordillera [Ph.D. dissert.]: University Park, The Pennsylvania State University, 269 p.

DeWitt, E., Armstrong, R.L., Sutter, J.F., and Zartman, R.E., 1984, U-Th-Pb, Rb-Sr, and Ar-Ar mineral and whole-rock isotopic systematics in a metamorphosed granitic

terrane, southeastern California: Geological Society of America Bulletin, v. 95, p. 723-729.

Dickinson, W.R., 1996, Kinematics of transrotational tectonism in the California Transverse Ranges and its contribution to cumulative slip along the San Andreas transform fault system: Boulder, Colorado, Geological Society of America Special Paper 305, 46 p.

Dickinson, W.R., and Wernicke, B.P., 1997, Reconciliation of San Andreas slip discrepancy by a combination of interior Basin and Range extension and transrotation near the coast: Geology, , v. 25, p. 663-665.

Dokka, R.K., 1992, The eastern California shear zone and its role in the creation of young extensional zones in the Mojave Desert region, *in* Craig, S.D., ed., Structure, Tectonics, and mineralization of the Walker Lane: Reno, Nevada, Geological Society of Nevada, p. 161-186.

Dokka, R.K., and Travis, C.J., 1990, Late Cenozoic strike-slip faulting in the Mojave Desert: Tectonics, v.9, p. 311-340.

Dunne, G.C., 1977, Geology and structural evolution of Old Dad Mountain, Mojave Desert, California: Geological Society of America Bulletin, v. 88, p. 737-748.

Dunne, G.C., and Walker, J.D., 1993, Age of Jurassic volcanism and tectonism, southern Owens Valley region, east-central California: Geological Society of America Bulletin, v. 105, p. 1223-1230.

Fleck, R.J., 1970, Tectonic style, magnitude, and age of deformation in the Sevier orogenic belt in southern Nevada and eastern California: Geological Society of America Bulletin, v. 81, p. 1705-1720.

Fleck, R.J., Mattinson, J.M., Busby, C.J., Carr, M.D., Davis, G.A., and Burchfiel, B.C., 1994, Isotopic complexities and the age of the Delfonte volcanic rocks, eastern Mescal Range, southeastern California: Stratigraphic and tectonic implications: Geological Society of America Bulletin, v. 106, p. 1242-1253.

Fossen, H., and Tikoff, B., 1993, The deformation matrix for simultaneous simple shearing, pure shearing and volume change, and its application to transpression-transtension tectonics: Journal of Structural Geology, v. 15, p. 413-422.

Fowler, T.K., Jr., Friedmann, S.J., Davis, G.A., and Bishop, K.M., 1995, Two-phase evolution of the Shadow Valley Basin, south-eastern California: a possible record of footwall uplift during extensional detachment faulting: Basin Research, v. 7, p. 165-179.

Friedmann, S.J., Davis, G.A., and Fowler, T.K., 1996, Geometry, paleodrainage, and geologic rates from the Miocene Shadow Valley supradetachment basin, eastern Mojave Desert, California, *in* Beratan, K.K., ed., Reconstructing the History of Basin and Range Extension Using Sedimentology and Stratigraphy: Boulder, Colorado, Geological Society of America Special Paper 303, p. 85-105.

Garfunkel, Z., 1974, Model for the Late Cenozoic tectonic history of the Mojave Desert, California, and for its relation to adjacent regions: Geological Society of America Bulletin, v. 85, p. 1931-1944.

Hammond, J.G., 1986, Geochemistry and petrogenesis of Proterozoic diabase in the southern Death Valley region of California: Contributions to Mineralogy and Petrology, v. 93, p. 312-321.

Hartman, M.T., 1997, A geophysical investigation of Silver Lake: A playa near the Garlock/Southern Death Valley Fault zone intersection, [M.S. thesis]: New Orleans, Louisiana, University of New Orleans, p. 82.

Heaman, L.M., and Grotzinger, J.P., 1992 1.08 Ga diabase sills in the Pahrump Group, California: Implications for development of the Cordilleran miogeocline; Geology, v. 20, p. 637-640.

Hodges, K.V., and Walker, J.D., 1992, Extension in the Cretaceous Sevier orogen, North American Cordillera: Geological Society of America Bulletin, v. 104, p. 560-569.

Holm, D.K., Geissman, J.W., and Wernicke, B., 1993, Tilt and rotation of the footwall of a major normal fault system: Paleomagnetism of the Black Mountains, Death Valley extended terrane, California: Geological Society of America Bulletin, v. 105, p. 1373-1387.

Kerrick, D.M., 1974, Review of metamorphic mixed volatile (H_2O-CO_2) equilibria: American Mineralogist, v. 59, p. 729-762.

Kerrick, D.M., 1990, The Al_2SiO_5 polymorphs: Reviews in Mineralogy, Volume 22, Mineralogical Society of America, Washington, D.C., 406 p.

Koons, P.O., 1990, Two-sided orogen: Collision and erosion from the sandbox to the Southern Alps, New Zealand: Geology, v. 18, p. 679-682.

Koons, P.O., 1994, Three-dimensional critical wedges: Tectonics and topography in oblique collisional orogens: Journal of Geophysical Research, v. 99, n. B6, p. 12,301-12,315.

Kupfer, D.K., 1960, Thrust faulting and chaos structure, Silurian Hills, San Bernardino County, California: Geological Society of America Bulletin, v. 71, p. 181-214.

Link, P.K., Christie-Blick, N., Devlin, W.J., Elston, D.P., Horodyski, R.J., Levy, M., Miller, J.M.G., Pearson, R.C., Prave, A., Stewart, J.H., Winston, D., Wright, L.A., and Wrucke, C.T., 1993, Middle and Late Proterozoic stratified rocks of the western U.S. Cordillera, Colorado Plateau, and Basin and Range province, *in* Reed, J.C., Jr., Bickford, M.E., Houston, R.S., Link, P.K., Rankin, D.W., Sims, P.K., and Van Schmus, W.R., eds., Precambrian: Conterminous U.S.: Boulder, Colorado, Geological Society of America, The Geology of North America, v. C-2.

Livaccari, R.F., 1991, Role of crustal thickening and extensional collapse in the tectonic evolution of the Sevier-Laramide orogeny, western United States: Geology, v. 19, p. 1104-1107.

Luyendyk, B.P., 1991, A model for Neogene crustal rotations, transtension, and transpression in southern California: Geological Society of America Bulletin, v. 103, 1528-1536.

Martin, M.W., Glazner, A.F., Walker, J.D., and Schermer, E.R., 1993, Evidence for right-lateral faulting accommodating en echelon Miocene extension, Mojave Desert, California: Geology, v. 21, p. 355-358.

Martin, M.W., and Walker, J.D., 1992, Extending the western North American Proterozoic and Paleozoic continental crust through the Mojave Desert: Geology, v. 20, p. 753-756.

Martin, M.W., and Walker, J.D., 1995, Stratigraphy and paleogeographic significance of metamorphic rocks in the Shadow Mountains, western Mojave Desert, California: Geological Society of America Bulletin, v. 107, p. 354-366.

Mbuyi, K, and Prave, A.R, 1993, Unconformities in the Mid-Late Proterozoic Pahrump Group: stratigraphic evidence from the upper member Crystal Spring Formation.: Geological Society of America Cordilleran Section, Abstracts with Program, Reno v. 25, n. 5, p. A116.

McMackin, M.R., 1992, Tectonic evolution of the Kingston Range, Death Valley, California [Ph.D. dissert.]: University Park, The Pennsylvania State University, 158 p.

McMackin, M.R., and Prave, A.R., 1994, Duplication of tectonostratigraphic facies by lateral faulting in the Shadow Valley basin, California: Geological Society of America, Cordilleran Section, Abstracts with Programs, San Bernardino, v. 26, n. 2, p. A72.

Miller, D.M., Walker, J.D., DeWitt, E., and Nakata, J.K., 1994, Mesozoic episodes of horizontal crustal extension, U.S. Cordillera: Geological Society of America, Cordilleran Section, Abstracts with Programs, San Bernardino, v. 26, n. 2, p. A74.

Miller, E.L., Miller, M.M., Stevens, C.H., Wright, J.E., and Madrid, R., 1992, Late Paleozoic paleogeographic and tectonic evolution of the western U.S. Cordillera, *in* Burchfiel, B.C., Lipman, P.W., and Zoback, M.L., eds. The Cordilleran Orogen: Conterminous U.S.: Boulder, Colorado, Geological Society of America, The Geology of North America, v. G-3.

Miller, J.M.G., 1987, Paleotectonic and stratigraphic implications of the Kingston Peak-Noonday contact in the Panamint Range, eastern California: Journal of Geology, v. 95, p. 75-85.

Patterson, S.R., Vernon, R.H., and Tobish, O.T., 1989, A review of criteria for the identification of magmatic and tectonic foliations in granitoids: Journal of Structural Geology, v. 11, p. 349-363.

Passchier, C.W., and Trouw, R.A.J., 1996, Microtectonics: Berlin, Germany, Springer-Verlag, 289 p.

Pavlis, T.L., 1995, Fabric development in syn-tectonic intrusive sheets as a consequence of melt-dominated flow and thermal softening of the crust: Tectonophysics, v. 253, p. 1-31.

Poole, F.G., Stewart, J.H., Palmer, A.R., Sandberg, C.A., Madrid, R.J., Ross, R.J., Jr., Hintze, L.F., Miller, M.M., and Wruck, C.T., 1992, Latest Precambrian to latest Devonian time; Development of a continental margin, *in* Burchfiel, B.C., Lipman, P.W., and Zoback, M.L., eds., The Cordilleran Orogen: Conterminous U.S.: Boulder, Colorado, Geological Society of America, The Geology of North America, v. G-3.

Prave, A.R., 1994, The Pahrump Group: Alternative speculations on the Neoproterozoic geodynamic development of the Death Valley region: Geological Society of America, Cordilleran Section, Abstracts with Programs, San Bernardino, v. 26, n. 2, p. A82.

Ramsay, J.G., and Huber, M.I., 1983, The Techniques of Modern Structural Geology, Volume 1: Strain Analysis: Academic Press, Inc., New York, 307 p.

Ramsay, J.G., and Huber, M.I., 1987, The Techniques of Modern Structural Geology, Volume 2: Folds and Fractures: Academic Press, Inc., New York.

Reches, Z., 1978, Analysis of faulting in three-dimensional strain field: Tectonophysics, v. 47, p. 109-129.

Reches, Z., 1983, Faulting of rocks in three-dimensional strain field: II. Theoretical analysis: Tectonophysics, v. 95, p. 133-156.

Roberts, M.T., 1976, Stratigraphy and depositional environments of the Crystal Spring Formation, southern Death Valley region, California, *in* Troxel, B.W., and Wright, L.A., eds., Geologic features of Death Valley, California: California Division of Mines and Geology Special Report 106, p. 35-43.

Rodosta, T., 1997, A fault kinematic study of Red Pass and Soda Avawatz fault zones; northeastern Mojave Desert, California [M.S. thesis]: New Orleans, Louisiana, University of New Orleans, 62 p.

Ross, T.M., Luyendyk, B.P., and Haston, R.B., 1989, Paleomagnetic evidence for Neogene clockwise tectonic rotations in the central Mojave Desert, California: Geology, v. 17, p. 470-473.

Schermer, E.R., Luyendyk, B.P., and Cisowski, S., 1996, Late Cenozoic structure and tectonics of the northern Mojave Desert: Tectonics, v. 15, p. 905-932.

Schermer, E.R., and Busby, C., 1994, Jurassic magmatism in the central Mojave Desert: Implications for arc paleogrography and preservation of continental volcanic sequences: Geological Society of America Bulletin, v. 106, p. 767-790.

Serpa, L., and Pavlis, T.L., 1996, Three-dimensional model of the late Cenozoic history of the Death Valley region, southeastern California: Tectonics, v. 15, p. 1113-1128.

Simpson, C., and De Paor, D.G., 1993, Strain and kinematic analysis in general shear zones: Journal of Structural Geology, v. 15, p 1-20.

Snow, J.K., 1992, Large-magnitude Permian shortening and continental-margin tectonics in the southern Cordillera: Geological Society of America Bulletin, v. 104, p. 80-105.

Snow, J.K., and Wernicke, B., 1989, Uniqueness of geological correlations: An example from the Death Valley extended terrain: Geological Society of America Bulletin, v. 101, p. 1351-1362.

Spear, F.S., 1995, Metamorphic Phase Equilibria and Pressure-Temperature-Time Paths: Mineralogical Society of America Monograph, Washington, D.C., 799 p.

Spencer, J.E., 1990, Late Cenozoic extensional and compressional tectonism in the southern and western Avawatz Mountains, southeastern California *in* Wernicke, B.P., ed., Basin and Range extensional tectonics near the latitude of Las Vegas, Nevada: Boulder, Colorado, Geological Society of America Memoir 176.

Stephens, K.A., 1994, Mesozoic tectonic evolution of the Tiefort Mountains, NE Mojave Desert, CA [M.S. thesis]: Bellingham, Washington, Western Washington University 130 p.

Sutter, J.F., 1968, Geochronology of major thrusts, southern Great Basin, California [M.A. thesis]: Houston, Texas, Rice University, 32 p.

Streckeisen, A., 1976, To each plutonic rock its proper name: Earth-Science Reviews, v. 12, p. 1-33.

Wadsworth, W.B., Ferriz, H., Rhodes, D.D., 1995, Structural and stratigraphic development of the Middle Jurassic magmatic arc in the Cowhole Mountains, central-eastern Mojave Desert, California, in Miller, D.M., and Busby, C., Jurassic Magmatism and Tectonics of the North American Cordillera: Boulder, Colorado, Geological Society of America Special Paper 299.

Walker, J.D., and Wardlaw, B.R., 1989, Implications of Paleozoic and Mesozoic rocks in the Soda Mountains, northeastern Mojave Desert, California, for late Paleozoic and Mesozoic Cordilleran orogenesis: Geological Society of America Bulletin, v. 101, p. 1574-1583.

Walker, J.D., Burchfiel, B.C., and Davis, G.A., 1995, New age controls on initiation and timing of foreland belt thrusting in the Clark Mountains, southern California: Geological Society of America Bulletin, v. 107, p. 742-750.

Walker, J.D., Martin, M.W., Bartley, J.M., and Coleman, D.S., 1990, Timing and kinematics of deformation in the Cronese Hills, California, and implications for Mesozoic structure of the southwestern Cordillera: Geology, v. 18, p. 554-557.

Ward, P.L., 1995, Subduction cycles under western North America during the Mesozoic and Cenozoic eras, in Miller, D.M., and Busby, C., Jurassic magmatism and tectonics of the North American Cordillera: Boulder, Colorado, Geological Society of America Special Paper 299, p. 1-45.

Wells, M.L., Dallmeyer, R.D., and Allmendinger, R.W., 1990, Late Cretaceous extension in the hinterland of the Sevier thrust belt, northwestern Utah and southern Idaho: Geology, v. 18, p. 929-933.

Wernicke, B., Axen, G.J., and Snow, J.K., 1988, Basin and Range extensional tectonics at the latitude of Las Vegas, Nevada: Geological Society of America Bulletin, v. 100, p. 1738-1757.

Willett, S., Beaumont, C., and Fullsack, P., 1993, Mechanical model for the tectonics of doubly vergent compressional orogens: Geology, v. 21, p. 371-374.

Williams, E.G., Wright, L.A., and Troxel, B.W., 1976, The Noonday Dolomite and equivalent stratigraphic units, southern Death Valley, California, *in* Troxel, B.W., and Wright, L.A., eds., Geologic features of Death Valley, California: California Division of Mines and Geology Special Report 106, p. 35-43.

Willis, D.K., 1993, The southern Death Valley fault zone: A study of Plio-Pleistocene folding along a strike-slip system in the vicinity of the Noble Hills, California [M.S. thesis]: New Orleans, Louisiana, University of New Orleans, 84 p.

Withjack, M.O., and Jamison, W.R., 1986, Deformation produced by oblique rifting: Tectonophysics, v. 126, p. 99-124.

Wright, L.A., 1954, Geology of the Silver Lake talc deposits, San Bernardino County, California: California Division of Mines Special Report 38, 30 p.

Wright, L.A., 1976, Late Cenozoic fault patterns and stress fields in the Great Basin and westward displacement of the Sierra Nevada block: Geology, v. 4, p. 489-494.

Wright, L.A., and Troxel, B.W., 1967, Limitations on right-lateral, strike-slip displacement, Death Valley and Furnace Creek Fault zones, California: Geological Society of America Bulletin, v. 78, p. 933-950.

Wright, L.A., and Troxel, B.W., 1973, Shallow-fault interpretation of Basin and Range Structure, Southwest Great Basin *in* DeJong, K.A., and Scholten, R., eds., Gravity and tectonics: New York, John Wiley and Sons, pp. 397-407.

Wright, L.A., Thompson, R.A., Troxel, B.W., Pavlis, T.L., DeWitt, E.H., Otton, J.K., Ellis, M.A., Miller, M.G., and Serpa, L.F., 1991, Cenozoic magmatic and tectonic evolution of the east-central Death Valley region, California: *in* Walawender, M.J., and Hanan, B.B., eds., Geological excursions in southern California and Mexico, Geological Society of America Guidebook: San Diego, California, p. 93-127.

Wrucke, C.T., Stevens, C.H., and Wooden, J.L., 1995, The Butte Valley and Layton Well Thrusts of eastern California: Distribution and regional significance: Tectonics, v. 14, p. 1165-1171.

APPENDIX

Neutron Activation Data

Sample #	99	error	129	error	131A	error	153B	error	Uncertainty
FeO (%)1	7.86 ±	0.02	2.89 ±	0.01	5.16 ±	0.02	2.59 ±	0.01	5%
Na2O (%)	3.69 ±	0.00	5.16 ±	0.01	4.67 ±	0.00	3.98 ±	0.01	3%
K2O (%)	1.7 ±	0.1	2.8 ±	0.2	2.9 ±	0.1	4.1 ±	0.3	15%
Sc (ppm)	24.10 ±	0.02	3.99 ±	0.01	6.63 ±	0.01	4.89 ±	0.01	3%
Cr (ppm)	6 ±	1	< 1.1E+01		< 1.1E+01		< 1.6E+01		10%
Co (ppm)	21.30 ±	0.09	2.00 ±	0.03	5.39 ±	0.05	2.36 ±	0.04	5%
Ni (ppm)	< 1.5E+023		< 6.3E+01		< 9.0E+01		< 8.7E+01		12%
Zn (ppm)	100 ±	12	77 ±	5	115 ±	8	75 ±	7	15%
As (ppm)	< 3.0E+00		< 5.1E+00		< 4.2E+00		< 5.7E+00		5%
Sb (ppm)	< 3.3E-01		0.44 ±	0.03	1.12 ±	0.05	0.31 ±	0.03	5%
Se (ppm)	< 5.1E+00		< 2.6E+00		1.6 ±	0.3	< 3.3E+00		5%
Rb (ppm)	70 ±	3	69 ±	2	97 ±	2	93 ±	2	10%
Cs (ppm)	1.29 ±	0.12	1.11 ±	0.06	3.49 ±	0.08	1.71 ±	0.08	5%
Sr (ppm)	660 ±	46	422 ±	22	543 ±	30	424 ±	24	12%
Ba (ppm)	745 ±	70	1090 ±	76	1340 ±	63	683 ±	48	10%
La (ppm)	28.4 ±	0.1	153.0 ±	0.3	41.6 ±	0.2	170.0 ±	0.5	3%
Ce (ppm)	53.1 ±	0.4	228.0 ±	0.5	72.1 ±	0.4	292.0 ±	0.6	7%
Nd (ppm)	27.8 ±	1.2	78.8 ±	1.7	32.0 ±	1.4	105.0 ±	1.4	12%
Sm (ppm)	5.92 ±	0.02	12.00 ±	0.04	6.02 ±	0.02	16.90 ±	0.03	5%
Eu (ppm)	1.71 ±	0.02	2.39 ±	0.02	2.01 ±	0.02	2.85 ±	0.03	5%
Tb (ppm)	0.89 ±	0.03	0.93 ±	0.02	1.04 ±	0.15	1.21 ±	0.04	5%
Yb (ppm)	2.3 ±	0.1	3.0 ±	0.2	4.0 ±	0.2	2.7 ±	0.1	5%
Lu (ppm)	0.30 ±	0.02	0.28 ±	0.03	0.50 ±	0.02	0.29 ±	0.02	5%
Zr (ppm)	124 ±	17	160 ±	7	210 ±	11	139 ±	9	10%
Hf (ppm)	5.61 ±	0.10	12.20 ±	0.06	15.40 ±	0.08	11.10 ±	0.07	5%
Ta (ppm)	0.44 ±	0.03	0.26 ±	0.02	0.92 ±	0.03	0.62 ±	0.03	5%
W (ppm)	< 2.9E+00		< 4.8E+00		1.2 ±	0.4	< 3.9E+00		12%
Hg (ppm)	< 1.5E-01		< 8.1E-02		< 1.1E-01		< 1.0E-01		5%
Th (ppm)	3.3 ±	0.1	35.6 ±	0.1	10.1 ±	0.1	50.6 ±	0.1	5%
U (ppm)	1.2 ±	0.3	1.5 ±	0.4	1.5 ±	0.5	2.0 ±	0.5	7%
Au (ppb)	< 2.9E-02		< 3.6E-02		< 3.6E-02		< 3.3E-02		10%
Ir (ppb)	< 6.3E-02		< 6.0E-02		< 5.7E-02		< 8.1E-02		10%
Os (ppb)	<-2.0E+00		<-2.0E+00		<-2.0E+00		<-2.0E+00		10%

Sample #	159	error	162	error	166	error	175A1	error	Uncertainty
FeO (%)	1.29 ±	0.01	2.53 ±	0.01	1.87 ±	0.01	2.12 ±	0.01	5%
Na2O (%)	3.15 ±	0.01	4.54 ±	0.01	3.77 ±	0.01	2.95 ±	0.01	3%
K2O (%)	4.0 ±	0.2	2.9 ±	0.2	3.6 ±	0.3	4.1 ±	0.2	15%
Sc (ppm)	2.97 ±	0.01	4.55 ±	0.01	3.74 ±	0.01	3.73 ±	0.01	3%
Cr (ppm)	< 7.2E+00		6 ±	1	< 1.0E+01		5 ±	1	10%
Co (ppm)	0.90 ±	0.02	2.73 ±	0.04	2.91 ±	0.04	4.11 ±	0.04	5%
Ni (ppm)	< 3.9E+01		< 6.3E+01		23 ±	7	< 5.4E+01		12%
Zn (ppm)	24 ±	4	68 ±	7	39 ±	7	38 ±	5	15%
As (ppm)	< 3.3E+00		1.9 ±	0.5	< 3.3E+00		< 3.3E+00		5%
Sb (ppm)	0.12 ±	0.02	0.30 ±	0.03	0.21 ±	0.03	0.10 ±	0.02	5%
Se (ppm)	< 2.6E+00		1.9 ±	0.4	1.3 ±	0.3	2.0 ±	0.2	5%
Rb (ppm)	77 ±	1	66 ±	2	89 ±	2	107 ±	2	10%
Cs (ppm)	0.52 ±	0.04	2.07 ±	0.07	0.82 ±	0.07	0.81 ±	0.04	5%
Sr (ppm)	118 ±	14	360 ±	27	239 ±	24	267 ±	19	12%
Ba (ppm)	761 ±	52	1540 ±	68	870 ±	51	918 ±	47	10%
La (ppm)	29.4 ±	0.2	95.3 ±	0.3	34.3 ±	0.2	38.3 ±	0.2	3%
Ce (ppm)	52.6 ±	0.4	145.0 ±	0.4	56.8 ±	0.4	64.4 ±	0.4	7%
Nd (ppm)	19.7 ±	0.8	50.1 ±	1.5	19.6 ±	0.9	22.9 ±	1.1	12%
Sm (ppm)	3.81 ±	0.02	8.83 ±	0.03	3.80 ±	0.02	3.86 ±	0.02	5%
Eu (ppm)	0.74 ±	0.01	1.77 ±	0.02	0.81 ±	0.02	0.86 ±	0.01	5%
Tb (ppm)	0.53 ±	0.01	0.83 ±	0.03	0.46 ±	0.02	0.48 ±	0.09	5%
Yb (ppm)	2.81 ±	0.04	2.4 ±	0.2	1.7 ±	0.1	1.56 ±	0.04	5%
Lu (ppm)	0.39 ±	0.02	0.31 ±	0.03	0.22 ±	0.02	0.22 ±	0.02	5%
Zr (ppm)	46 ±	4	104 ±	9	57 ±	8	57 ±	6	10%
Hf (ppm)	3.79 ±	0.04	8.30 ±	0.07	4.90 ±	0.06	4.17 ±	0.05	5%
Ta (ppm)	0.32 ±	0.01	0.82 ±	0.03	0.51 ±	0.02	1.32 ±	0.02	5%
W (ppm)	1.0 ±	0.3	1.9 ±	0.5	< 4.5E+00		< 2.6E+00		12%
Hg (ppm)	< 6.0E-02		< 1.0E-01		0.04 ±	0.01	< 6.6E-02		5%
Th (ppm)	12.5 ±	0.1	26.8 ±	0.1	11.7 ±	0.1	21.7 ±	0.1	5%
U (ppm)	0.8 ±	0.2	1.7 ±	0.5	< 3.9E+00		2.9 ±	0.4	7%
Au (ppb)	0.01 ±	0.00	0.01 ±	0.00	< 2.1E-02		< 2.4E-02		10%
Ir (ppb)	< 3.6E-02		< 6.6E-02		< 5.1E-02		< 4.5E-02		10%
Os (ppb)	<-2.0E+00		<-2.0E+00		<-2.0E+00		<-2.0E+00		10%

Sample #	175A2	error	175A3	error	1131	error	1132	error
FeO (%)	3.10 ±	0.01	5.04 ±	0.02	8.87 ±	0.03	9.36 ±	0.03
Na2O (%)	4.30 ±	0.01	4.24 ±	0.01	4.10 ±	0.01	3.70 ±	0.01
K2O (%)	1.3 ±	0.3	1.6 ±	0.3	1.2 ±	0.3	1.6 ±	0.3
Sc (ppm)	3.56 ±	0.01	9.83 ±	0.02	18.90 ±	0.02	26.00 ±	0.03
Cr (ppm)	3 ±	1	< 1.0E+01		72 ±	2	132 ±	2
Co (ppm)	4.88 ±	0.03	9.43 ±	0.07	24.60 ±	0.12	28.40 ±	0.11
Ni (ppm)	< 4.5E+01		31 ±	9	< 1.6E+02		< 1.8E+02	
Zn (ppm)	46 ±	4	80 ±	9	92 ±	13	98 ±	15
As (ppm)	< 3.6E+00		< 4.8E+00		< 6.6E+00		< 6.9E+00	
Sb (ppm)	0.13 ±	0.02	0.22 ±	0.04	0.36 ±	0.07	0.21 ±	0.04
Se (ppm)	< 1.7E+00		< 4.2E+00		< 5.7E+00		< 6.0E+00	
Rb (ppm)	40 ±	1	69 ±	3	48 ±	4	50 ±	4
Cs (ppm)	0.70 ±	0.04	1.40 ±	0.08	2.25 ±	0.13	2.01 ±	0.15
Sr (ppm)	382 ±	16	385 ±	33	744 ±	45	706 ±	54
Ba (ppm)	233 ±	37	341 ±	57	548 ±	48	417 ±	46
La (ppm)	36.6 ±	0.2	51.1 ±	0.3	25.2 ±	0.2	16.3 ±	0.2
Ce (ppm)	60 9 ±	0.3	92.6 ±	0.6	60.8 ±	0.8	38.3 ±	0.6
Nd (ppm)	22.1 ±	1.0	38.7 ±	1.5	35.0 ±	2.0	22.8 ±	2.5
Sm (ppm)	3.60 ±	0.01	6.21 ±	0.03	6.87 ±	0.03	6.55 ±	0.03
Eu (ppm)	1.00 ±	0.01	1.46 ±	0.02	1.95 ±	0.03	1.95 ±	0.03
Tb (ppm)	0.41 ±	0.01	0.78 ±	0.02	0.80 ±	0.03	0.83 ±	0.04
Yb (ppm)	1.5 ±	0.1	2.0 ±	0.1	2.1 ±	0.1	2.0 ±	0.1
Lu (ppm)	0.18 ±	0.01	0.20 ±	0.02	0.28 ±	0.02	0.29 ±	0.02
Zr (ppm)	75 ±	5	74 ±	9	91 ±	17	105 ±	17
Hf (ppm)	5.55 ±	0.04	4.36 ±	0.07	4.60 ±	0.11	4.94 ±	0.13
Ta (ppm)	0.36 ±	0.01	0.37 ±	0.03	0.60 ±	0.04	0.59 ±	0.04
W (ppm)	< 4.2E+00		< 5.1E+00		< 7.5E+00		< 8.1E+00	
Hg (ppm)	< 5.4E-02		< 1.3E-01		< 1.7E-01		< 1.9E-01	
Th (ppm)	6.30 ±	0.04	6.18 ±	0.07	1.93 ±	0.12	1.86 ±	0.14
U (ppm)	1.0 ±	0.3	< 3.3E+00		< 4.5E+00		< 2.7E+00	
Au (ppb)	< 2.0E-02		< 2.5E-02		0.015 ±	0.004	0.014 ±	0.003
Ir (ppb)	< 2.8E-02		< 5.1E-02		< 7.5E-02		< 8.4E-02	
Os (ppb)	<-2.0E+00		<-2.0E+00		<-2.0E+00		<-2.0E+00	

Sample #	180	error	SS2	error	SS3	error	Uncertainty
FeO (%)	12.20 ±	0.02	16.30 ±	0.03	15.10 ±	0.03	5%
Na2O (%)	2.43 ±	0.01	0.31 ±	0.00	2.93 ±	0.01	3%
K2O (%)	1.7 ±	0.4	3.5 ±	0.3	2.9 ±	0.5	15%
Sc (ppm)	50.00 ±	0.05	24.60 ±	0.03	24.20 ±	0.02	3%
Cr (ppm)	< 2.1E+01		12 ±	2	16 ±	2	10%
Co (ppm)	47.90 ±	0.14	53.40 ±	0.16	52.30 ±	0.16	5%
Ni (ppm)	< 1.7E+02		51 ±	16	97 ±	22	12%
Zn (ppm)	132 ±	22	189 ±	12	239 ±	16	15%
As (ppm)	< 6.3E+00		5.4 ±	0.8	2.6 ±	0.8	5%
Sb (ppm)	< 6.3E-01		0.83 ±	0.07	0.40 ±	0.07	5%
Se (ppm)	< 8.1E+00		< 4.5E+00		< 7.8E+00		5%
Rb (ppm)	54 ±	6	129 ±	4	60 ±	5	10%
Cs (ppm)	2.02 ±	0.20	14.60 ±	0.13	2.59 ±	0.16	5%
Sr (ppm)	461 ±	75	1540 ±	49	241 ±	66	12%
Ba (ppm)	343 ±	54	359 ±	50	397 ±	55	10%
La (ppm)	12.0 ±	0.1	30.0 ±	0.2	28.0 ±	0.2	3%
Ce (ppm)	28.4 ±	1.2	64.0 ±	1.2	57.8 ±	1.8	7%
Nd (ppm)			41.5 ±	3.1	35.8 ±	3.0	12%
Sm (ppm)	4.83 ±	0.02	8.74 ±	0.04	7.82 ±	0.03	5%
Eu (ppm)	1.50 ±	0.03	3.40 ±	0.03	3.02 ±	0.03	5%
Tb (ppm)	0.68 ±	0.05	1.13 ±	0.03	1.00 ±	0.04	5%
Yb (ppm)	1.9 ±	0.1	3.0 ±	0.1	2.8 ±	0.1	5%
Lu (ppm)	0.26 ±	0.02	0.37 ±	0.02	0.32 ±	0.02	5%
Zr (ppm)	< 2.0E+02		196 ±	18	169 ±	23	10%
Hf (ppm)	2.04 ±	0.13	5.89 ±	0.11	5.60 ±	0.15	5%
Ta (ppm)	0.45 ±	0.05	1.03 ±	0.04	0.94 ±	0.05	5%
W (ppm)	3.6 ±	0.9	< 8.4E+00		< 7.5E+00		12%
Hg (ppm)	< 2.4E-01		< 1.7E-01		< 2.2E-01		5%
Th (ppm)	1.97 ±	0.16	4.61 ±	0.12	4.3 ±	0.2	5%
U (ppm)	< 4.5E+00		< 4.2E+00		2.6 ±	0.5	7%
Au (ppb)	< 3.3E-02		< 3.3E-02		< 3.9E-02		10%
Ir (ppb)	< 1.0E-01		< 7.2E-02		< 9.0E-02		10%
Os (ppb)	<-2.0E+00		<-2.0E+00		<-2.0E+00		10%

C1 Chondrite Normalization

Sample	99	129	131A	153B	159	C1 chondrite Lit. Values
Cs	5.22	4.49		6.92	2.09	0.247
Rb	23.13	22.76	31.88	30.63	25.43	3.04
K	19.57	31.16	32.73	46.01	44.77	0.0889
Th	83	892	253	1,268	313	0.0399
U	108	136	140	184	76	0.0107
Sr	63.46	40.58	52.21	40.77	11.35	10.40
Ba	248.33	363.33	446.67	227.67	253.67	3.00
La	91.03	490.38	133.33	544.87	94.23	0.312
Ce	65.31	280.44	88.68	359.16	64.70	0.813
Nd	46.10	130.68	53.07	174.13	32.67	0.603
Sm	30.05	60.91	30.56	85.79	19.34	0.197
Eu	23.11	32.30	27.16	38.51	9.95	0.074
Gd*	22.00	28.70	24.64	38.45	13.55	0.260
Tb	18.83	19.70	22.13	25.74	11.34	0.047
Yb	11.10	14.10	18.95	12.86	13.38	0.210
Lu	9.38	8.58	15.57	8.95	12.07	0.0323
Sc	3.13	0.52	0.86	0.64	0.39	7.7
Zr	25.31	32.65	42.86	28.37	9.43	4.9
Hf	35.73	77.71	98.09	70.70	24.14	0.157
Ta	21.46	12.78	45.07	30.15	15.46	0.0205

C1 Chondrite Normalization

Sample	162	166	175A1	175A2	175A3	C1 chondrite Lit. Values
Cs	8.38	3.32	3.27	2.83	5.67	0.247
Rb	21.68	29.38	35.20	13.19	22.76	3.04
K	32.28	40.27	46.12	14.51	18.22	0.0889
Th	672	293	544	158	155	0.0399
U	158	n.a.	269	90	n.a.	0.0107
Sr	34.62	22.98	25.67	36.73	37.02	10.40
Ba	513.33	290.00	306.00	77.67	113.67	3.00
La	305.45	109.94	122.76	117.31	163.78	0.312
Ce	178.35	69.86	79.21	74.91	113.90	0.813
Nd	83.08	32.50	37.98	36.65	64.18	0.603
Sm	44.82	19.29	19.59	18.27	31.52	0.197
Eu	23.92	11.00	11.61	13.51	19.73	0.074
Gd*	24.13	12.22	12.69	11.11	20.46	0.260
Tb	17.70	9.72	10.21	8.66	16.49	0.047
Yb	11.19	7.86	7.43	7.14	9.52	0.210
Lu	9.50	6.75	6.69	5.54	6.22	0.0323
Sc	0.59	0.49	0.48	0.46	1.28	7.7
Zr	21.22	11.57	11.67	15.22	15.12	4.9
Hf	52.87	31.21	26.56	35.35	27.77	0.157
Ta	39.85	24.93	64.39	17.46	18.05	0.0205

C1 Chondrite Normalization

Sample	1131	1132	180	SS2	SS3	C1 chondrite Lit. Values
Cs	9.11	8.14	8.18	59.11	10.49	0.247
Rb	15.63	16.35	17.73	42.43	19.74	3.04
K	13.95	18.45	19.35	39.26	32.06	0.0889
Th	48	47	49	116	108	0.0399
U	n.a.	n.a.	n.a.	n.a.	238	0.0107
Sr	71.54	67.88	44.33	148.08	23.17	10.40
Ba	182.67	139.00	114.33	119.67	132.33	3.00
La	80.77	52.24	38.46	96.15	89.74	0.312
Ce	74.78	47.11	34.93	78.72	71.09	0.813
Nd	58.04	37.81	0.00	68.82	59.37	0.603
Sm	34.87	33.25	24.52	44.37	39.70	0.197
Eu	26.35	26.35	20.27	45.95	40.81	0.074
Gd*	21.58	21.82	17.25	29.49	26.19	0.260
Tb	16.98	17.68	14.47	24.04	21.28	0.047
Yb	9.76	9.57	9.10	14.43	13.14	0.210
Lu	8.76	8.95	8.08	11.46	9.81	0.0323
Sc	2.45	3.38	6.49	3.19	3.14	7.7
Zr	18.63	21.43	n.a.	40.00	34.49	4.9
Hf	29.30	31.46	12.99	37.52	35.67	0.157
Ta	29.22	28.59	21.85	50.24	45.61	0.0205

The following information was provided by the Radiation Center of Oregon State University regarding the reported data.

The error value listed for each individual elemental abundance is a counting error. This error should be used only if it is larger than the analytical uncertainty listed in the right-hand column on each data sheet. This may actually be the case for elements with relatively short-lived radionuclides such as potassium. In order to provide an indication of the magnitude of the counting errors, they may be reported to more significant figures than the analytical value.

1. Total Fe expressed as weight percent FeO.

2. Where an individual error is reported for a specific analytical result, it is based on one standard deviation of the sample's net counts in the photopeak of interest. Because the net counts in some photopeaks were relatively high, the standard deviation value shown for the corresponding analytical result turned out to be comparatively small (i.e., less than 1 or 2 % of the analytical result). If these small standard deviation values are used as the only measure of confidence in the reported results, they will indicate an unreasonably high level of analytical accuracy. In these cases, a better estimate of the analytical accuracy can be obtained by using the percent uncertainty value listed for the element under consideration. This value is the percent of relative standard deviation (using one standard deviation) obtained for the specific element being considered, based on repeated counts of appropriate standards for this same element.

3. Certain concentration values have been reported as maximum undetectable activity (MUA), which has been indicated in each case by the "<" symbol on the data sheets. When an MUA value is given, it represents a situation where no photopeak was clearly evident at an acceptable statistical confidence level (or at an acceptable sensitivity level). In these cases, the MUA gives the maximum possible concentration for the element or oxide which could remain undetected (based on the counts obtained) at a confidence level of three sigma (99.7%). Therefore, the MUA value establishes an upper limit concentration value for the element or oxide involved. The actual concentration value may be less than the MUA, but should not exceed this value.

The statistical confidence limit set for photopeak acceptability (i.e., the "sensitivity level" mentioned above) is defined as the uncertainty permitted for a photopeak that is to be allowed in the determination of a specific nuclide. It is essentially the relative standard deviation of the net counts in the photopeak (expressed as a percent value), and is calculated by:

$$\% \text{ Sensitivity Level} = \frac{\sqrt{\text{Gross Counts} + \text{Background Countns}}}{\text{Net Counts}}$$

When the sensitivity level exceeded 33% for a suspected photopeak, the MUA value was reported. To state this another way, when one standard deviation of the net counts in a photopeak exceeded 33% of the total net counts involved in the peak, we felt that the uncertainty was too great and reported the MUA.

4. Values listed for the non-volatile C1 chondrite normalization were modified from Anders, E. and Ebihara, M., 1982, Solar System Abundances of the Elements: Geochimica et Cosmochimica Acta, v. 6, p. 2363-2380.

VITA

John Comstock was born November 3, 1953, in Palm Springs, California, and grew up in the suburbs of Los Angeles. He enlisted in the U. S. Air Force in 1973, serving in Thule, Greenland and Phoenix, Arizona before transferring to the California Air National Guard where he became a weather forecaster and National Guard bum. He attended various colleges during the late 1970's and early 1980's, majoring in philosophy, history and political science, and scratched out an existence by substitute teaching. From 1983 through 1992, after a brief flirtation with the Episcopal priesthood, he worked in the medical equipment industry. Initially working for others, he was invited to seek opportunity elsewhere, so he started and managed his own company. The expansion of government regulation and the encroachment of corporate managed health care provided the incentive to return to college. He started in the geology program at Sonoma State University in Rohnert Park, California in 1991 and graduated with a B.S. in Geology in May, 1995. He started graduate studies at the University of New Orleans in the fall semester of 1995 and will graduate with a M.S. in Geology in December 1997. He is currently enrolled in the Ph.D. program in geology at Rice University in Houston, Texas.